Print parameter optimisation for three-dimensional bioprinting of hydrogel scaffolds

M Hibbert

orcid.org/ 0000-0002-3235-2620

Dissertation submitted in fulfilment of the requirements for the degree Master of MSc Pharmaceutics at the North-West University

Supervisor: Prof L du Plessis

Co-Supervisor: Prof J Viljoen

Examination: March 2021

PREFACE AND DISCLAIMER

This dissertation is presented in article form, therefore, British English was used as per the author guidelines of scientific journals. The reference style is the Harvard style of the NWU only for the examination of the dissertation and will be changed before submission of the article. The article was written for the journal Bioprinting and will be submitted for publication.

The dissertation is compiled in the article format according to the guidelines of the North-West University and consist of an Introduction, including the problem statement, aim and objectives in Chapter 1, the Literature review in Chapter 2, the article entitled *Print parameter optimisation for a PF127 and alginate hybrid hydrogel* in Chapter 3 and the Conclusion and Recommendations in Chapter 4. The formulation and evaluation of hybrid hydrogel bioink results is presented in Annexure A, the printability of the alginate PF127 hybrid hydrogel results are presented in Annexure B and the print parameter optimisation study is presented in Annexure C.

Author contribution and permission statements

I, Monja Hibbert, am the main researcher responsible for the proposal, planning and execution of this study, along with (i) extensive review of relevant literature, (ii) assessment and optimisation of the bulk of the experimental protocol and methods, (iii) collection, analysis, interpretation and presentation of data, (iv) design, planning and writing of research articles, and (v) writing of all sections of this thesis.

Prof. Lissinda H. Du Plessis

Supervisor responsible for guidance, intellectual input and evaluation of research outputs.

Prof. J.M. Viljoen

Co-supervisor responsible for guidance, intellectual input and evaluation of research outputs.

I hereby confirm that the study was approved by the Health Science Ethics Committee at the North-West University with the ethics clearing number: NWU-00510-19-A1 (Annexure D).

Statement by co-authors

I hereby confirm my role related to the publication entitled *Print parameter optimisation for three-dimensional bioprinting of hydrogel scaffolds,* I give consent that Monja Hibbert may include the manuscript in her dissertation.

This study was funded in part by the National Research Foundation (NRF) of South-Africa grant of Lissinda du Plessis (Grant number 85297).

DISCLAIMER

Any opinion, finding, and conclusion or recommendation expressed in this material is that of the authors, and the South African National Research Foundation does not accept any liability in this regard.

ACKNOWLEDGEMENTS

First of all, I want to give thanks to our creator YHVH for granting me this opportunity to further my knowledge, for gifting me the mental capabilities to pursue my dreams, and for accompanying this capacity with the needed endurance, wisdom and patience to follow through. I give all honour to You.

I would like to acknowledge the following people for their support, guidance and motivation throughout this study:

My supervisor, Prof Lissinda Du Plessis, for your patience through every step, none of this would have even been possible without you. Thank you for your guidance and time, for you open door and listening ears, be it study related or not. Thank you for sharing your knowledge with me and for forming me into the researcher I am today.

My co-supervisor, Prof Joe Viljoen, for your guidance, input and for your time and patience. Thank you for teaching me within this journey.

My dearest husband, Alex Hibbert, thank you for keeping things together when I failed to do so, thank you for every cup of coffee and conversations of encouragement and motivation. Thank you for helping me when I struggled and for always being so proud of me even when I felt it was undeserved. I thank YHVH for blessing me with a life partner such as you. I love you!

My friend, my partner in crime, my master's companion, Riana van Wyk, thank you for always listening to my venting, unpacking of failed experiments and frustrations, thank you for always finding a way to relate and for being by my side in this endeavour that both of us decided to take on and for keeping me company on campus. May your journey in life always be favourable.

My mother and father, René and Ramon van der Linde, for always supporting me in everything I approach. Thank you for the sacrifices you have made to help me achieve my goals and for always knowing what to say to calm my racing mind and heart. Thank you for always being my rock and support system – no words could encompass my gratitude.

My mother- and father-in-law, Carlene and Paul Hibbert, thank you for your unwavering support throughout this journey.

My grandfather and -mother, Jan and Antoinette Vermeulen, for the legacy that has allowed me to fulfil my dreams, may this dissertation bring you great feelings of accomplishment, pride and joy.

ABSTRACT

In drug discovery and delivery research, there is a continuing need for valid and reliable alternatives for in vitro drug efficacy and toxicity studies, and consequently tissue engineering has caught the attention of researchers within this field. The mechanical properties, bioactivity and printability of these tissue constructs/scaffolds, however, still remain a challenge. Various studies have focused on investigating alternative printers, biopolymers and cross-linking methods of the hydrogels/bioinks and recent papers mainly focus on the final tissue constructs; nonetheless, few have focused on the performance of the printing process.

The aim of this study was to systematically optimise the printing parameters required to successfully 3D bioprint a preselected computer-aided design (CAD) model into a sustainable scaffold with a preformulated hybrid hydrogel. The optimised parameters include nozzle size, printing speed, pneumatic extrusion pressure as well as temperature. The formulated hybrid hydrogel, which consisted of alginate, a naturally derived biomaterial and Pluronic F-127 (PF127), a synthetic poloxamer, had to undergo characterisation studies which included determining the optimal concentration of alginate, the ionic cross-linking solution used, as well as the cross-linking method.

An alginate concentration between 4 and 6% (w/v) yielded successful cross-linking with a 2% (w/v) CaCl2 cross-linking solution. PF127 was consequently added in various concentrations, classifying it as a hybrid hydrogel, also had to undergo characterisation studies to determine the optimal PF127 concentration as well as determining the properties of the hybrid hydrogel. Porosity, degradation rate, viscosity and cross-linking capabilities were measured. A concentration of 6% (w/v) alginate (A) mixed with a 46% (w/v) PF127 in a 2:1 ratio, displayed the most positive results, with an average porosity of 50.50±3.1%, a low degradation rate that can be attributed to the PF127 addition, and a rheological characterisation of a non-Newtonian fluid.

Cross-linking the 6%A:46%PF127 hybrid hydrogel had to be done with a 4% (w/v) CaCl2 cross-linking solution as the 2% (w/v) CaCl2 caused insufficient cross-linking. This was ascribed to PF127's chemical inertness, as it does not undergo ionic cross-linking, but entangle within the polymer chains formed from the alginate. This hybrid hydrogel (6%A:46%PF127) was consequently used to systematically optimise the printing parameters. The parameter optimisation index (POI), described by Webb and Doyle (2017), was implemented in combination with a newly formulated scoring method to help determine the optimal printing parameters.

It was found that in combination with these grading methods, the visual appearance plays a similarly important role in selecting optimal printing parameters. The CAD model was printed to 8 to 12% completion, photographed and enlarged to ease line width and corner drag measurements as they determine the POI as well as the score allocation that form part of the newly formulated grading method. Optimal printing parameters to yield a successful scaffold print were found to be a nozzle size of 27G, extrusion pressure of 70kPa and a printing speed of 30mm/s at 37ºC.

The printed scaffold was submerged into a 4% (w/v) CaCl2 cross-linking solution for 24h. The swelling ratio of the printed scaffold was also determined to be the better in 2% (w/v) CaCl2 at 37ºC. Although the printing parameters were successfully optimised with the formulated hybrid hydrogel, high concentrations of PF127 could possibly have a negative effect on cell proliferation in the event that they are included in the bioink, therefore a clear need for the design and development for alternative polymer support materials is needed.

Keywords: 3D bioprinting, pneumatic extrusion, biomaterials, tissue engineering, scaffold, printing parameter optimisation, hybrid hydrogel, hydrogel characterisation, alginate, Pluronic F-127, parameter optimisation index (POI).

TABLE OF CONTENTS

LIST OF TABLES

LIST OF FIGURES

LIST OF ABBREVIATIONS

.stl:	Standard Tessellation Language or STereoLithography
2D:	Two dimensional
3D:	Three dimensional
A:	Alginate
ABS:	Acrylonitrile butadiene styrene
AM:	Additive manufacturing
CAD:	Computer-aided design
Ca^{2+}:	Calcium
$CaCl_2$:	Calcium chloride
ECM:	Extracellular matrix
G:	Gauge (nozzle size)
dH_2O:	Distilled water
H:	Hydrogen
HLB:	Hydrophilic-lipophilic balance
kPa:	Kilo pascal
min:	Minutes
mm/s:	Milli-meters per second
PBS:	Phosphate buffered saline
PEG:	Poly(ethylene gly-col)
PEO:	Polyethylene oxide
PF127:	Pluronic F127
PLA:	Polylactide
POI:	Parameter optimisation index
PPF:	Poly(propyl fumarate)
PPO:	Poly(oxyethylene–oxypropylene)
RP:	Rapid prototyping
s:	Seconds
SR:	Swelling ratio
US FDA:	United States Food and Drug Administration
w/v:	Weight per volume

CHAPTER 1: INTRODUCTION

1.1 Introduction

In drug discovery and drug delivery research, there is a continuing need for valid and reliable alternatives for *in vitro* drug efficacy and toxicity testing (Herrera, 2019; Koçak *et al.,* 2021). Launching a new drug usually composes of two major stages, namely the preclinical phase which involves drug discovery, and the clinical phase, which involves drug development; where drug development focuses on the safety and efficacy of possible new drug candidates (Zhu, 2016). Monitoring and studying the mechanisms, toxicities and effects of possible new drugs are of great importance and for this purpose, animal models are used and very rarely animals, since unnecessary animal use is ethically inappropriate. By utilising the field of three-dimensional (3D) bioprinting, it allows for *in vitro* cell models to be printed, thereby providing an alternative to two-dimensional (2D) and animal models (Koçak *et al*., 2021).

Research has shown that cells in a 2D culture display dramatic differences in cell behaviour compared to 3D cultures, which provides a more relevant physiology and environment native to cells (Zhu, 2016). One of the main advantages that 3D multi-layer cell culture systems have, is the ability to recreate *in vivo* conditions that 2D cell cultures lack. Consequently, the fabrication of synthetic tissue, known as tissue engineering, has caught the attention of many researchers seeking an alternative from the classically known methods of drug efficacy and toxicity testing (Peng *et al*., 2017).

Existing tissue engineering technologies have contributed immensely in creating novel tissue models for drug efficacy and toxicity testing. However, classic tissue engineering methods have several disadvantages, as they lack the ability to fabricate complex biometric structures. This leads to over-simplified tissue constructs that are inaccurate with unrealistic cell microenvironments (Vijayavenkataraman *et al*., 2018). 3D bioprinting, on the other hand, allows cell-cell and cell-extracellular matrix (ECM) interaction, whereas this is absent in 2D tissue constructs (Wu *et al*., 2018). A study conducted by Suo *et al*. (2019) proved that breast cancer cells from a hydrogel culture portrayed higher invasion/migration abilities than that of a 2D culture, and therefore cell-laden hydrogels open a wide range of research possibilities and therapeutic models.

There are various novel technologies available in tissue engineering; for example, additive manufacturing (AM) for the direct fabrication of 3D tissue constructs or scaffolds, also known as biofabrication, is one successful approach (Tytgat *et al*., 2019; Peng *et al*., 2017). AM can be

described as the process of joining materials to fabricate a 3D object by means of a layer-by-layer method (Wu *et al*., 2018). The process was originally conceived by Charles Hull in 1986 and consists of printing successive layers of a material on top of each other to 'print' objects (Bishop *et al*., 2017; Ngo *et al*., 2018). Material extrusion is an AM technology where the material is extruded through a syringe or nozzle system onto an appropriate platform to create an object (Leberfinger *et al*., 2019). The object can be any design; from a simple line to a complex organ model, which is designed by computer-aided design (CAD) software (ISO, 2015); however, most tissue constructs use a scaffold architecture in a geometric pattern (grid with different pore sizes) (Datta *et al*., 2018; O'Brien, 2011; Ozbolat & Hospodiuk, 2016).

3D bioprinting can be defined as the stacking and assembling of organic materials that can contain living cells, or not, and other bioinks in spatial patterns using a computer-aided layer-by-layer deposition approach, creating a well-arranged 3D structure (Datta *et al*., 2018; O'Brien, 2011; Ozbolat & Hospodiuk, 2016). Although some biofabrication products can be described as non-living, they are still biological, which means that not all biofabrication processes involve live cells (Mironov *et al.,* 2009). Successful 3D bioprinting relies on two characteristics, namely cell viability and geometric accuracy. Both these features depend on the properties of the biomaterial being used and are influenced by the bioprinting parameters (Webb & Doyle, 2017).

Biofabrication processing methods can be subdivided into four main groups, namely laser-based bioprinting, droplet-based bioprinting, extrusion-based bioprinting and vat polymerisation (Vijayavenkataraman *et al*., 2018; Lee *et al*., 2018). These groups' subdivisions are stated in Table 2-1 in Chapter 2. Extrusion-based bioprinting has the ability to bioprint a wide range of bioinks with various viscosities and can be subdivided into two groups, namely pneumatic extrusion and mechanical extrusion; however, only pneumatic extrusion has the ability to adjust the air pressure used during extrusion, and this leads to a lower rate of cell death when compared to mechanical extrusion methods (Hölzl *et al*., 2016; Li *et al*., 2020; Bishop, 2017). Pneumatic extrusion has been selected for this study and is visually displayed in Figure 1-1.

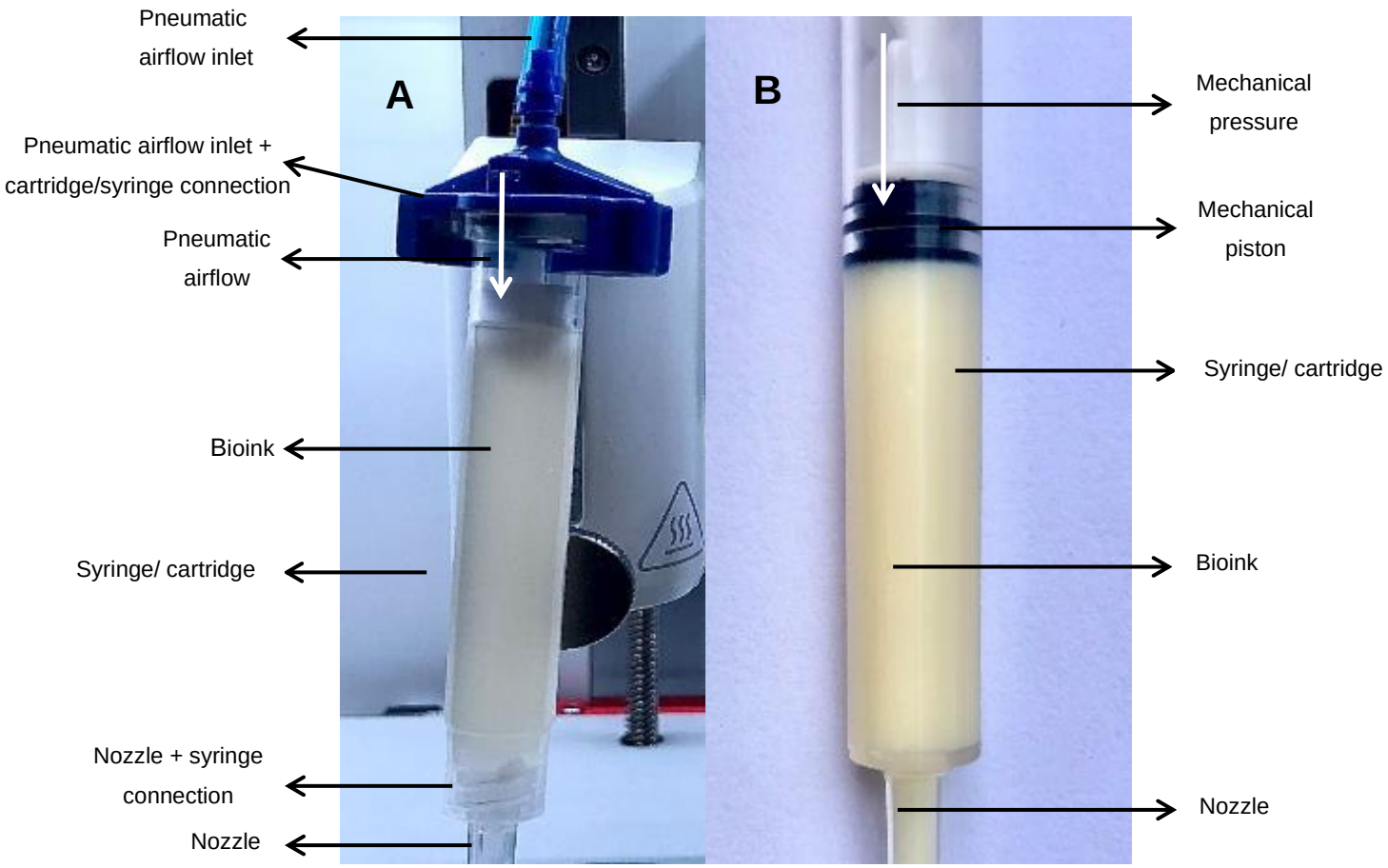

Figure 1-1: Photographic representation of A) pneumatic extrusion and B) mechanical extrusion

Biopolymers are used as the bioink when utilising pneumatic extrusion-based bioprinting, which should portray the necessary characteristics within the printed scaffold, including biocompatibility, biodegradability, good degradation kinetics, safe degradation by-products and being able to enhance cell migration and adhesion (or tissue biomimicry) (Cojocaru *et al*., 2019; Liu *et al*., 2019). Bioinks are bioprintable materials that are based on natural and synthetic polymers (Parak *et al*., 2017), and are defined as cell-containing/cell-free formulations that are able to be processed by biofabrication technology (Van Kampen *et al*., 2019) and are usually prepared with hydrogels.

Hydrogels are defined as 3D porous networks of hydrophilic polymers that are cross-linked and capable of retaining large amounts of biological fluids. Owing to their high biocompatibility, they demonstrate a similar structure to the ECM, including suitable viscosity and shape fidelity (Wang *et al.,* 2018; Chimene *et al*., 2020). Many formulated bioinks are adapted from low viscosity

hydrogels through modulation, such as adding thickeners or by means of partial cross-linking (Williams *et al*., 2018).

Alginate was selected as the basis of the hybrid hydrogel and is considered a natural, soft biopolymer that is derived from the cell walls of brown algae (Emami *et al*., 2018; Puguan *et al*., 2014; Feng *et al*., 2019). Alginate owns a few unique properties, i.e. hydrophobicity, non-toxicity, biocompatibility as well as chelating ability (Derkus *et al*., 2014). Sodium alginate used in this study is the salt form of the alginate, consisting of the sodium salt of alginic acid that is a mixture of polyuronic acids. It is slowly soluble in water, forming a viscous, colloidal solution. (BP, 2018). The free aldehyde groups on the oxidised sodium alginate structure can react with amine groups to form a chemical hydrogel that has a wide variety of uses in fields such drug delivery, wound healing, and tissue and bone engineering (Emami *et al*., 2018). The alginate concentration had to be optimised between 1 and 10% (w/v) according to Webb and Doyle (2017), upon which this study is based, and the optimal cross-linking concentration and method had to be determined (Paxton *et al.,* 2019).

Although alginate provides desirable biocompatibility, it alone did not have the mechanical properties required to successfully support a structure, or even a subsequent layer: and for this reason alginate also had to undergo cross-linking with ionic cross-linking agents, such as calcium (Ca^{+}) and calcium chloride ($CaCl_2$) that cause polymer chains to form and the gel to become more rigid (Berg *et al*., 2018; Chimene *et al*., 2020). Since many formulated bioinks are adapted from low viscosity hydrogels, combining the alginate with high molecular weight polymers have also been implemented to increase the resolution of alginate printing (Panwar & Tan, 2016; Williams *et al*., 2018), and therefore Pluronic F-127 (PF127) was selected as the second component of the hybrid hydrogel for this study.

In contrast to alginate, PF127 falls into the category of being a synthetic, water-soluble, nontoxic poly(oxyethylene–oxypropylene) (PPO), biodegradable poloxamer that displays reverse thermo-responsive properties in aqueous solutions, which have various applications in gelling systems (Grassi *et al*., 2006; Rarokar *et al*., 2018). PF127 is a free-flowing liquid that undergoes thermo-reversible gelation at body temperature (37ºC) and should be prepared using the ‘cold method’ which involves dissolving the PF127 crystals in an aqueous phase at 4ºC (Rarokar *et al*., 2018). The United States Food and Drug Administration (US FDA) guidelines have declared PF127 a safe, inactive, low toxic, biodegradable ingredient that may be used in certain preparations because of their chemical inertness (Rarokar *et al*., 2018), which concludes that it will not partake in the ionic cross-linking process that alginate undergoes. According to Rarokar *et al*. (2018), although PF127 does not partake in alginate cross-linking, it entangles within the polymer chains formed and therefore forms part of the final scaffold.

In this study, this excipient was added to the basis alginate hydrogel, making it a hybrid hydrogel, even though it is synthetic and not of natural origin, which contributed positively to the hybrid hydrogel's characteristics that allowed for printing to take place before alginate cross-linking could occur. Various hybrid alginate/PF127 hydrogels were formulated in the past, e.g. for the use of an application hydrogel, such as a gel-paving system to cover stents inserted in the artery during interventions (Barba *et al*., 2014); however, up to date, an alginate and PF127 hybrid hydrogel has never been used during pneumatic extrusion-based bioprinting.

The degradation rate and porosity of the hybrid hydrogel formulation had to be taken into consideration, as a scaffold printed for tissue engineering purposes is not meant to be permanent, and requires a sufficient porosity to ensure that nutrients are easily transported throughout the structure to where they are required and waste products to be easily removed from within the scaffold for when the hybrid hydrogel is seeded with cells (Roehm, 2018; Calejo *et al*., 2018; Cao *et al*., 2017). Porosity was calculated using a method from Cao *et al*. (2017) which can be seen in Chapter 2 section 2.10.2, and the degradation formula was adapted from a study conducted by Montalbano *et al*. (2018) which is presented in Chapter 2 section 2.10.1.

Furthermore, bioinks should be biocompatible, presenting a high cell viability post printing, be porous enough to allow nutritional transport, and encourage cell adhesion and growth (Parak *et al*., 2019; Chimene *et al*., 2020). The viscosity determines the printability of the bioink, and hydrogels with shear thinning properties are preferred due to the reduced viscosity during the extrusion process (Schwab *et al*., 2020). Hydrogels that have shear thinning properties are classified as non-Newtonian fluids, since the apparent viscosity is dependent on the shear rate (Chimene *et al*., 2020). It was therefore confirmed that the preformulated hybrid hydrogel selected as bioink for the parameter optimisation study, fell into this classification. The swelling ratio was observed since it is an important factor to take into consideration when engineering tissue constructs and when it is used for drug release studies. It can usually be observed with the naked eye how the structure shrinks after its removal from an aqueous solution and again when it is resubmerged, absorbing the aqueous solution back into the scaffold (Wang *et al.,* 2019; Cui *et al*., 2014).

When printing with hydrogels, considerable effort is required to determine the optimum printing parameters to ensure successful printing. These parameters include nozzle temperature and diameter, printing time and speed as well as dispensing pressure. These are often optimised and established in the absence of cells. These parameters also directly influence cell viability, since they determine the shear forces within the bioinks when printing (Webb & Doyle, 2017). The printability of a bioink should present with structural precision and accuracy post printing, withstand forces during the printing process and possess characteristics that render the bioink

printable. The properties of the bioink can be improved by mixing it with hydrogels that have the required and distinct characteristics (Berg *et al*., 2018). Webb and Doyle (2017) explain the parameter optimisation index (POI), providing a better understanding of the relationship between shear stress and accuracy. Printing accuracy is directly related to the geometry of the printed lines, where shear stress is associated with the fluid mechanics of extruding the hydrogel through a thin nozzle, which means the shear stress is directly dependent on the extrusion pressure (Webb & Doyle, 2017). The POI is further explained in Chapter 2 section 2.11.1.

The bioprinting process of hydrogels occurs in three phases (Vijayavenkataraman *et al*., 2018; Varkey *et al*., 2019), and specific tasks within each phase are presented in Figure 1-2. The first phase is known as the pre-processing phase. During this phase, a CAD model was selected, preliminary hydrogel studies on alginate were conducted to ensure a sufficient concentration thereof is present, an optimal cross-linking solution concentration and cross-linking method were determined. The alginate/PF127 hybrid hydrogel formulation concentration was optimised by determining the degradation rate and porosity. Line tests were also conducted to determine the printability of each hybrid hydrogel formulation.

During the next phase, known as the processing phase, an optimal hybrid hydrogel was selected based on the results obtained from the pre-processing phase. This hybrid hydrogel was rheologically measured to ensure its viscosity fell within the required classification. The hybrid hydrogel was used to optimise the printing parameters that allowed for a 100% complete and successful scaffold print. In the next phase, known as the post-processing phase, the 100% printed scaffolds were subjected to swelling ratio measurements as this property allows for nutrients and waste products to move in the structure. The experimental design is described in more detail in section 1.2.3.

1.1.1 Research problem

The continuing need for useful, valid and consistent alternatives for drug discovery and delivery research has led to the utilisation of biofabrication methods such as pneumatic extrusion-based bioprinting for the fabrication of tissue constructs that can be used as *in vitro* biomimetic tissue models. 3D cultures provide a more relevant physiology and environment native to the cells, where 2D models lack *in vivo* conditions and display dramatically different cell behaviour compared to 3D cultures, leading to inaccurate results (Peng *et al*., 2017; Zhu, 2016; Ma *et al*., 2018). However, a number of challenges still remain, especially pertaining to mechanical properties, printability and bioactivity of these printed constructs or scaffolds.

There are studies that have investigated the use of alternative printers, biopolymers and cross-linking methods while printing with hydrogels; nonetheless, few studies have focused on the performance of the printing process to ensure validity, accuracy and precision of the printed scaffold. The specific research question of this study was to systematically optimise the printing parameter required to successfully 3D print a CAD scaffold using a preformulated hybrid hydrogel. This study focused on optimising an alginate/PF127 hybrid hydrogel that was used in a print parameter optimisation study where the printing parameters considered were: printing temperature (ºC), extrusion time (mm/s), extrusion pressure (kPa) and nozzle size (G).

For this study to be successfully conducted, a hybrid hydrogel was formulated and characterised. Optimising the hybrid hydrogel formulation is of importance since various biofabrication techniques require certain properties to be present within the hybrid hydrogel (Hölzl *et al*., 2016), and to ensure that the optimal hybrid hydrogel formulation was selected, it underwent porosity, viscosity and degradation rate studies as these factors are all of importance. After the hybrid hydrogel was selected and printing parameters were optimised, the swelling ratio of the scaffold was also determined as part of the scaffold characterisation study.

1.2 Aims and objectives

1.2.1 Aim

The aim of this study was to systematically optimise the different printing parameters during the 3D bioprinting process of a pre-formulated hybrid hydrogel scaffold.

1.2.2 Objectives

The specific objectives of this study were to:

1. conduct preliminary alginate hydrogel studies to optimise the concentration thereof;
2. determine the ionic cross-linking concentration needed for successful alginate cross-linking;
3. formulate and characterise a biopolymer-based hybrid hydrogel to be used as bioink with alginate and PF127, and combinations thereof in different ratios;
4. characterise the formulated hybrid hydrogels by means of quantifying the porosity value and degradation rate as a measure of stability in order to select the optimal hybrid hydrogel bioink for the print parameter optimisation study;
5. determine the printability with each hybrid hydrogel formulation using an adaptation of the single fibre extrusion test;

6. evaluate rheological properties (viscosity) of the selected optimal hybrid hydrogel by using a rotational rheometer to confirm the non-Newtonian property of the hybrid hydrogel;
7. develop a scaffold print scoring method;
8. determine the optimal nozzle size and temperature first by evaluating the capability of producing an 8 to 12% completed cell-free scaffold base within the predetermined bioprinting parameters;
9. determine the optimal extrusion speed and pressure thereafter by evaluating the scaffold integrity with image analyses of 8 to 12% printed scaffold bases with formulated scoring method;
10. calculate the POI and establish whether there is a correlation between the print score and the POI;
11. evaluate the visual appearance and cross-linking method of the hybrid hydrogel scaffold with a 100% complete print with optimised print parameters;
12. evaluate bioactivity of the hybrid hydrogel scaffold by calculating the swelling ratio.

1.2.3 Experimental design

The planned methods for this study were based on the three phases of the bioprinting process (Vijayavenkataraman *et al*., 2018; Varkey *et al*., 2019) as outlined in Figure 1-1, namely pre-processing, processing and post-processing.

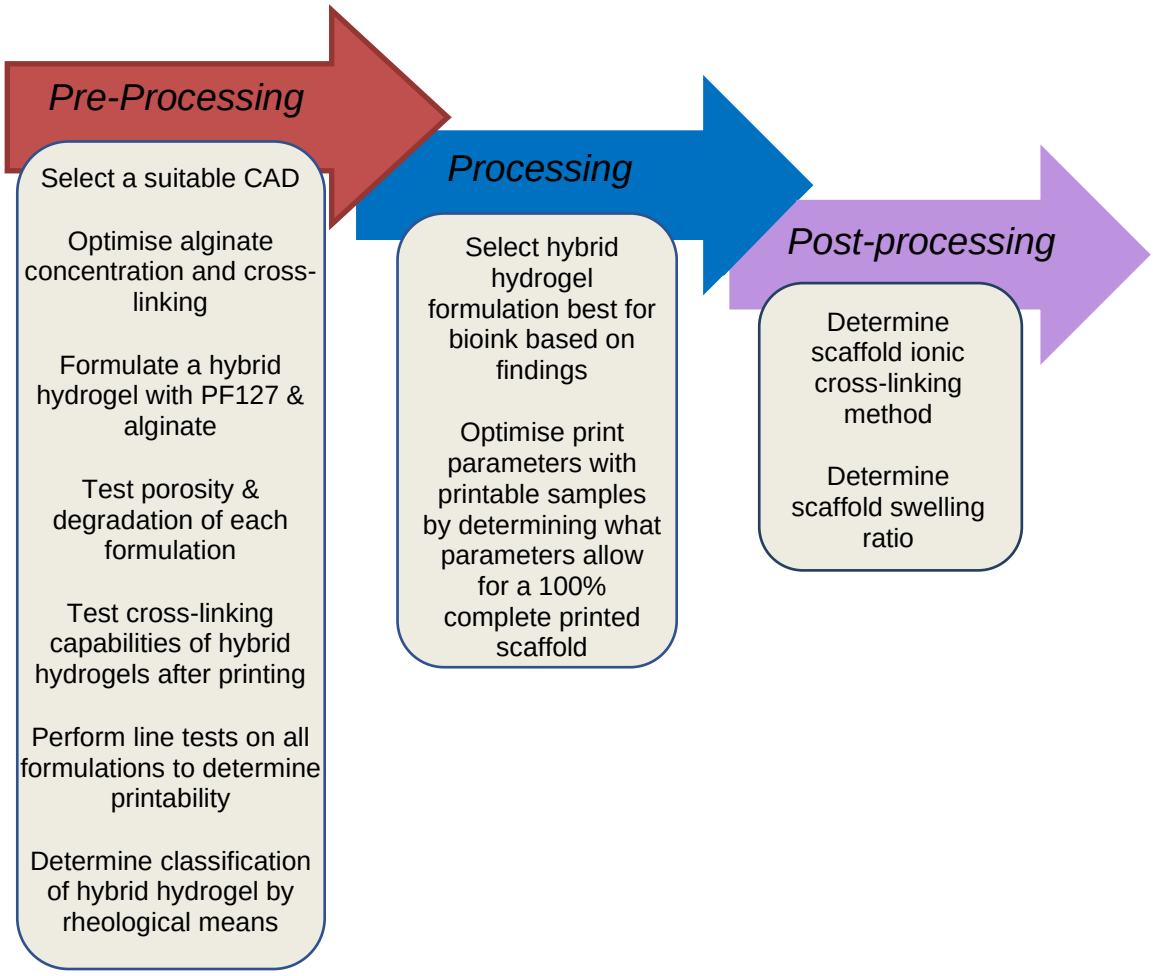

Figure 1-2: Three phase experimental design adapted from Varkey *et al*. (2019)

The first phase, known as the pre-processing phase, started with the selection of a suitable scaffold design that was created with CAD software. A scaffold design with 10mm x 10mm x 10mm dimensions was downloaded from the Bioverse website (Bioverse.co). This is the collaborative 3D bioprinting community that shares CAD designs that have already been sliced and are ready to use. The files are provided in .stl (Standard Tessellation Language or STereoLithography) format, which is the native file format of stereolithography and the standard file format in AM. This file format can be used by any 3D bioprinter, since it is a universal binary file.

Alginate was used as the basis of the hydrogel, and the optimal concentration thereof to be used within the hybrid hydrogel was determined. According to Webb and Doyle (2017), the study that this study is based on, an optimal concentration of alginate ranges between 1 and 10% (w/v), and therefore four concentrations were tested: 2, 4, 6 and 8% (w/v). Cross-linking of the alginate had

to take place and the extent of ionic cross-linking with a $CaCl_2$ cross-linking solution in various concentrations were tested to determine the most suitable concentration required to successfully cross-link alginate. These results can be found in Annexure A.

After the preliminary hydrogel formulation with alginate (A) was conducted, PF127 was introduced into the alginate solution in a 2:1 (A:PF127) ratio, respectively. A higher amount of alginate in relation to the PF127 was selected, since alginate is the biopolymer of importance. Formulations with various concentrations were formulated and characterisation studies were conducted as the properties of a hybrid hydrogel will determine whether or not it is suitable for the end-use purpose. These studies include porosity and degradation and the results can be found in Chapter 3, sections 10.4 to 10.5. The cross-linking capabilities of the various concentrations of the hybrid hydrogel formulations were tested as the scaffold underwent cross-linking during the processing and post-processing phase.

PF127 is described as being chemically inert and did not participate in the ionic cross-linking process as alginate does. However, it was determined that entanglement within the cross-linked alginate polymer chains occurred, and resulted in PF127 forming part of the end-use scaffold as described by Rarokar *et al*. (2018). Line tests were also performed during this phase that evaluated the printability of each formulation and determined how successful cross-linking of each formulation was. These results can be observed in Annexure B. From the results obtained during the pre-processing phase, an optimal hybrid hydrogel formulation was chosen to continue with to the next phase, known as the processing phase.

This chosen optimal hybrid hydrogel underwent rheological studies to determine the classification of the hybrid hydrogel according to its viscosity since a non-Newtonian bioink was required. These results can be seen in Annexure B. During the processing phase, the printing parameters were optimised with the selected hybrid hydrogel that was used as bioink. Two parameters namely, extrusion temperature and nozzle size, were kept constant while the printing speed and extrusion pressure were tested, photographed and compared within these constantly kept parameters. The CAD model was only printed between 8 to 12% completion, as this base of the scaffold already provided sufficient evidence to conclude whether the parameter was usable or not. These results can be observed in Annexure C.

The next phase, known as the post-processing phase, involved the step where the scaffold degraded and the tissue had to mature had there been cells incorporated into the bioink. Live cells can be seeded into the hydrogel during the pre-processing phase, and tissue maturation needs to occur before *in vitro* or *in vivo* usage (Bishop *et al*., 2017) during the post-processing phase. For this study, no live cells had been incorporated and therefore the only post-processing

studies included the cross-linking methods of printed scaffolds and determining the swelling ratio thereof. The swelling ratio is an important factor, because this characteristic is responsible for nutrients and waste products moving within the structure, as this is directly related to hydrogels' ability to retain large amounts of fluid (Chimene *et al*., 2020).

1.3 References

1. Barba, A.A., Lamberti, G., Rabbia, L., Grassi, M., Larobina, D. & Grassi, G. 2014. Modelling of the reticulation kinetics of alginate/pluronic blends for biomedical applications. *Materials Science and Engineering C*, 37:327–331.

2. Berg, J., Hiller, T., Kissner, M.S., Qazi, T.H., Duda, G.N., Hocke, A.C., Hippenstiel, S., Elomaa,L., Weinhart, M., Fahrenson, C. & Kurreck, J. 2018. Optimization of cell-laden bioinks for 3D bioprinting and efficient infection with influenza A virus. *Scientific Reports,* 8:13877.

3. Bishop, E.S., Mostafa, S., Pakvasa, M., Luu, H.H., Lee, M.J., Moriatis Wolf, J., Ameer, G.A., He, T.C. & Reid, R.R. 2017. 3-D bioprinting technologies in tissue engineering and regenerative medicine: Current and future trends. *Genes & Diseases*, 4(4):185–195.

4. BP, 2018. British Pharmacopoeia. In: *Alginate.*

5. Cao, D., Zhang, Y., Cui, Z., Du, Y. & Shi, Z. 2017. New strategy for design and fabrication of polymer hydrogel with tunable porosity as artificial corneal skirt. *Materials Science & Engineering C*, 70:665–672.

6. Chimene, D., Kaunas, R. & Gaharwar, A.K. 2020. Hydrogel Bioink Reinforcement for Additive Manufacturing: A Focused Review of Emerging Strategies. *Advanced Material Science*, 32:1902026.

7. Cojocaru, F., Balan, V., Popa, M.I., Lobiuc, A., Antoniac, A., Antoniac, I.V. & Verestiuc, L. 2019. Biopolymers: Calcium phosphates composites with inclusions of magnetic nanoparticles for bone tissue engineering. *International Journal of Biological Macromolecules,* 125:612–620.

8. Cui, L., Jia, J., Guo, Y., Liu, Y. & Zhu, P. 2014. Preparation and characterization of IPN hydrogels composed of chitosan and gelatin cross-linked by genipin. *Carbohydrate Polymers,* 508 99:31–38.

9. Datta, P., Barui, A., Wu, Y., Ozbolat, V., Moncal, K.K. & Ozbolat, I.T. 2018. Essential steps in bioprinting: From pre- to post-bioprinting. *Biotechnology Advances*, 36:1481–1504.

10. Derkus, B., Emregul, E., Emregul, K. & Yucesan, C. 2014. Alginate and alginate-titanium dioxide nanocomposite as electrode materials for anti-myelin basic protein immune sensing. *Sensors and Actuators,* B:294–302.

11. Emami, Z., Ehsani, M., Zandi, M. & Foudazi, R. 2018. Controlling alginate oxidation conditions for making alginate-gelatin. *Carbohydrate Polymers,* 198:509–517.

12. Feng, P., He, J., Peng, S., Gao, G., Zhao, Z., Xiong, S. & Shuai, C. 2019. Characterizations and interfacial reinforcement mechanisms of multicomponent biopolymer based scaffold. *Materials Science & Engineering C,* 100:809–825.

13. Grassi, G., Crevatin, A., Farra, R., Guarnieri, G., Pascotto, A., Rehimers, B., Lapasin, R. & Grassi, M. 2006. Rheological properties of aqueous Pluronic–alginate systems containing liposomes. *Journal of Colloid and Interface Science*, 301:282–290.

14. Herrera, C. 2019. The pre-clinical toolbox of pharmacokinetics and pharmacodynamics: *in vitro* and *ex vivo* models. *Frontiers in Pharmacology*, 10:578.

15. Hölzl, K., Lin, S., Tytgat, L., Van Vlierberghe, S., Gu, L. & Ovsianikov, A. 2016. Bioink properties before, during and after 3D bioprinting. *Biofabrication*, 8:032022.

16. International organisation for standardization (ISO). 2015. Standard Terminology for Additive Manufacturing – General Principles – Terminology. (ISO/ASTM52900).

17. Koçak, E., Yıldız, A. & Acartürk, F. 2021. Three dimensional bioprinting technology: Applications in pharmaceutical and biomedical area. *Colloids and Surfaces B: Biointerfaces*, 197:111396

18. Leberfinger, A.N., Dinda, S., Wuc, Y., Koduru, S.V. & Ozbolat, V. 2019. Bioprinting functional tissues. *Acta Biomaterialia,* 95:32–49.

19. Lee, J.M., Sing, S.L., Zhou, M. & Yeong, W.Y. 2018. 3D bioprinting processes: A perspective on classification and terminology. *International Journal of Bioprinting*, 4(2): 151.

20. Li, J., Wu, C., Chu, P.K. & Gelinsky, M. 2020. 3D printing of hydrogels: Rational design strategies and emerging biomedical applications. *Materials Science & Engineering R,* 140:100543.

21. Liu, J., Sun, L., Xu, W., Wang, Q., Yu, S. & Sun, J. 2019. Current advances and future perspectives of 3D printing natural-derived biopolymers. *Carbohydrate Polymers,* 207:297–316.

22. Ma, X., Liu, J., Zhu, W., Tang, M., Lawrence, N., Yu, C., Gou, M. & Chen, S. 2018. 3D bioprinting of functional tissue models for personalized drug screening and *in vitro* disease modelling. *Advanced Drug Delivery Reviews*, 132:235–251

23. Montalbano, G., Toumpaniari, S., Popov, A., Duan, P., Chen, J., Dalgarno, K., Scott III, W.E. & Ferreira, A.M. 2018. Synthesis of bioinspired collagen/alginate/fibrin based hydrogels for soft tissue engineering. *Materials Science & Engineering C,* 91:236–246.

24. Mironov, V., Trusk, T., Kasyanov, V., Little, S., Swaja, R. & Markwald, R. 2009. Biofabrication: a 21st century manufacturing paradigm. *Biofabrication 1*, 022001.

25. Ngo, T.D., Kashani, A., Imbalzano, G., Nguyen, K.T.Q. & Hui, D. 2018. Additive manufacturing (3D printing): A review of materials, methods, applications and challenges. *Composites Part B*, 143:172–196.

26. O'Brien, F.J. 2011. Biomaterials & scaffolds for tissue engineering. *Materials Today*, 14(3):88-95.

27. Ozbolat, I. & Hospodiuk, M. 2016. Current advances and future perspectives in extrusion-based. *Biomaterials,* 76:321–343.

28. Panwar, A. & Tan, L. 2016. Current status of bioinks for micro-extrusion-based 3D bioprinting. *Molecules,* 1:2–26.

29. Parak, A., Pradeep, P., Du Toit, L.C., Kumar, P., Choonara, Y.E. & Pillay, V. 2019. Functionalizing bioinks for 3D bioprinting applications. *Drug Discovery Today,* 24:198205.

30. Paxton, N.C., Allenby, M.C., Lewis, P.M. & Woodruff, M.A. 2019. Biomedical applications of polyethylene. *European Polymer Journal*, 118:412–428.

31. Peng, W., Datta, P., Ayan, B., Ozbola, V., Sosnoski, D. & Ozbolat, I.T. 2017. 3D bioprinting for drug discovery and development in pharmaceutics. *Acta Biomaterialia,* 57:26–46.

32. Puguan, J., Yu, X. & Kim, H. 2014. Characterization of structure, physico-chemical properties and diffusion. *Journal of Colloid and Interface Science,* 432:109–116.

33. Rarokar, N.R., Saoji, S.D. & Khedekar, P.B. 2018. Investigation of effectiveness of some extensively used polymers on thermoreversible properties of Pluronic tri-block copolymers. *Journal of Drug Delivery Science and Technology*, 44:220–230.

34. Roehm, K. 2018. Bioprinting cell laden structures with chitosan-gelatin for neural tissue applications. United States of America: New Jersey Institute of Technology (Dissertation – PhD).

35. Schwab, A., Levato, R., D'Este, M., Piluso, S., Eglin, D. & Malda, J. 2020. Printability and Shape Fidelity of Bioinks in 3D Bioprinting. *Chemical Reviews*, 120:11028–11055.

36. Suo, A., Xu, W., Wang, Y., Sun, T., Ji, L. & Qian, J. 2019. Dual-degradable and injectable hyaluronic acid hydrogel mimicking extracellular matrix for 3D culture of breast cancer MCF-7 cells. *Carbohydrate Polymers,* 211:336–348.

37. Tytgat, L., Van Damme, L., Arevalo, M.D.P.O., Declarcq, H., Thienpont, H., Otteveare, H., Blondeel, P., Dubruel, P. & Van Vlierberghe, S. 2019. Extrusion-based 3D printing of photo-cross-linkable gelatin and κ-carrageenan hydrogel blends for adipose tissue regeneration. *International Journal of Biological Macromolecules*, 140:929–938.

38. Van Kampen, K.A., Scheuring, R.G., Terpstra, M.L., Levato, R., Groll, J., Malda, J., Mota, C. & Moroni, L. 2019. Biofabrication: From additive manufacturing to bioprinting. *Elsevier.*

39. Varkey, M., Visscher, D.O., Van Zuijlen, P.P.M., Atala, A. & Yoo, J.J. 2019. Skin bioprinting: the future of burn wound reconstruction?. *Burns & Trauma.* 7(4):3.

40. Vijayavenkataraman, S., Yan, W.C., Lu, W.F., Wang, C.H. & Fuh, J.Y.H. 2018. 3D bioprinting of tissues and organs for regenerative medicine. *Advanced Drug Delivery Reviews,* 32:296–332.

41. Wang, Q.Q., Liu, Y., Zhang, C.J., Zhang, C. & Zhu, P. 2019. Alginate/gelatin blended hydrogel fibers cross-linked by Ca2+ and oxidized starch: Preparation and properties. *Materials Science & Engineering C,* 99:1469–1476.

42. Webb, B. & Doyle, B. 2017. Parameter optimization for 3D bioprinting of hydrogels. *Bioprinting*, 8:8–12.

43. Williams, D., Thayer, P., Martinez, H., Gatenholm, E., Khademhosseinic, A. & Khademhosseini, A. 2018. A perspective on the physical, mechanical and biological

specifications of bioinks and the development of functional tissues in 3D bioprinting. *Bioprinting,* 9:19–36.

44. Wu, Y., Lin, Z.Y.W., Wenger, A.C., Tam, K.C. & Tanga, X.S. 2018. 3D bioprinting of liver-mimetic construct with alginate/cellulose nanocrystal hybrid bioink. *Bioprinting,* 9:1–6.

45. Zhu, W. 2016. 3D printing of functional biomaterials for tissue modeling. San Diego, CA: University of California. (Dissertation – PhD).

CHAPTER 2: LITERATURE REVIEW

2.1 Introduction

In drug discovery and drug delivery research, there is a continuing need for valid and reliable alternatives for *in vitro* drug efficacy and toxicity testing, before the clinical trials and during the early stages of the drug discovery process, to prevent an enormous failure in the time and financial investment that the launch of a new commercial drug demands (Peng *et al.,* 2017; Herrera, 2019). In order to reduce the long lead time and high costs involved with the drug development process, pharmaceutical companies have started moving away from the traditional drug development paradigm to a “quick-win, fast-fail” alternative paradigm (Vijayavenkataraman *et al*., 2018; Peng *et al*., 2017).

To make this new paradigm work, the high rate of drugs that fail testing has to be overcome by lowering the technical uncertainties during the early stages of drug development, and this is where 3D bioprinting could play a vital role (Vijayavenkataraman *et al*., 2018). A high percentage (approximately 94%) of drugs that pass the pre-clinical trials, fail during the clinical phase and this can be ascribed to the non-availability of biomimetic 3D models. Most drug toxicity assays and tests are conducted with the traditional 2D monolayer model, which lacks the native 3D cell microenvironment (Vijayavenkataraman *et al*., 2018; Peng *et al*., 2017) leading to unpredictable or misleading effects and results (Koçak *et al*., 2021). Animal models cause ethical concerns and are at times not successful enough at imitating mechanisms of the human body. Biofabrication for tissue engineering purposes has started to reduce the use of these models resulting in an animal-free drug development system (Koçak *et al*., 2021) and consequently forms part of the alternative drug development paradigm (Vijayavenkataraman *et al*., 2018).

Biofabrication processes have opened a new field of possibilities within tissue engineering and regenerative medicine, and have many applications in the field of pharmacy. This is owing to the fact that alternative and more accurate drug testing biomimetic models are becoming available that portray more accurate results. Drug delivery systems are optimised to increase the efficacy of the active ingredients, even allowing for multiple and incompatible drugs to be formulated into a single dosage, thereby increasing patient compliance (Vijayavenkataraman *et al*., 2018; Koçak *et al*., 2021).

2.2 Tissue engineering

Due to the significantly long organ transplant waiting lists worldwide, it has become evident that the lack of viable tissue for transplant is large enough to require a solution, and therefore tissue

engineering technology was proposed in 1993 as an effective method to save lives (Koçak *et al*., 2021). By utilising the emerged technology of 3D bioprinting, the fabrication of complex and biologically tailored tissue constructs with all its native tissue architecture and cellular components, is possible and can be used to replicate *in vitro* culture environments leading to the fact that they can be used as *in vitro* biomimetic tissue models (Ma *et al*., 2018).

Extrusion-based bioprinting has shown the most promising results with regard to tissue engineering, since it provides us with the ability of scaling, and therefore human sized tissues can be produced, which is impossible using any other method of bioprinting (Vijayavenkataraman *et al*., 2018). Other bioprinting methods can lead to a severe decrease in cell viability, leading to unsuccessful tissue constructs (Roehm, 2018).

2.3 Additive manufacturing

There are various novel technologies available in tissue engineering, including a successful approach termed additive manufacturing (AM) for the direct fabrication of three-dimensional (3D) tissue constructs or scaffolds (Tytgat *et al*., 2019; Peng *et al*., 2017). AM can be described as the process of joining materials to fabricate a 3D object where the materials are usually joined together by means of a layer-by-layer method (Wu *et al*., 2018). The process was originally conceived by Charles Hull in 1986 and consists of printing successive layers of a material on top of each other to 'print' objects (Bishop *et al*., 2017; Ngo *et al*., 2018). The first AM machine was capable of curing photosensitive resins in layer-by-layer form and is known as stereolithography (SLA) (Kodama, 1981; Ngo *et al*., 2018).

Originally, these techniques were mainly used in aerospace and in the automotive industry for the production of metallic prototypes as well as by architects and designers for the production of functional prototypes due to its cost-effective prototyping capabilities (Greul *et al*., 1995; Ngo *et al*., 2018). Additive processes used to be exclusive for rapid prototyping (RP), but have grown over the past 34 years into many different technologies. RP refers to a group of technologies for fabricating a physical object from a computer-aided design (CAD) model and has been used to construct models for design verification (Levy *et al*., 2003; Jee & Sachs, 1999).

AM typically uses hard materials such as metals, plastics and resins; however, it has expanded into a variety of fields that require them to make use of soft materials, such as polymers used for food applications (Chaudhary *et al*., 2010; Moreira *et al*., 2019). There are seven different AM fabrication technologies and they include: material extrusion, powder-bed fusion, vat photopolymerisation, material jetting, binder jetting, sheet lamination and direct energy deposition (Gao *et al*., 2015).

Material jetting is the process whereby droplets of the building material are selectively deposited. Binder jetting, conversely, is the process in which a liquid bonding agent is selectively deposited to join powder materials. Inkjet printing, also known as drop-on-demand printing, is the most commonly used type of printer for biological and non-biological applications. It is used to print complex and advanced structures by delivering controlled volumes of a liquid to predefined locations, that can be applied in tissue engineering to print complex tissue scaffolds (Ngo *et al*., 2018; Murphy & Atala, 2014).

Material extrusion is an AM technology where the material is extruded through a syringe or nozzle system onto an appropriate platform to create an object (Leberfinger *et al*., 2019). The object can be any design; from a simple line to a complex organ model, which is designed by CAD (ISO, 2015). These are the technologies that directly stemmed from inkjet printing and became synonymous with 3D printing. In most literature, the term 3D printing may refer to any AM fabrication technology, but is usually limited to low-end machines (ISO, 2015).

Today, AM has numerous applications in the medical field and a wide range of biomedical materials can now be processed and have rapidly progressed in tissue engineering and regenerative medicine (Van Kampen *et al*., 2019; Zadpoor & Malda, 2017). Various AM techniques allow for the fabrication of complex geometries with high precision and are free standing, which cannot be achieved by existing assembly methods (Sano *et al*., 2018). Other advantages include flexibility in design, personal customisation and maximum material saving (Ngo *et al*., 2018).

AM processes are capable of fabricating medical instruments and prosthetics at a fraction of the price in comparison to classic methods and when utilised with the correct materials, this fabrication process is capable of producing scaffolds that are seeded with cells for tissue engineering purposes. Pharmaceutical applications for AM mostly consist of a specific field within AM known as bioprinting and they include the fabrications of complex drug delivery systems that could be utilised in all phases of drug discovery and drug testing models (Vijayavenkataraman *et al*., 2018; Zadpoor & Malda, 2017).

2.4 Three-dimensional bioprinting

3D printing is an RP process that can be defined as the stacking and assembling of organic materials with the presence of living cells, or not, and other biological inks (bioinks) in spatial patterns by using a computer-aided layer-by-layer deposition approach, creating a well-arranged 3D structure. The 3D structure can be any design, but most tissue constructs use a scaffold

architecture in a geometric pattern (grid with different pore sizes) (Datta *et al*., 2018; O'Brien, 2011; Ozbolat & Hospodiuk, 2016; Jee & Sachs, 1999).

The biofabrication process encompasses the generation of tissue constructs and organs through bioprinting, bio/self-assembly and subsequently tissue maturation (Zadpoor & Malda, 2017; Ngo *et al*., 2018). Biofabrication processing methods can be subdivided into four main groups, namely; laser-based bioprinting, droplet-based bioprinting, extrusion-based bioprinting and vat polymerisation (Vijayavenkataraman *et al*., 2018; Lee *et al*., 2018).

Table 2-1: Classification of bioprinting technologies (Vijayavenkataraman *et al*., 2018; Lee *et al*., 2018)

Bioprinting			
Laser-based bioprinting	*Droplet-based bioprinting*	*Extrusion-based bioprinting*	*Vat polymerisation*
- Laser-induced forward transfer (LIFT)	- Inkjet-based bioprinting	- Pneumatic extrusion	- Stereo-lithography (SLA)
- Direct writing	- Electrohydrodynamic jetting	- Piston-based extrusion	- Direct light projection
- Biological laser processing	- Acoustic wave jetting	- Screw-based extrusion	- Two-photon polymerisation
	- Microvalve-based bioprinting		

There are various methods, materials and equipment involved in 3D printing and it has evolved over the years, giving it the ability to transform manufacturing processes (Ngo *et al*., 2018). The three primary types of 3D bioprinting all have the capability to print scaffolds for cell seeding and to build tissue constructs by encapsulating cells within the scaffold. They include: extrusion-based, inkjet-based and light-assisted printing (Ma *et al.,* 2017). Material extrusion with biopolymers has been successfully implemented in tissue engineering, and initially this specific application was termed biofabrication, micro-fabrication or 3D bioprinting (Moroni *et al*., 2018; Yanagawa *et al*., 2016).

Patient specific and customised products in smaller quantities and at a relatively low cost have been made possible through 3D printing (Ngo *et al*., 2018; Zadpoor & Malda, 2017). The development of aqueous-based, solvent-free systems enables the direct printing of biological materials into 3D scaffolds, which, in combination with the ability to control external as well as the internal shape and architecture of the generated biological structures, allows for a positive influence on tissue engineering and integration (Murphy & Atala, 2014; Zadpoor & Malda, 2017).

Biopolymers are utilised and fabricated into hydrogels that are used as the bioink during the printing process that has the necessary characteristics, including biocompatibility, biodegradability, good degradation kinetics, safe degradation by-products and they should be able to enhance cell migration and adhesion (or tissue biomimicry) (Cojocaru *et al*., 2019; Liu *et al*., 2019). Bioinks are loaded into the printing cartridge/syringe and are extruded by means of mechanical or pneumatic forces through a nozzle, as seen in Figure 2-1 (Bishop, 2017).

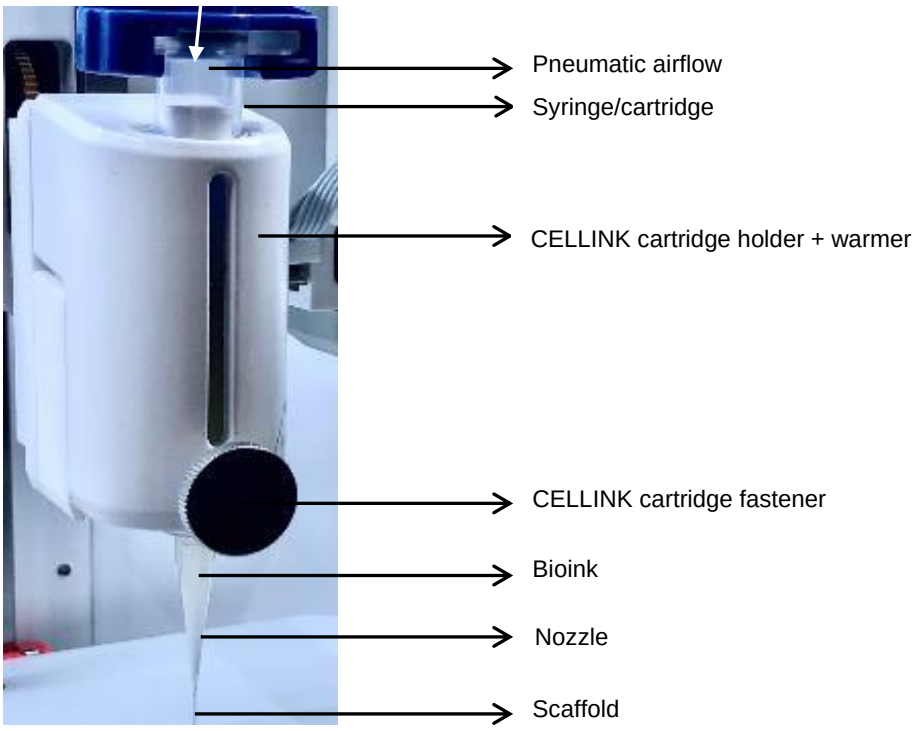

Figure 2-1: Schematic example of pneumatic extrusion based bioprinting illustrating the pneumatic printhead from Cellink® (Gothenburg, Sweden)

During mechanical extrusion, the pressure applied to the bioink to extrude it through the nozzle, cannot be changed as in the case with pneumatic extrusion. Pneumatic extrusion allows the air pressure to be optimised to reduce the shear stress as an increase in the shear rate can result in cell membrane rupture and thereby lead to cell death (Lee *et al*., 2018; Chimene *et al*., 2020). In this study, the BioX™ 3D bioprinter from Cellink® (Gothenburg, Sweden) with a HeartOS operating system, was used. The pneumatic-driven extrusion printhead as presented in Figure 2-1 was used. Both the printhead and the printbed of the bioprinter are temperature controlled which allowed for more precise temperature control when working with the bioinks.

Successful 3D bioprinting relies on two characteristics: cell viability and geometric accuracy. Both these characteristics depend on the properties of the biomaterial being used and are both influenced by the bioprinting parameters (Webb & Doyle, 2017). Bioinks are bioprintable materials that are based on natural and synthetic polymers (Parak *et al*., 2017) and are defined as cell-containing formulations that are able to be processed by biofabrication technology (Van Kampen *et al*., 2019); however, the print parameter optimisation process usually occurs in the absence of live cells. After the CAD model has been printed, tissue maturation has to transpire. It is a time-dependent process and should commence under very strict circumstances as the environment plays a distinct role in cell-cell and cell-extracellular matrix interaction (Datta *et al*., 2018).

The aim of tissue engineering is to create synthetic tissues by combining cells with scaffolds that have the relevant geometry, cues for cell growth and differentiation, enough porosity for cellular infiltration and domains for cellular binding (Roehm, 2018). Classic tissue engineering methods have several disadvantages, as they lack the ability to fabricate complex biometric structures. This leads to over-simplified tissue constructs that are inaccurate with unrealistic cell microenvironments (Vijayavenkataraman *et al*., 2018). Soft and hard tissue can be fabricated when utilising the field of bioprinting. Tissue that surrounds, connects and/or supports other organs and other tissues in the body are classified as soft tissue, whereas bones and teeth are classified as hard tissue. Hard tissue has its place in the tissue engineering field, especially with regard to dentistry (Fuchs *et al*., 2019); however, this study focused on parameter optimisation for scaffolds that could possibly be used as alternative drug testing models and soft tissue is more often used and therefore more relevant.

3D bioprinting allows cell-cell and cell-extracellular matrix interaction, whereas this is absent in 2D tissue constructs. (Wu *et al*., 2018). A recent study proved that breast cancer cells from a hydrogel culture portrayed higher invasion/migration abilities than that of a 2D culture (Suo *et al*., 2019); therefore, cell-laden hydrogels open a wide range of research possibilities and therapeutic models. Pharmaceutical applications include inexpensive, tailor-made drug delivery systems to improve patient compliance as well as providing multiple dosages or containing various incompatible combinations of active ingredients within a single dose. Cancer tumour models can be fabricated that mimic the complex tumour ECM, this allows for the study of tumour mechanisms and metastasis for accurate personalised anti-cancer drug screening and personalised treatment (Vijayavenkataraman *et al*., 2018; Koçak *et al*., 2021).

2.5 Hydrogels and bioinks

Hydrogels are 3D networks of polymer chains containing hydrophilic groups capable of absorbing large quantities of water (Rashid *et al*., 2019; Gyles *et al*., 2017). The biomedical application of

hydrogels' initial concern was over the limitations to operate within physiological conditions and the toxicity of their cross-linking agents. However, advances in physiology and increased research on the chemistry of hydrogel cross-linking have led to more biocompatible and innovative scientific designs that overcome these problems (Gyles *et al*., 2017).

3D bioprinting of living cells requires a stringent set of conditions that are best met by hydrogels and subsequently they are used as the basis of almost all bioink formulations. They can absorb their dry weight in water numerous times and usually consists of 70 to 99% water, making them highly porous and permeable. The less stringent the biocompatibility requirements are, the wider the range of materials that can be used to meet the requirements for successful biofabrication (Zadpoor & Malda, 2017). While most hydrogels are suited for cell growth, they lack the mechanical properties required to sustain a subsequently printed layer. This can be resolved through the addition of another biopolymer or by means of cross-linking (Chimene *et al*., 2020).

Bioink properties can be improved through mixing it with hydrogels that have the required, distinct characteristics (Berg *et al*., 2018). Owing to their good biocompatibility and high water content, they demonstrate a similar structure to the ECM and have the ability to mimic tissue environments (Wang *et al*., 2018; Yap & Yang, 2016). The hydrogels/bioinks used in the process of scaffold printing and its degradation products should be biocompatible to avoid an immune response in patients receiving 3D printed tissue constructs (Kuo & Ma, 2001). The characteristics of a bioink should both meet the requirements for bioprinting as well as ensuring cell survival within the construct (Hölzl *et al*., 2016).

The viscosity of hydrogels to be used as bioinks should be characterised as a non-Newtonian fluid. Non-Newtonian fluids display a decrease in viscosity as the shear stress increases. The shear stress is related to the nozzle size as well as the air pressure applied to extrude the bioink. The smaller the nozzle and the higher the air pressure applied, the higher the shear stress will be. A high shear stress can have a negative effect on live cells as it can cause ruptures in the cell membrane, ultimately resulting in cell death. However, decreasing the viscosity of the hydrogel during extrusion will result in a more positive outcome on cell viability (Chimene *et al*., 2020; Webb & Doyle, 2017). Alginate hydrogels have shown the most promising results in the delivery systems of bioactive agents and tissue engineering technologies, as they retain some similarities in structural components to the ECM of soft tissue (Lee & Mooney, 2017).

2.6 Cross-linking

Many formulated bioinks are adapted from low viscosity hydrogels through modulation such as adding thickeners or by partial cross-linking (Williams *et al*., 2018). Cross-linking can be

physical/ionic or chemical. Physical/ionic cross-linking involves cross-linking of the physical polymer chains with each other. This is achieved through the metal ion reacting with the carboxyl group by means of hydrophobic association, hydrogen bonding, crystallisation, entanglement etc. (Hu *et al*., 2018). Chemical cross-linking can be described as when a covalent bond is formed between the added chemical cross-linking agent and the hydrogel, causing the gel to be more rigid. Cross-linking causes irreversible bonds to form between the polymer chains and or cross-linking solution that can be broken by changing the physical conditions or by applying stress (Gyles *et al*., 2017). Chemical cross-linking could possibly have a negative effect on cell proliferation as the chemicals can be harsh on developing cells and therefore physical or ionic cross-linking was selected as the cross-linking method for this study.

Only low-viscosity bioinks can be 3D printed and consequently an additional cross-linking step is required after the scaffold has been printed to secure the structure and therefore its integrity (Vijayavenkataraman *et al*., 2018). This setback can also be resolved by adding viscous synthetic polymers such as poly(ethylene gly-col) (PEG), poly(propyl fumarate) (PPF) and poloxamers; or by mixing it with other naturally-derived bioinks including alginate, chitosan derivatives, silk, hyaluronic acid and fibrin (Panwar & Tan, 2016; Yap & Yang, 2016).

Ionically cross-linking alginate is most frequently conducted with $CaCl_2$. However, this cross-linker typically leads to rapid and non-uniform gelation that can be resolved with the addition of a buffer. The phosphate group in phosphate buffered saline (PBS) competes with the carboxylate groups of alginate that react with the calcium ions to form polymer chains, which is the result of cross-linking (Lee & Mooney, 2012; Chimene *et al.,* 2020), and therefore the addition of PBS aided to better control the gelation of alginate in the presence of $CaCl_2$.

2.7 3D bioprinting of bioink

The bioprinting process of hydrogels occurred in three phases (Varkey *et al*., 2019; Vijayavenkataraman *et al*., 2018). The first phase is the pre-processing phase where the scaffold designed with CAD software had to be selected and the hybrid hydrogel had to be formulated and optimised to meet the stringent criteria for successful bioprinting. This criteria included sufficient viscosity, good degradation rates and permeability as the nutrients imperative for the survival of living cells, as well as the removal of waste products, have to be able to transfer within the structure (Roehm, 2018). The hybrid hydrogel had to undergo a set of tests to determine its biocompatibility with the biofabrication process utilised, which, in the case for this study, is pneumatic extrusion.

Following was the processing phase where the actual hybrid hydrogel scaffold was manufactured layer-by-layer. During the processing phase, the hybrid hydrogel that was formulated and optimised in the previous phase, was used as the bioink on which the printing parameters should be optimised. When printing with hydrogels, considerable effort is required to determine the optimal printing parameters to ensure successful printing. These parameters include nozzle diameter, printing time, speed and temperature and dispensing pressure. The printing parameters are often optimised and established in the absence of cells in the bioink. In the event that an oversized nozzle is used, it could lead to less accurate scaffold printing and the bioink can start to flow out the nozzle before the printing process has started, since low viscosity hydrogels are used as bioinks for 3D bioprinting.

If a nozzle size is used that is too small, it could lead to an increased extrusion pressure requirement that increases the shear stress and ultimately has a negative effect on cell proliferation. Non-Newtonian hydrogels display a decrease in viscosity when the bioink is extruded through the nozzle, which results in a low shear stress rate that has a positive effect on cell proliferation. These parameters also directly influence cell viability, since the parameters determine the shear forces within the bioinks when printing (Webb & Doyle, 2017; Roehm, 2018).

If the parameters are not optimised, it can lead to structures with a printed compromised infill grid that will result in an inaccurately printed final structure, if it even allows for the structure to be printed to 100% completion. The post-processing phase involved the steps where the hybrid hydrogel had to degrade and in the event that cells were added, tissue maturation had to occur before *in vitro* or *in vivo* usage (Bishop *et al*., 2017). The only post-processing tests conducted included the cross-linking method of the printed scaffolds and determining the swelling ratio thereof since no live cells were incorporated.

From Figure 2-2, a compromised printed infill grid can be observed. Continuing to extrude the bioink on top of these unsuccessful layers will lead to a structure with unknown levels of structural integrity. During this study, a self-collapsing effect was observed (Figure 3-12A) whenever the parameters weren't optimal. This effect could possibly be attributed to the properties of the biomaterials within the hydrogel as they also play a vital role in successful 3D bioprinting (Gyles *et al*., 2017; Li *et al*., 2020).

Figure 2-2: Four-layer printed grid scaffold using a sacrificial polypropylene oxide gel, Cellink® Start, top and side view of preselected CAD model, without optimised parameters

It is also important to note that when working with live cells, a sterile environment is required to prohibit any other growth than the cells incorporated into the bioink. The BioX™ printer used in this study is equipped with a closed chamber printing system and a UV sterilisation chamber that allows for a sterile printing environment.

2.8 Biomaterials

A wide range of materials can be used for 3D printing and they include metals, concrete, ceramics and polymers. Polymers are considered the most common material used in 3D printing since they are significantly diverse and can easily adopt different printing techniques and processes (Ngo *et al*., 2018). The primary polymers used during 3D printing are polylactide (PLA), which is a polyester derived from lactic acid and acrylonitrile butadiene styrene (ABS) (Basu *et al*., 2016; Ngo *et al*., 2018), or soft biopolymers including gelatine and alginate (Bilal & Iqbal, 2019). Biopolymers are polymers that are found in living organisms, for instance cellulose or proteins. They can be divided into two groups, namely plastic/hard biopolymers that are hard and tough and soft/gel biopolymers that are soft and weak (Li *et al*., 2020).

Plastic biopolymers are not flexible but have a longer biodegradable time, as some of them are used in food packaging where biodegradability should only start to occur after a predetermined time (Chaudhary *et al*., 2010). Gel biopolymers, conversely, are soft and flexible and have been successfully used in the past to manipulate and sustain a predetermined scaffold (Feng *et al*., 2019). The biodegradation process of gel biopolymers is faster, and therefore, the scaffold should be able to break down within a few days (Roehm, 2018).

The biomaterials will determine whether the hydrogel will be characterised as a natural, synthetic or a hybrid hydrogel. Natural hydrogels are those that are made of biomaterials that are of natural origin, such as alginate and gelatine, where, on the other hand, synthetic biomaterials such Pluronic F-127 (PF127) are used for synthetic and hybrid hydrogels and are synthesised from polymers such as PEG (Gyles *et al*., 2017). In this study, a hybrid hydrogel was formulated using alginate and PF127.

Multi-material inks/hybrid hydrogels have slowly been replacing natural hydrogels as they provide a higher gel strength and water absorption capacity, and therefore, they have been widely explored for solutions to the shortcomings of single component gels (Gyles *et al*., 2017; Li *et al*., 2020). When engineering soft tissue, other biomaterials are often used in comparison to the fabrication of hard tissue. Hard tissue and soft tissue cells react differently within scaffolds as they need to undergo different cell maturation processes to obtain the final tissue construct (Verrier *et al*., 2004) which consequently concludes that they require a different set of stringent requirements and subsequently require different hydrogels made from other biomaterials.

2.8.1 Alginate

Alginate is a naturally occurring, anionic polymer derived from the cell walls of various species of brown algae (Emami *et al*., 2018; Puguan *et al*., 2014; Lee & Mooney, 2012). It is a polysaccharide consisting of a linear chain of β-D-mannuronic acid and α-L-guluronic acid (Puguan *et al*., 2014). Alginate owns a few unique properties, i.e. hydrophobicity, non-toxicity, biocompatibility as well as chelating ability (Derkus *et al*., 2014) and has a molecular weight of approximately 216g/mol and density of 1,6g/cm^3. Sodium alginate (Figure 2-3) is the salt form of the alginate as this is how alginate is processed to a powder, consisting of the sodium salt of alginic acid that is a mixture of polyuronic acids and it is slowly soluble in water, forming a viscous, colloidal solution (BP, 2018).

Sodium alginate is usually a powder form that is a light yellow-greenish colour that can be reconstituted into any concentration desired, having a greenish-brown, semi-translucent appearance after being dissolved and is derived from alginic acid that has a molecular weight of 398.32 g/mol and a density of 1.6g/cm^3. A combination of both these structures is present in the powder form. Alginate also has other salt forms, such as calcium and magnesium; however, the only form that is soluble in water and that results in a gel that can be cross-linked with a calcium salt aqueous solution after reconstitution, is sodium alginate. It has a sodium atom attached to the alginate structure as seen in Figure 2-3. For these reasons, sodium alginate was used in this study.

Sodium alginate has a pH of around 3 to 3.5 and becomes more viscous as the pH increases as the carboxylate backbone group of the alginate becomes more pronated and causes hydrogen bonds to form, resulting in polymer chains being tighter together, resulting in a higher viscosity (Lee & Mooney, 2012). The free aldehyde groups on the oxidised sodium alginate can react with amine groups to form a chemical hydrogel that has a wide variety of uses in fields such drug delivery, wound healing, and tissue and bone engineering (Emami *et al*., 2018). The carboxylate group discussed earlier is responsible for the ionic cross-linking process it undergoes when exposed to a $CaCl_2$ solution and can be observed in Figure 2-3, on the top left of the chemical structure. This group consists of a carbon atom that is double bonded to an oxygen atom. The alginate is dissolved in PBS since the phosphate group competes with this carboxylate group resulting in a slower and more controlled form of cross-linking (lee & Mooney, 2012).

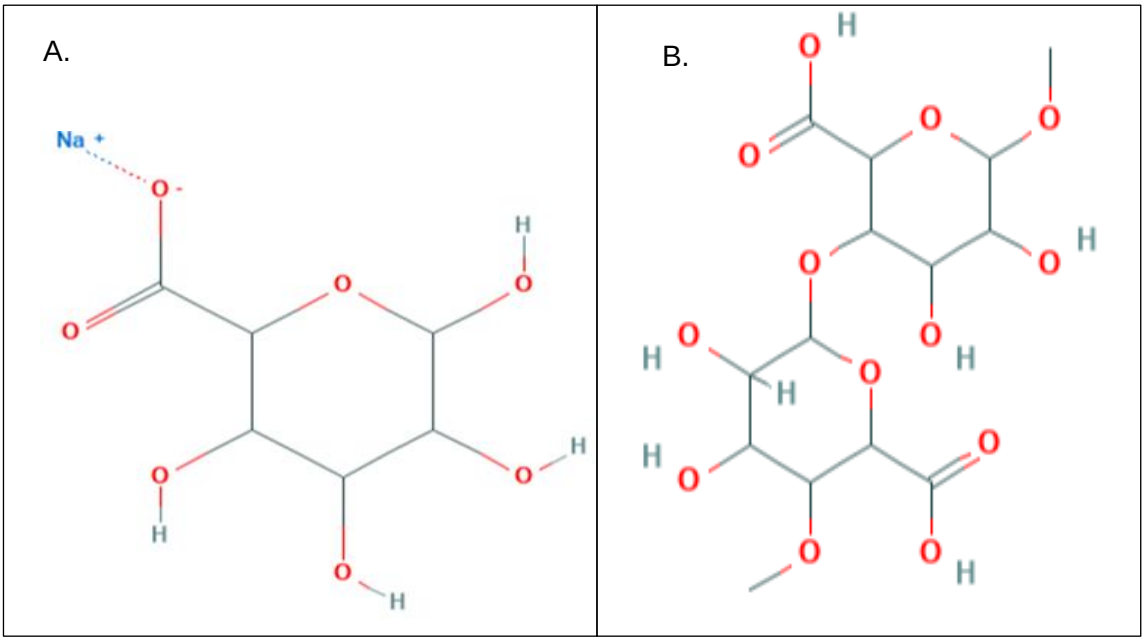

Figure 2-3: **A) Sodium alginate chemical structure with the linear formula of $C_6H_9NaO_7$ and B) alginic acid chemical structure with the molecular formula of $C_{12}H_{22}O_{13}$**

Although alginate provides desirable biocompatibility and mechanical stability, it lacks biomimetic properties since it does not provide cellular adhesion motifs. This is due to the lack of essential protein components (Berg *et al*., 2018). Combining the alginate with high molecular weight polymers has been implemented to increase the resolution of alginate printing (Panwar & Tan, 2016).

2.8.2 Pluronic F-127

PF127 is a non-ionic copolymer surfactant with a hydrophilic-lipophilic balance (HLB) of 18 to 23. PF127 gelling systems undergo sol-gel transition and fall into the category of a nontoxic, synthetic, poly(oxyethylene-oxypropylene) (PPO), water soluble, biodegradable poloxamer that displays reverse thermo-responsive properties in aqueous solutions that have various applications in gelling systems (Grassi *et al*., 2006; Rarokar *et al*., 2018). The US FDA guidelines have declared PF127 as a safe, inactive, low toxic, biodegradable ingredient that may be used in certain preparations because of its chemical inertness (Rarokar *et al*., 2018). It is also known as Poloxamer 407.

PF127 is a free-flowing liquid when kept at 4ºC, with an approximate molecular weight of 12600g/mol and a mannuronic to guluronic acid (M/G) ratio of 1.56, which undergoes thermo-reversible gelation above lower critical solution temperatures and should be prepared using the 'cold method' (Choi *et al*., 1999). It behaves as a low viscosity solution below its sol-gel transition point, which is dependent on the temperature as well as the concentration PF127 present, while it forms cubic liquid crystalline structures at higher temperatures, i.e. above its sol-gel transition point (Grassi *et al*., 2006).

This poloxamer consists of hydrophilic polyethylene oxide (PEO) and hydrophobic PPO blocks; it loses the solubility of the PPO blocks, leading to micelle formation and therefore the liquid transforms into a gel (Rarokar *et al*., 2018; Yap & Yang, 2016). The PF127 chemical structure displays a CH_2CH_2O group that is repeated 100 times. Following, is a CH_2CHCH_3O group that is repeated 65 times, while the last CH_2CH_2O is repeated 100 times. It therefore consists of PPO blocks with two 99-unit hydrophilic PEO blocks.

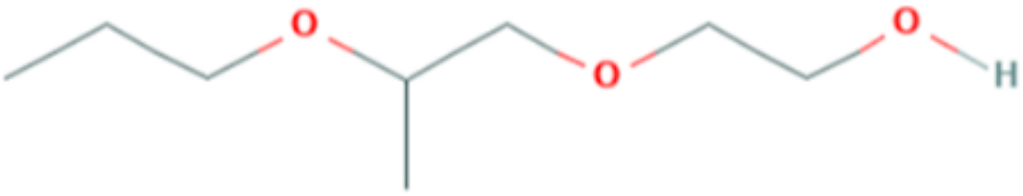

Figure 2-4: Pluronic 127 chemical structure with the linear formula of $(C_3H_6O{\cdot}C_2H_4O)x$

Concentrations of 30% (w/v) and above have shown to start gelation at 25ºC, while concentrations lower than 20% (w/v) only start gelation at 35ºC and higher. This concludes that the sol-gel

transition temperature of PF127 is strongly concentration dependent (Khalil *et al.,* 2006; Wei, *et al*., 2002) and for this study higher concentrations (40–50% w/v) were used to ensure its sol-gel transition temperature is reached below 37ºC.

2.9 Characterisation of hybrid hydrogel

Hydrogels can be formulated in a number of ways and the polymeric structure can be designed with tailored properties according to the intended application. It is important to align the characterisation of the hydrogel with the formulation, but also with the intended application in mind (Ahmed, 2015). There are various standardised and non-standardised methods to characterise hydrogels. Since this was not the primary aim of this study, only characterisation methods relevant to 3D bioprinting were considered, including porosity, degradation or stability, viscosity and swelling ratio. The ideal hybrid hydrogel considered, needed to have the following functional features:

- Suitable rate of absorption, described as porosity, for 3D bioprinting;
- High absorption capacity in phosphate buffered saline (PBS);
- Suitable viscosity, with non-Newtonian characteristics; and
- High durability and stability in the swelling environment and during storage (Ahmed, 2015).

2.9.1 Porosity

High porosity in scaffolds is essential for tissue engineering since this property contributes to all nutrients and waste products to be removed from within the construct (Calejo *et al*., 2018). Moreover, a uniform structure with an interconnected and highly porous network will facilitate diffusion of nutrients to the cells incorporated (Kuo, 2002). Hydrogels consist mostly of water, rendering them easy to permeate and therefore very porous compounds (Roehm, 2018).

It was consequently important to study the porosity abilities of the cross-linked hydrogel as this is directly related to the ability of hydrogels to retain large amounts of fluid and its ability to move nutrients and waste products in the scaffold (Rashid *et al*., 2019; Gyles *et al*., 2017). Normally, the surface morphology can be inspected with the naked eye and the porosity can be calculated with a formula described by Cao *et al*., (2017). Porosity tests were conducted and calculated according to the Archimedes principle described by Cao *et al*., (2017), where the porosity for eight respective hydrogels was calculated using the following formula:

$$\%\text{Porosity} = 100(m_2 - m_1)/(m_2 - m_3) \quad [1]$$

Where m_1 is the mass of dry hybrid hydrogel, m_2 is the mass of the swollen hybrid hydrogel and m_3 is the mass of swollen hybrid hydrogel suspended in water.

2.9.2 Degradation/stability

Alginate hydrogels follow a degradation process that involves the loss of divalent ions into surrounding media (Li *et al*., 2020). Since alginate scaffolds are not aimed at being permanent, degradation should occur uniformly, under physiological conditions and should produce non-toxic degradation products as the tissue develops and starts to occupy a larger volume (Kuo, 2002; Liu *et al*., 2019). The scaffold should therefore degrade and be replaced by the ECM of the cells (Roehm, 2018). An enzymatic degradation of alginate has been proposed in a study conducted by Kuo (2002) to test the stability and degradation of alginate; however, this method was not used for this study as the focus was on printing parameter optimisation.

The hydrolytic degradation was measured by using an adaptation from the method described by Montalbano *et al*. (2018) by creating hybrid hydrogel discs in well-plates from the six different hybrid hydrogel formulations. These discs had to be incubated at 37ºC inside dH_2O where the discs were subsequently weighed at predetermined time intervals. The culture media was changed every time a weight measurement was taken after removing any excess water with a paper towel (Montalbano *et al*., 2018).

2.9.3 Characterisation of swelling ratio

The swelling ratio of the hybrid hydrogels is an important factor to consider when used in drug release studies and in scaffolds used for tissue engineering, as this provides us with additional insight into the hydrogels' aqueous stability. Swelling of the hydrogels can usually be seen by with naked eye as they grow in structure when absorbing substances from outside the hydrogel and are based on the Van der Waal forces on hydrogen (H) bonds between the water and the hydrogel (Mazi & Surmelihindi, 2021; Cui *et al*., 2014; Wang *et al*., 2019; Mulakkal *et al*., 2018).

The swelling capabilities of a scaffold can be influenced by a number of factors, including: temperature, degree of bioink cross-linking and the pH of the swelling medium, while temperature and swelling medium pH have more pronounced effects. An increase in the swelling capabilities of a hydrogel at higher temperatures can be referred to as positive temperature-sensitive hydrogels, whereas hydrogels that can be affected by the pH are referred to as pH-sensitive hydrogels. Hydrogels that are sensitive to pH changes have many applications in drug delivery and in the medical field due to their good biocompatibility (Mazi & Surmelihindi, 2021). The 3D printed scaffolds therefore had to be evaluated for their swelling ratio in different swelling mediums at different temperatures. As we know, $CaCl_2$ lowers the pH of dH_2O as the calcium hydrolyses

in the water resulting in free hydrogen ions. This will subsequently be added to the swelling medium to determine its swelling capabilities in an altered pH.

2.9.4 Viscosity

Rheology can be defined as the study of flow and deformation of materials. Li *et al*. (2020) describes viscosity as the resistance of a fluid to flow under an applied stress and is predominantly determined by its concentration and molecular weight. A hydrogel used in 3D bioprinting needs to possess a sufficient viscosity for the scaffold to be able to maintain its structure during and post printing. Profiling the viscosity of a gel can contribute to recognising and regulating how a gel product will perform when it is used (Abouhussein *et al*., 2018). Deformation (strain) and flow (strain rate) indicate the distance a sample moves by means of an external force/stress. The equations utilised for viscosity is described as follows:

$$viscosity = \frac{Stress}{Strain\ rate} \qquad [2]$$

The viscosity of the hybrid hydrogel chosen to continue printing parameter optimisation studies with, was measured using the ARES-G2 Rheometer that can be described as a rotational rheometer equipped with a 40mm steel cone plate with a 2º angle. A sample was placed on top of the bottom plate and the top cone plate was closed over it, creating a 30µm truncation gap. The bottom plate remained still while the top cone plate oscillated. This increased the shear stress, and the viscosity is consequently measured at varying shear rates (Li *et al*., 2020).

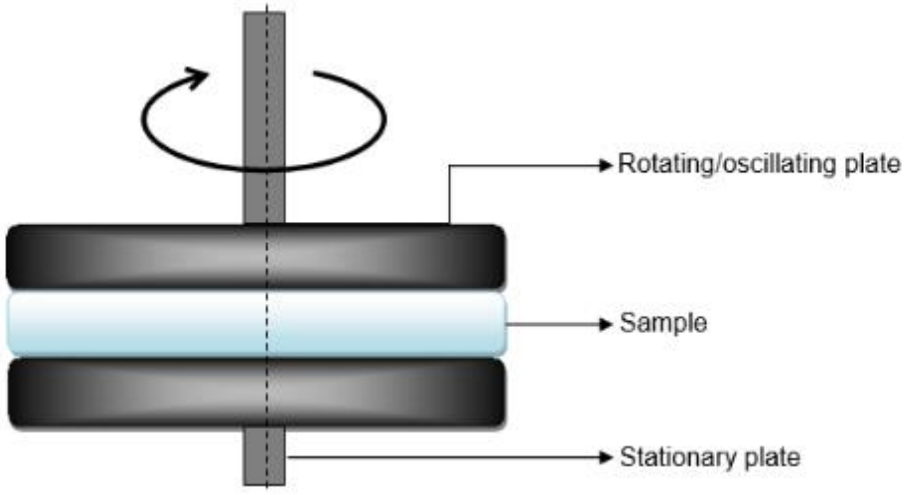

Figure 2-5: Schematic example of a rotation rheometer

Viscosity and other rheological behaviours are properties that determine a substance's processability and end-use performance. Most bioinks used in extrusion-based bioprinting are regarded as non-Newtonian fluids, which denotes that the gel's apparent viscosity depends on the shear stress. As the shear rate increases, the apparent viscosity decreases due to large polymer chains being reoriented and a disruption of the electrostatic interactions (Chimene *et al*., 2020). This characteristic contributes a positive result in cell viability post printing as an increase in the shear stress can result in cell membrane ruptures that subsequently leads to cell death (Roehm, 2018; Vijayavenkataraman *et al*., 2018). The hydrogel was consequently evaluated to ensure that it fell into the non-Newtonian fluid class.

2.10 Printability of bioink

The printability of the bioink/hydrogel should present with structural precision and accuracy post printing. It should withstand forces during the printing process and should possess characteristics that render the bioink printable. Furthermore, the bioink should be biocompatible, presenting a high cell viability post printing, be porous enough to allow nutritional transport and encourage cell adhesion and growth (Parak *et al*., 2019).

2.10.1 Line test

The printability of each formulation was determined using an adaptation of the single fibre extrusion/line test, as described by Trachtenberg *et al*. (2016). This method enabled optimisation of the hybrid hydrogel bioink formulation and extrusion with the bioprinter before the 10mm x 10mm x 10mm scaffold was printed. A single square (line) of 10mm in length and diameter was printed without the grid infill pattern that was used during the scaffold printing process. Line width measurements were taken as described in Figure 3-1 in Chapter 3, and the method is described in Chapter 3 section 4.1. These measurements were compared to determine the printability of the hybrid hydrogel as well as its cross-linking capabilities.

The print parameters, including the nozzle temperature and size, printing time, speed and dispensing pressure, were kept constant. A single nozzle size of 250µm (inner diameter) or 25G was used at a temperature of 35ºC with a single print speed of 10 mm/s and an extrusion pressure of 30kPa for the line tests performed for each of the six hybrid hydrogel formulations. Each line length and diameter was measured using digital callipers (Grip, 0-150mm). Photographs were taken after each line test with an iPhone 8 Plus equipped with a 12-megapixel wide-angle and telephoto lens. Image dimensions were employed to establish a scale in order to quantify line length and diameter. This method is explained in Chapter 3 section 4.1 and Annexure B.

2.11 Print parameter optimisation

When compared to conventional manufacturing processes, AM systems require more interaction between the parameters and the materials used and therefore necessitate more controllable parameters (Gao *et al*., 2015). Printing with materials such as hybrid hydrogels, the delicate balance between the parameters affects the printing results and consequently the influence of each parameter should be fully understood (Webb & Doyle, 2017). Complex structures are able to be fabricated through bioprinting processes and for these structures to show accurate results in geometry, the printing parameters need to be optimal to ensure a successful construct is printed (Tytgat *et al*., 2019; Peng *et al*., 2017; Vijayavenkataraman *et al*., 2018). Webb and Doyle (2017) made use of a POI to standardise the optimisation process; however, this was not the only method used to determine the optimal printing parameters during this study. A new grading method was implemented that allowed the scaffolds to be compared within predetermined groups even though they had varying parameters used to fabricate them. This grading method is thoroughly explained in Chapter 3 section 4 and 5. The visual appearance and observance of the scaffold bases printed and used for line width and corner drag measurements, as described in Chapter 3 section 4 and 5, were taken into consideration in combination with the grading methods.

2.11.1 Parameter optimisation index

To standardise the printing parameter optimisation process, the POI method was introduced as this describes the relationship between the variables. The printing accuracy is directly related to the geometry of the printed line, while the shear stress relationships are associated with the fluid mechanics of extruding a hybrid hydrogel through a thin nozzle. From fluid mechanics, we know that shear stress in fluids flowing through straight cylinders is dependent on the pressure applied to extrude it through a nozzle. The higher the pressure, the higher the shear rate leading to a decrease in viscosity, while an increase in the nozzle diameter reduces the velocity and therefore the shear stress (Webb & Doyle, 2017; Lewicki *et al*., 2019; Chimene *et al*., 2020).

The POI can consequently be calculated using the following two equations:

$$POI = \frac{1}{t_{line} \cdot D_G \cdot p} \quad [3]$$

$$POI_i = \frac{POI_i}{POI_{MAX,n}} \quad [4]$$

Where t_{line} = printed line width, D_G = needle gauge, p = extrusion pressure, POI_i = POI for an individual set of parameter, POI_{MAX} = maximum POI of the range tested and n = total number

of parameter combinations. The POI_i can assume values between 0 (worst) and 1 (best) (Webb & Doyle, 2017; Lewicki *et al*., 2019).

2.12 References

1. Ahmed, E.M. 2015. Hydrogel: Preparation, characterization, and applications: A review. *Journal of Advanced Research*, 6:105–121.

2. Abouhussein, D.M.N., Khattab, A., Bayoumi, N.A., Mahmoud, A.F. & Sakr, T.M. 2018. Brain targeted rivastigmine mucoadhesive thermosensitive *In situ* gel: Optimization, *in vitro* evaluation, radiolabeling, *in vivo* pharmacokinetics and biodistribution. *Journal of Drug Delivery Science and Technology,* 43:129–140.

3. Basu, A., Langer, R. & Domb, A. 2016. Special issue: Polylactide (PLA) based biopolymers. *Advanced Drug Delivery Reviews,* 107:1–2.

4. Berg, J., Hiller, T., Kissner, M.S., Qazi, T.H., Duda, G.N., Hocke, A.C., Hippenstiel, S., Elomaa, L., Weinhart, M., Fahrenson, C. & Kurreck. J. 2018. Optimization of cell-laden bioinks for 3D bioprinting and efficient infection with influenza A virus. *Scientific Reports,* 8:13877.

5. Bilal, M. & Iqbal, H. 2019. Naturally-derived biopolymers: Potential platforms for enzyme 491 immobilization. *International Journal of Biological Macromolecules,* 130:462–482.

6. Bishop, E.S., Mostafa, S., Pakvasa, M., Luu, H.H., Lee, M.J., Moriatis Wolf, J., Ameer, G.A., He, T.C. & Reid, R.R. 2017. 3-D bioprinting technologies in tissue engineering and regenerative medicine*:* Current and future trends*. Genes & Diseases*, 4(4):185–195.

7. BP, 2018. British Pharmacopoeia. In: *Alginate.*

8. Calejo, M.T., Ilmarinen, T., Skottman, H. & Kellomäki, M. 2018. Breath figures in tissue engineering and drug delivery: State-of-the-art and future perspectives. *Acta Biomaterialia*, 66:44–66.

9. Cao, D., Zhang, Y., Cui, Z., Du, Y. & Shi, Z. 2017. New strategy for design and fabrication of polymer hydrogel with tunable porosity as artificial corneal skirt. *Materials Science & Engineering C*, 70:665–672.

10. Chaudhary, D., Dong, Y. & Kar, K. 2010. Hydrophilic plasticized biopolymers: Morphological influence on physical properties. *Materials Letters,* 64:872–875.

11. Chimene, D., Kaunas, R. & Gaharwar, A.K. 2020. Hydrogel Bioink Reinforcement for Additive Manufacturing: A Focused Review of Emerging Strategies. *Advanced Material Science*, 32:1902026.

12. Choi, H.G., Lee, M.K., Kim, M.N. 1999. Oxidation Behavior of Hot-pressed Si_3N_4 with Re_2O_3 (Re=Y, Yb, Er, La). *Journal of the European Ceramic Society*, 19:2757–2762.

13. Cojocaru, F., Balan, V., Popa, M.I., Lobiuc, A., Antoniac, A., Antoniac, I.V. & Verestiuc, L. 2019. Biopolymers – Calcium phosphates composites with inclusions of magnetic nanoparticles for bone tissue engineering. *International Journal of Biological Macromolecules,* 125:612–620.

14. Cui, L., Jia, J., Guo, Y., Liu, Y. & Zhu, P. 2014. Preparation and characterization of IPN hydrogels composed of chitosan and gelatin cross-linked by genipin. *Carbohydrate Polymers,* 508(99):31–38.

15. Datta, P., Barui, A., Wu, Y., Ozbolat, V., Moncal, K.K. & Ozbolat, I.T. 2018. Essential steps in bioprinting: From pre- to post-bioprinting. Biotechnology Advances, 36:1481–1504.

16. Derkus, B., Emregul, E., Emregul, K. & Yucesan, C. 2014. Alginate and alginate-titanium dioxide nanocomposite as electrode materials for anti-myelin basic protein immune sensing. *Sensors and Actuators,* B:294–302.

17. Emami, Z., Ehsani M., Zandi, M. & Foudazi, R. 2018. Controlling alginate oxidation conditions for making alginate-gelatin. *Carbohydrate Polymers,* 198:509–517.

18. Feng, P., He, J., Peng, S., Gao, G., Zhao, Z., Xiong, S. & Shuai, C. 2019. Characterizations and interfacial reinforcement mechanisms of multicomponent biopolymer based scaffold. *Materials Science & Engineering C,* 100:809–825.

19. Fuchs, A., Youssef, A., Seher, A., Hartmann, S., Brands, R.C., Müller-Richter, U.D.A., Kübler, A.C. & Linz, C. 2019. A new multilayered membrane for tissue engineering of oral hard- and soft tissue by means of melt electrospinning writing and film casting – An in vitro study. *Journal of Cranio-Maxillo-Facial Surgery*, 47:695–703.

20. Hu, C., An, R., Han, L., Wang, X., Shi, Y. & Ran, R. 2018. Preparation of high strength double physically cross-linked hydrogels by immersion method—How to avoid uneven soaking. *Colloids and Surfaces A,* 559:74–82.

21. Koçak, E., Yıldız, A. & Acartürk, F. 2021. Three dimensional bioprinting technology: Applications in pharmaceutical and biomedical area. *Colloids and Surfaces B: Biointerfaces*, 197:111396.

22. Kodama, H. 1981. Automatic method for fabricating a three-dimensional plastic model with photo-hardening polymer. *Review of Scientific Instruments,* 52:1770–1773.

23. Kuo, C.K. 2002. Ionically cross-linked alginate hydrogels as scaffolds for tissue engineering. United States of America: The University of Michigan (Thesis – PhD).

24. Kuo, C.K. & Ma, P.X. 2001. Ionically cross-linked alginate hydrogels as scaffolds for tissue engineering: Part 1. Structure, gelation rate and mechanical properties. *Biomaterials*, 22:511–521.

25. Gao, W., Zhang, Y., Ramanujan, D., Ramani, K., Chen, Y., Williams, C.B., Wang, C.C.L., Shin, Y.C., Zhang, S. & Zavattieri, P.D. 2015. The status, challenges, and future of additive manufacturing in engineering. *Computer-Aided Design*, 69:65–89.

26. Grassi, G., Crevatin, A., Farra, R., Guarnieri, G., Pascotto, A., Rehimers, B., Lapasin, R. & Grassi, M. 2006. Rheological properties of aqueous Pluronic–alginate systems containing liposomes. *Journal of Colloid and Interface Science*, 301:282–290.

27. Greul, M., Pintat, T. & Greulich, M. 1995. Rapid prototyping of functional metallic parts. *Computers in Industry,* 28:23–28.

28. Gyles, D.A., Castro, L.D., Silva, J.O.C. Jnr. & Ribeiro-Costa, R.M. 2017. A review of the designs and prominent biomedical advances of natural and synthetic hydrogel formulations. *European Polymer Journal*, 88:373–392.

29. Herrera, C. 2019. The pre-clinical toolbox of pharmacokinetics and pharmacodynamics: *in vitro* and *ex vivo* models. *Frontiers in Pharmacology*, 10:578.

30. Hölzl, K., Lin, S., Tytgat, L., Van Vlierberghe, S., Gu, L. & Ovsianikov, A. 2016. Bioink properties before, during and after 3D bioprinting. *Biofabrication*, 8:032022.

31. International organisation for standardization (ISO). 2015. Standard Terminology for Additive Manufacturing – General Principles – Terminology. (ISO/ASTM52900).

32. Jee, H.J. & Sachs, E. 1999. A visual simulation technique for 3D printing. *Advances in Engineering Software,* 31:97–106.

33. Khalil, E., Schaefer, U.F. & Sallam, A. 2006. Release characteristics of diclofenac diethylamine from emulgels containing Pluronic F127. *Journal of Drug Delivery Science and Technology,* 16(5):381–387.

34. Leberfinger, A.N., Dinda, S., Wuc, Y., Koduru, S.V. & Ozbolat, V. 2019. Bioprinting functional tissues. *Acta Biomaterialia,* 95:32–49.

35. Lee, J.M., Sing, S.L., Zhou, M. & Yeong, W.Y. 2018. 3D bioprinting processes: A perspective on classification and terminology. *International Journal of Bioprinting*, 4(2): 151.

36. Lee, K.Y. & Mooney, D.J. 2012. Alginate: Properties and biomedical applications. *Progress in Polymer Science*, 37:106–126.

37. Levy, G.N., Schindel, R. & Kruth, J.P. 2003. Rapid manufacturing and rapid tooling with layer manufacturing (LM) technologies, state of the art and future perspectives. *CIRP Annals*, 52(2)589–609.

38. Lewicki, J., Bergman, J., Kerins, C. & Hermanson, O. 2019. Optimization of 3D bioprinting of human neuroblastoma cells using sodium alginate hydrogel. *Bioprinting*, 16:e00053.

39. Li, J., Wu, C., Chu, P.K. & Gelinsky, M. 2020. 3D printing of hydrogels: Rational design strategies and emerging biomedical applications. *Materials Science & Engineering R,* 140:100543.

40. Liu, J., Sun, L., Xu, W., Wang, Q., Yu, S. & Sun, J. 2019. Current advances and future perspectives of 3D printing natural-derived biopolymers. *Carbohydrate Polymers,* 207:297–316.

41. Ma, X., Liu, J., Zhu, W., Tang, M., Lawrence, N., Yu, C., Gou, M. & Chen, S. 2018. 3D bioprinting of functional tissue models for personalized drug screening and *in vitro* disease modelling. *Advanced Drug Delivery Reviews*, 132:235–251.

42. Mazi, H. & Surmelihindi, B. 2021. Temperature and pH-sensitive Super absorbent Polymers based on Modified Maleic Anhydride. *Journal of Chemical Science*, 13.

43. Montalbano, G., Toumpaniari, S., Popov, A., Duan, P., Chen, J., Dalgarno, K., Scott III, W.E. & Ferreira, A.M. 2018. Synthesis of bioinspired collagen/alginate/fibrin based hydrogels for soft tissue engineering. *Materials Science & Engineering C,* 91:236–246.

44. Moreira, T.F.M., De Oliveira, A., Da Silva, T.B.V., Dos Santos, A.R., Gonçalves, O.H., Da Silva Gonzalez, R., Droval, A.A. & Leimann, F.V. 2019. Hydrogels based on gelatin: Effect of lactic and acetic acids on microstructural modifications, water absorption mechanisms and antibacterial activity. *LWT – Food Science and Technology,* 103:69–77.

45. Moroni, L., Boland, T., Burdick, J.A., De Maria, C., Derby, B., Forgacs, G., Groll, J., Li, Q., Malda, J., Mironov, V.A., Mota, C., Nakamura, M., Shu, W., Takeuchi, S., Woodfield, T.B.F., Xu, T., Yoo, J.J. & Vozzi, G. 2018. Biofabrication: A guide to technology and terminology. *Trends in Biotechnology,* 36(4):384–402.

46. Mulakkal, M., Trask, R., Ting, V. & Seddon, A. 2018. Responsive cellulose-hydrogel composite ink for 4D printing. *Materials and Design,* 160:108–118.

47. Murphy, S.V. & Atala, A. 2014. 3D bioprinting of tissues and organs. *Nature Biotechnology*, 32(8):773–785.

48. Ngo, T.D., Kashani, A., Imbalzano, G., Nguyen, K.T.Q. & Hui, D. 2018. Additive manufacturing (3D printing): A review of materials, methods, applications and challenges. *Composites Part B*, 143:172–196.

49. O'Brien, F.J. 2011. Biomaterials & scaffolds for tissue engineering. *Materials Today*, 14(3):88-95.

50. Ozbolat, I. & Hospodiuk, M. 2016. Current advances and future perspectives in extrusion-based. *Biomaterials,* 76:321–343.

51. Panwar, A. & Tan, L. 2016. Current status of bioinks for micro-extrusion-based 3D bioprinting. 558 *Molecules,* 1:2–26.

52. Parak, A., Pradeep, P., Du Toit, L.C., Kumar, P., Choonara, Y.E. & Pillay, V. 2019. Functionalizing bioinks for 3D bioprinting applications. *Drug Discovery Today,* 24:198–205.

53. Peng, W., Datta, P., Ayan, B., Ozbola, V., Sosnoski, D. & Ozbolat, I.T. 2017. 3D bioprinting for drug discovery and development in pharmaceutics. *Acta Biomaterialia,* 57:26–46.

54. Puguan, J., Yu, X. & Kim, H. 2014. Characterization of structure, physico-chemical properties and diffusion. *Journal of Colloid and Interface Science,* 432:109–116.

55. Rarokar, N.R., Saoji, S.D. & Khedekar, P.B. 2018. Investigation of effectiveness of some extensively used polymers on thermoreversible properties of Pluronic tri-block copolymers. *Journal of Drug Delivery Science and Technology*, 44:220–230.

56. Rashid, F., Albayati, M. & Dodou, K. 2019. Studies on Novel Methods for Formulating Novel Cross-Linked Hydrogel Films of Hyaluronic Acid. *Cosmetics*, 6(59):2–19.

57. Roehm, K. 2018. Bioprinting cell laden structures with chitosan-gelatin for neural tissue applications. United States of America: New Jersey Institute of Technology (Thesis – PhD).

58. Sano, Y., Matsuzaki, R., Ueda, M., Todoroki, A. & Hirano, Y. 2018. 3D printing of 568 discontinuous and continuous fibre composites using. *Additive Manufacturing,* 24:521–527.

59. Suo, A., Xu, W., Wang, Y., Sun, T., Ji, L. & Qian, J. 2019. Dual-degradable and injectable 570 hyaluronic acid hydrogel mimicking extracellular matrix for 3D culture of breast cancer MCF-571 7 cells. *Carbohydrate Polymers,* 211:336–348.

60. Trachtenberg, J.E, Placone, J.K., Smith, B.T., Fisher, J.P. & Mikos, A.G. 2017. Extrusion-based 3D printing of poly(propylene fumarate) scaffolds with hydroxyapatite gradients. *Journal of Biomaterials Science: Polymer Edition.,* 28(6):532–554.

61. Tytgat, L., Van Damme, L., Arevalo, M.D.P.O., Declarcq, H., Thienpont, H., Otteveare, H., Blondeel, P., Dubruel, P. & Van Vlierberghe, S. 2019. Extrusion-based 3D printing of photo-cross-linkable gelatin and κ-carrageenan hydrogel blends for adipose tissue regeneration. *International Journal of Biological Macromolecules*, 140:929–938.

62. Van Kampen, K.A., Scheuring, R.G., Terpstra, M.L., Levato, R., Groll, J., Malda, J., Mota, C. & Moroni, L. 2019. Biofabrication: From additive manufacturing to bioprinting. *Elsevier.*

63. Varkey, M., Visscher, D.O., Van Zuijlen, P.P.M., Atala, A. & Yoo, J.J. 2019. Skin bioprinting: the future of burn wound reconstruction?. *Burns & Trauma.* 7(4):3.

64. Verrier, S., Blaker, J.J., Maquet, V., Hench, L.L. & Boccaccini, A.R. 2004. PDLLA/Bioglasss composites for soft-tissue andhard -tissue engineering: an in vitro cell biology assessment. *Biomaterials*, 25:3013–3021.

65. Vijayavenkataraman, S., Yan, W.C., Lu, W.F., Wang, C.H. & Fuh, J.Y.H. 2018. 3D bioprinting of tissues and organs for regenerative medicine. *Advanced Drug Delivery Reviews,* 32:296–332.

66. Wang, Q.Q., Liu, Y., Zhang, C.J., Zhang, C. & Zhu, P. 2019. Alginate/gelatin blended hydrogel fibers cross-linked by Ca2+ and oxidized starch: Preparation and properties. *Materials Science & Engineering C,* 99:1469–1476.

67. Webb, B. & Doyle, B. 2017. Parameter optimization for 3D bioprinting of hydrogels. *Bioprinting*, 8:8–12.

68. Williams, D., Thayer, P., Martinez, H., Gatenholm, E., Khademhosseinic, A. & Khademhosseini, A. 2018. A perspective on the physical, mechanical and biological specifications of bioinks and the development of functional tissues in 3D bioprinting. *Bioprinting,* 9:19–36.

69. Yanagawa, F., Sugiura, S. & Kanamori, T. 2016. Hydrogel microfabrication technology toward three dimensional tissue engineering. *Regenerative Therapy,* 3:45–57.

70. Yap, L.S. & Yang, M.C. 2016. Evaluation of hydrogel composing of Pluronic F127 and carboxymethyl hexanoyl chitosan as injectable scaffold for tissue engineering applications. *Colloids and Surfaces B: Biointerfaces*, 146:204–211.

71. Wu, Y., Lin, Z.Y.W., Wenger, A.C., Tam, K.C. & Tanga, X.S. 2018. 3D bioprinting of liver-mimetic construct with alginate/cellulose nanocrystal hybrid bioink. *Bioprinting,* 9:1–6.

72. Zadpoor, A.A. & Malda, J. 2017. Additive Manufacturing of Biomaterials, Tissues, and Organs. *Annals of Biomedical Engineering*, 45(1):1–11.

CHAPTER 3: PRINT PARAMETER OPTIMISATION FOR A PLURONIC F-127 AND ALGINATE HYBRID HYDROGEL

Manuscript to be submitted for the journal *Bioprinting*.

This article is written according to the journal instructions that can be found at https://www.elsevier.com/wps/find/journaldescription.cws_home/738378?generatepdf=true. The reference style followed was a numeric style and the language was British English as specified by the journal. This reference style and language were also kept constant throughout the dissertation to enable enhanced reading. There was not a strict adherence to word count for the purposes of the examination of the dissertation; however, the manuscript will be condensed for publication purposes. The journal allows for detailed methods to be included, which can allow other researchers to duplicate the methods. Before article submission, the results presented in the Annexures will be reformatted into supplementary material as required by the journal.

Title page

Print parameter optimisation for a Pluronic F-127 and alginate hybrid hydrogel

Monja Hibbert*, Joe M Viljoen, Lissinda H du Plessis

Centre of Excellence for Pharmaceutical Sciences, Faculty of Health Sciences, North-West University, Private Bag X6001, Potchefstroom 2520, South Africa

*corresponding author monjavdl@gmail.com

Abstract

The continuing need for valid and reliable alternatives for the classic drug efficacy and toxicity testing models that at times lead to inaccurate or unrealistic results since they fail to mimic all the intrinsic factors and cell micro-environments of the human physiology, has led to the utilisation of 3D bioprinting methods such as pneumatic-based extrusion for the fabrication of tissue constructs. These tissue constructs mimic the *in vitro* condition of the human body and can be utilised to diagnose and treat cancer. Biopolymers are used to create a hydrogel that is used as the bioink and with materials such as hydrogels, the delicate balance between the parameters affect the printing results, and therefore the influence of each parameter should be fully understood (Webb & Doyle, 2017).

The aim of this study was to systematically optimise the printing parameters required to successfully 3D bioprint a computer-aided design (CAD) model with a preformulated hybrid hydrogel. First, a hybrid hydrogel was formulated to conduct the printing parameter optimisation process. Preliminary hydrogel studies were conducted on alginate to determine the optimal concentration thereof as well as the cross-linking capabilities and concentration of the $CaCl_2$ cross-linker solution required. Subsequently, the second component of the hydrogel, known as Pluronic F-127 (PF127), was added and also characterised. A preliminary evaluation concluded that a concentration between 4 and 6% (w/v) alginate yielded the most positive results after being cross-linked with a 2% (w/v) $CaCl_2$ solution.

PF127 was added in various concentrations to the alginate solutions (4 and 6% (w/v)) to determine the optimal concentration and ratio of the two components. The hybrid hydrogel was evaluated in terms of porosity, degradation rate, rheological viscosity classification, and cross-linking capabilities. A hybrid hydrogel with 6% (w/v) alginate and 46% (w/v) PF127, mixed in a 2:1 ratio, respectively, displayed the most optimal characteristics to continue with the printing parameter optimisation part of the study. This hybrid hydrogel portrayed the highest porosity percentage and was classified as a non-Newtonian fluid, which is required for successful pneumatic extrusion. Parameters that were optimised include: nozzle size, printing speed, extrusion pressure and temperature. The parameter optimisation index (POI) was used in combination with a newly formulated scoring system to determine the optimal printing parameters. It was found that the visual observations in combination with grading methods of the 8 to 12% printed scaffolds, were a similarly important factor to take into consideration when selecting the optimal printing parameters.

Parameters that yielded a 100% complete scaffold print was a nozzle size of 27G using an extrusion pressure of 70kPa and printing speed of 30mm/s at 37ºC. Although these parameters are regarded as optimal, they are specific to the hybrid hydrogel formulated in this study and high concentrations of PF127 could possibly have a negative effect on cell proliferation. It is recommended that the parameters should be optimised for different hydrogels. The development of alternative polymers that can be utilised as supporting components within the hydrogel should be further researched.

Keywords: 3D bioprinting, pneumatic extrusion, biomaterials, tissue engineering, scaffold, printing parameter optimisation, hybrid hydrogel, hydrogel characterisation, alginate, Pluronic F-127, parameter optimisation index (POI).

1 Introduction

Many researchers are seeking alternatives to the classic drug efficacy and toxicity testing models (Herrera, 2019; Koçak *et al.,* 2021). Classic two-dimensional (2D) models display dramatic differences in cell behaviour when compared to three-dimensional (3D) models that provide a more realistic environment native to cells, and this can lead to inaccurate results. 3D bioprinting allows for *in vitro* cell models to be fabricated and therefore provides an alternative to known models (Peng *et al*., 2017; Zhu, 2016; Ma *et al*., 2018).

Tissue engineering has many fabrication technologies available; however, additive manufacturing (AM) for the direct fabrication of 3D tissue constructs, also known as biofabrication, has shown many advantages since it has the ability to fabricate complex biometric structures that recreate *in vivo* conditions (Tytgat *et al*., 2019; Peng *et al*., 2017; Vijayavenkataraman *et al*., 2018). 3D bioprinting is defined as the stacking and assembly of organic materials and bioinks, containing cells or not, into spatial patterns using a computer-added design (CAD) to create a 3D structure (Datta *et al*., 2018; O'Brien, 2011; Ozbolat & Hospodiuk, 2016; Mironov *et al.,* 2009).

3D bioprinting can be subdivided into four main groups, namely: laser-, droplet-, extrusion-based bioprinting and vat polymerisation. From these groups, extrusion-based bioprinting is the main focus for researchers within the medical field of tissue engineering and also has many applications in the pharmaceutical world. Extrusion-based bioprinting can be subdivided into pneumatic and mechanical extrusion. Pneumatic extrusion utilises air pressure to extrude the bioink, whereas mechanical extrusion uses mechanical force. Since pneumatic extrusion allows for air pressure control, it lowers the chances of cell death caused by shear stress (Roehm, 2018; Vijayavenkataraman *et al*., 2018).

Hydrogels are used as bioinks during extrusion-based printing and can be defined as 3D porous networks that are capable of retaining large amounts of fluid (Roehm, 2018). Bioinks are composed of natural and synthetic biopolymers; and because of their high biocompatibility, they mimic the extracellular matrix (ECM) more inherent to cells, including a suitable viscosity and shape fidelity. They should furthermore possess the characteristics required to ensure it can be printed into a scaffold rendering them printable (Wang *et al*., 2018; Chimene *et al*., 2020; Parak *et al.,* 2017).

The need for valid and consistent alternatives to the classic drug discovery and delivery research models has led to the utilisation of biofabrication methods allowing for the fabrication of tissue constructs that can be used as *in vitro* biomimetic tissue models by means of extrusion-based bioprinting (Peng *et al*., 2017; Zhu, 2016; Ma *et al*., 2018). A number of challenges still remain

pertaining to mechanical properties, printability and bioactivity of these printed constructs (Parak *et al*., 2019). Furthermore, the extrusion pressure and speed, nozzle size and printing temperature are printing parameters that had to be optimised to ensure a 100% complete successful print and the relationship between these parameters can be observed with the parameter optimisation index (Webb & Doyle, 2017).

In the first part of the study, it was important to optimise the bioink formulation to obtain a bioink that could be extruded and that had high shape fidelity after extrusion. In the second part, it was important to optimise the print parameters for the developed bioink. A print score was established using line width and corner drag measurements of the printed scaffolds. The aim of the print score was to find a set of parameters, including nozzle size, printing pressure and speed that resulted in an accurately printed scaffold.

This newly developed print score was compared to the printer optimisation index used by other studies (Webb & Doyle, 2017; Lewicki, 2019). Various research have investigated alginate bioinks for pneumatic extrusion; however, to date the combination of alginate and PF127 has not been investigated. Several studies have furthermore investigated print parameter optimisation; nonetheless, no standardised methods are available. Studies have however proven the importance of print parameter optimisation for any bioink (Webb & Doyle, 2017; Paxton *et al*., 2019), but it is of even greater importance for novel formulated bioinks.

2 Materials and methods

2.1 Materials

Alginic acid sodium salt (powder, 180947), phosphate buffered saline (PBS) (powder, P3813), Pluronic F-127 (powder, P2443) and anhydrous calcium chloride (granules, C1016) were purchased from Sigma-Aldrich (Merck, Darmstadt, Germany) and 3ml pneumatic syringe/cartridges and 22, 25 and 27G high-precision conical bioprinting nozzles were purchased from Cellink® (Gothenburg, Sweden).

2.2 Bioink formulation

Alginate was prepared in 30ml PBS at concentrations of 2, 4, 6 and 8% (w/v) as described by Berg *et al*. (2018). The PBS solution was heated to 40ºC before the alginate powder was gradually added while being magnetically stirred. After 10min of stirring, the solution depicted a consistency of a syrup and was placed in the fridge at 4ºC for 24h before it was used. $CaCl_2$ was prepared in dH_2O to create 1l of a 4.0% (w/v) solution that was diluted to 2.0, 1.5, 1.0 and 0.5% (w/v). The

solution was kept for 24h at 24ºC to ensure complete diffusion, dissolution and equilibrium was reached prior to utilisation.

Preliminary formulation studies of alginate at the concentrations listed, cross-linked with 0.5 to 2.0% $CaCl_2$ (w/v), did not yield suitable hybrid hydrogels for 3D bioprinting. It was concluded, to continue with 4 and 6% alginate (w/v) with various concentration of PF127 added to the formulation. The hybrid hydrogel bioink was cross-linked with 4% $CaCl_2$ (w/v) (Appendix A). PF127 was prepared using the cold method as described by Choi *et al*. (1999), and was prepared in concentrations between 40 and 50% (w/v) to ensure the structure holds its integrity while in the printing process. Distilled H_2O was refrigerated to 4ºC before PF127 was added. PF127 amounts of 40, 46 and 50g of PF127 were placed into containers and made up to volume (100ml). The solution was left in the fridge at 4ºC for two to four days.

Alginate and PF127 were combined in a 2:1 ratio, with varying concentrations as follow:

Hybrid hydrogel 1: 4% (w/v) Alginate + 40% (w/v) PF127

Hybrid hydrogel 2: 4% (w/v) Alginate + 46% (w/v) PF127

Hybrid hydrogel 3: 4% (w/v) Alginate + 50% (w/v) PF127

Hybrid hydrogel 4: 6% (w/v) Alginate + 40% (w/v) PF127

Hybrid hydrogel 5: 6% (w/v) Alginate + 46% (w/v) PF127

Hybrid hydrogel 6: 6% (w/v) Alginate + 50% (w/v) PF127

For this study, no live cells were incorporated into any of the hybrid hydrogel formulations and did thus received a ‘no risk’ status allocation from the North-West University Health Research Committee (NWU-HREC) (Annexure D). In the event that live cells are used, a new status will have to be allocated to the study based on the decision made by the ethics approval committee of the university.

3 Bioprinting process

The formulated hybrid hydrogel used as bioink underwent printing parameter optimisation with the BioX™ 3D bioprinter from Cellink® (Gothenburg, Sweden) with a HeartOS operating system. The printer is equipped with intelligent printhead mounts and a printbed capable of temperature control. Before each printing session, these printheads were calibrated with the surface on which the scaffold was printed. It is also equipped with clean chamber technology and UV curing systems that allow for a sterile printing environment. All scaffold prints were conducted with a 3ml

pneumatic syringe using 22G (410µm), 25G (250µm) and 27G (200µm) sterile high precision conical nozzles (Cellink®, Gothenburg, Sweden) that screw into the pneumatic syringe (Figure 1-1, Chapter 1) that is also regarded as the print cartridge.

These cartridges were loaded by using an adapter that screws onto the nozzle connection point wherein a simple mechanical syringe could be inserted to be filled with the bioink and extruded into the pneumatic syringe/cartridge. Following, the loaded cartridge was inserted into the printhead mount, tightened and connected to the pneumatic airflow inlet. A layer height of 0.2 to 0.3mm was printed, depending on the nozzle size used, with a grid infill pattern (Figure 3-1) and no supporting material. The extrusion pressure and printing speed were constantly changed as they were part of the printing parameter optimisation process.

4 Characterisation of hybrid hydrogel bioink

4.1 Line test

An adaptation from the single fibre extrusion test described by Trachtenberg *et al*. (2016) was performed on all six proposed formulations. A single line was printed into a 10x10 mm rectangle without infill employing a 25G nozzle at 35ºC with an extrusion pressure of 30kPa and a printing speed of 10mm/s. Photographs were taken with an iPhone 8 Plus equipped with a 12-megapixel wide-angle and telephoto lens. The photographs taken during the line test were compared using measurements taken from each line, as illustrated by Figure 3-1:

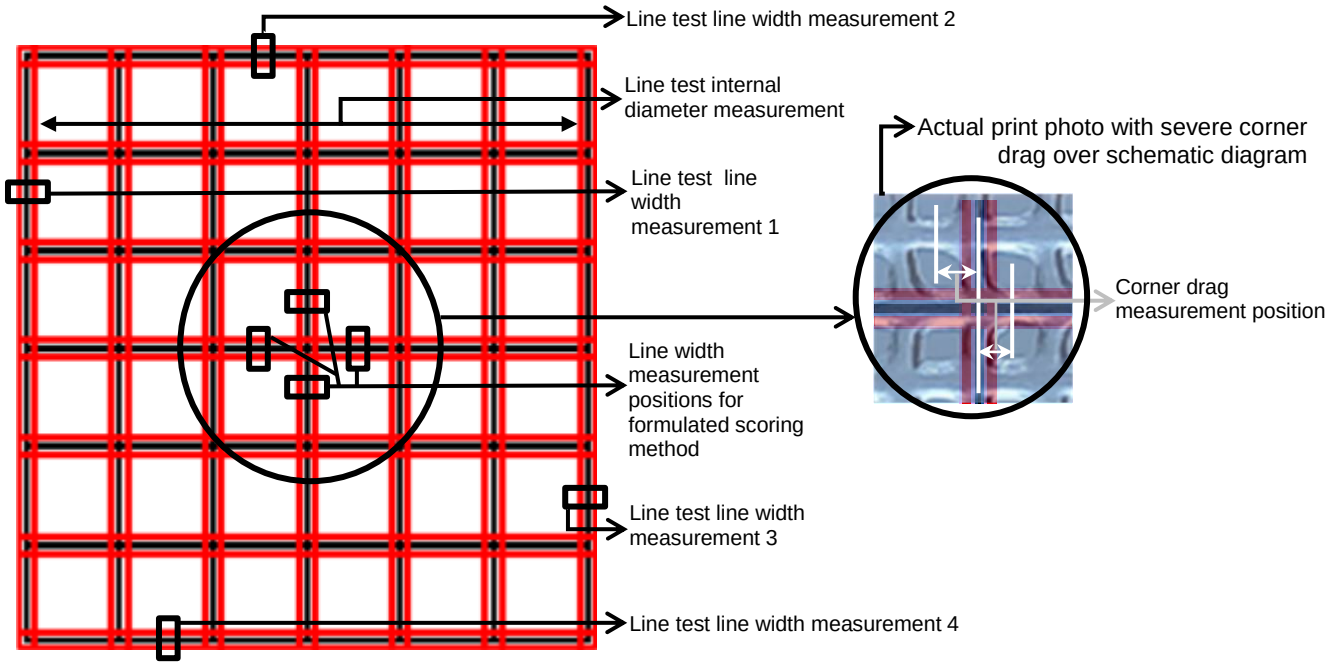

Figure 3-1: **Schematic diagram illustrating the location of each measurement taken for the line test, the newly formulated grading system and the grid infill pattern used on the bioprinter. The black lines represent the CAD design needle print position, while the red lines represent the printed hybrid hydrogel line volume**

These measurements, together with the visual appearance of the hybrid hydrogel after printing, were compared, before and after cross-linking commenced. During visual examination of single line scaffolds, the line width, integrity and volume were determined.

4.2 Degradation/stability

The degradation/stability method was adapted from Montalbano *et al*. (2018). A volume of 1ml of each hybrid hydrogel formulation was placed into a 24 well-plate and cross-linked with 4% (w/v) $CaCl_2$ for 24h at 37ºC to create a disc. Four discs of each hybrid hydrogel formulation were produced and tested in triplicate. After complete cross-linking, the discs were removed from the $CaCl_2$ solution and rinsed. These discs were weighed and placed back into the well-plates containing 3ml dH_2O. The well-plates were kept at 37ºC and the discs were weighed again after 24h, 48h, as well as one week (168h). The disc masses were compared to determine whether it started to degrade.

4.3 Porosity

The porosity of the hybrid hydrogel bioinks was determined and calculated according to the Archimedes principle described by Cao *et al*., (2017) were the porosity for eight respective hydrogels were calculated using Equation 1:

$$\%\text{Porosity} = 100(m_2 - m_1)/(m_2 - m_3) \quad [1]$$

Where m_1 is the mass of dry hydrogel, m_2 is the mass of the swollen hydrogel and m_3 is the mass of swollen hydrogel suspended in water.

A volume of 1ml of each hybrid hydrogel formulation was placed into a 1 x 7mm well-plate and cross-linked with 4% (w/v) $CaCl_2$ for 24h to create a disc. Four discs of each hybrid hydrogel formulation were formulated to ensure obtaining statistically significant results was achieved. After complete cross-linking, the discs were removed from the $CaCl_2$ solution and rinsed with dH_2O. These discs were left to dry for 30min on a paper towel to drain the excess dH_2O, where after it was weighed. The discs were resubmerged into dH_2O to allow for reabsorption. Subsequently, the discs were removed and weighed again; and once more suspended in dH_2O followed by weighing again (Cao *et al*., 2017). The test was conducted in triplicate.

4.4 Viscosity

The 6% (w/v) alginate (A) in combination with the 46% (w/v) PF127 mixed in a 2:1 ratio respectively (hydrogel 5) was the concluded optimal bioink and used during this process. The viscosity of hybrid hydrogel 5 (6%A:46%PF127) was analysed using a rotational rheometer (ARES G2, TA Instruments, New Castle, DE, USA). A flow sweep test was done in triplicate at 35ºC and 37ºC. The rheometer is equipped with a 40mm steel cone plate with a 2º angle and a 30µm truncation gap. A sample of approximately 6ml was used with a shear rate (γ)(1/s) range of 1 to100, increasing with 1 per second measured in time steps of 3s. Viscosity versus shear rate data was fitted using Power Law models (Li *et al*., 2020).

5 Print parameter optimisation of scaffold

Only the hybrid hydrogel 5 (6%A:46%PF127) was used in the print parameter optimisation. The print parameter optimisation process was divided into six groups, where the nozzle size and extrusion pressure were kept constant. The two variables were extrusion pressure (kPa) and extrusion speed (mm/s), with a range of 20 to 80kPa and 10 to 45mm/s, respectively. The six groups are as follows: (1) 22G at 35ºC; and (2) at 37ºC; (3) 25G at 35ºC; and (4) at 37ºC; (5) 27G

at 35ºC; and (6) at 37ºC. Printing parameters were optimised using a newly proposed grading method.

Scaffolds were only printed until 8 to 12% completion as this basis layer would already provide sufficient data to conclude whether or not a certain parameter should be taken into further consideration. Each 8 to 12% printed scaffold base was photographed and enlarged to roughly 50mm to improve the accuracy of the line width measurements. The hybrid hydrogel line width volume, as described in Figure 3-1, has been assigned a theoretical line width of 2mm on a 50mm extrapolation, resulting in an extrapolation value of 52mm.

This allowed a line width of 1mm into each square and caused the inner diameter of each individual square to decrease from 8mm to 6mm. From the CAD needle print position (middle point of hybrid hydrogel line volume), as depicted in Figure 3-1, the hybrid hydrogel line width can reach a maximum of 8mm with 4mm expanding into each square before the hybrid hydrogel lines would combine and the measurement of individual lines became impossible, thereby rendering the print unsuccessful. The line width should consequently be optimal and is dependent on the extrusion pressure as well as nozzle size.

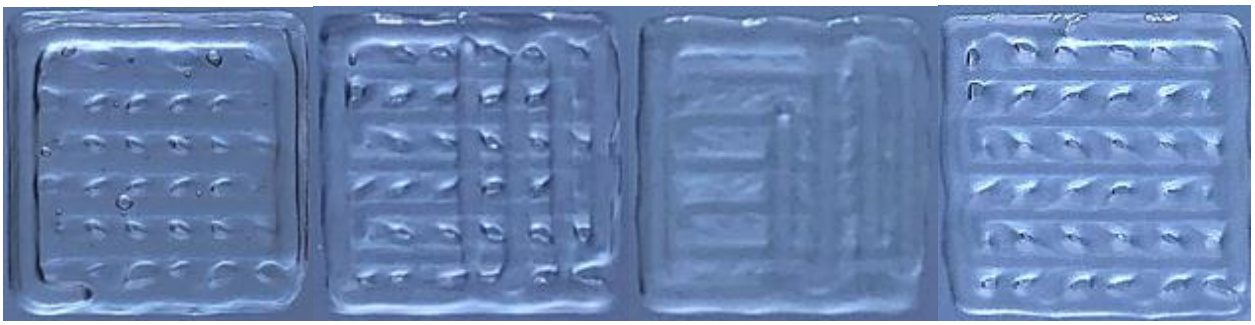

Figure 3-2: Photographs of 8 to 12% printed scaffolds of which the line width volumes exceed 8mm and 4mm expansion into each square within the design, on a 52mm extrapolation

These prints were unmeasurable and were therefore rendered unsuccessful. Where the red lines cross over each other, the hybrid hydrogel line width volume should still stay within the theoretical 2mm allocated value. Since these lines are printed through each other, the printing speed should be optimal. In the event that the printing speed is too high, it will cause the line that is being printed through to be dragged, resulting in a ‘corner drag’. As the dimensions stay the same at the corners of the squares, the corner drag should be a maximum of 4mm from the CAD needle print position

before they would start touching another, which as a results would render them unmeasurable. The ‘corner drag’ has been allocated a theoretical value of 1mm.

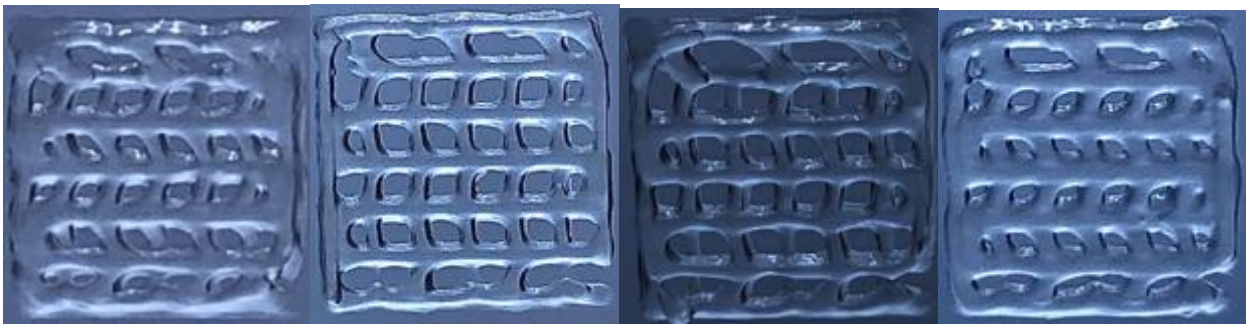

Figure 3-3: Photographs of 8 to 12% printed scaffolds of which the corner drag exceed 4mm into each square within the infill grid design, on a 52mm extrapolation

Although these prints were still measurable, they had compromised inner grids. Continuing to print on a compromised grid can cause a lack in structural integrity of the final scaffold that renders the print unsuccessful.

As 4mm was the width and corner drag limit within the square, this value was allocated a score of 0/10 with the minimum theoretical width being 1mm, allocated a score of 10/10. This means that for each 0.3mm the line width exceeded the minimum theoretical 2mm, or corner drag exceeded the theoretical minimum 1mm, one point was deducted from the 10/10 score. With these two formulated calculations, it allowed a value to be allocated to each print with its parameters, and for results that could be statistically analysed. Equation 2 was used to calculate the points lost for the line widths measurement. Equation 3 was used to calculate the points lost for the corner drag measurements, while Equation 4 was used to ultimately determine the score allocation out of 10.

$$PL = \frac{Lw_{ave} - 2}{0.3} \quad [2]$$

$$PL = \frac{Cd_{ave} - 1}{0.3} \quad [3]$$

$$S_{10} = 10 - PL \quad [4]$$

Where $PL =$ points lost, $Lw_{ave} =$ line width average extrapolated to 52mm, $Cd_{ave} =$ corner drag average extrapolated to 52mm, $S_{10} =$ score out of 10.

In Figure 3-4, photographs of scaffold bases portraying a good line width and corner drag are portrayed. The line width measurements barely exceed 2mm, if at all, and it can be clearly observed that the corner drag, as described, is hardly visible.

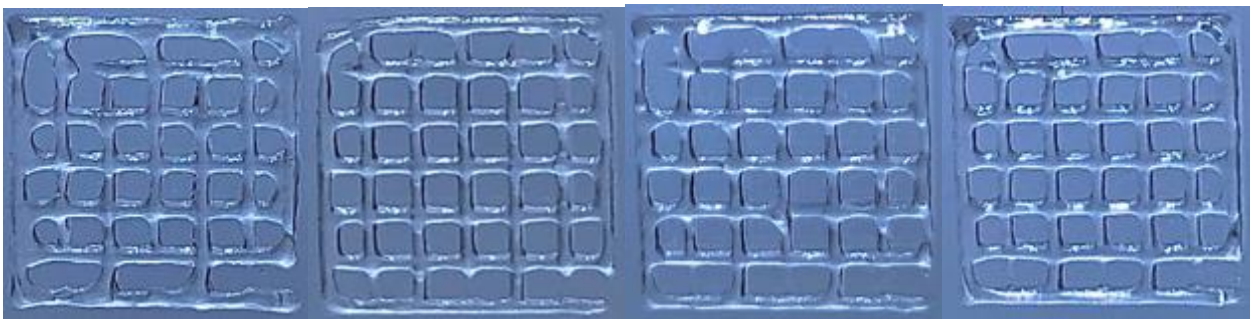

Figure 3-4: Photographs of 8 to 12% printed scaffolds of which the line width volumes barely exceeds 2mm and a corner drag measurement of 1mm into each square within the design, on a 52mm extrapolation

The 8 to 12% printed scaffolds from Figure 3-4 were all taken from within the parameters of 37ºC and 27G. They all had an average score of 10/10. It was observed that even though these scaffolds had scored an average of 10/10, they did not yield a 100% completely printed scaffold. During the printing process, they would start to display the self-collapsing effect that is displayed in Figure 3-12A, and would therefore be regarded as unsuccessful. The visual observation of the printing process had proven to show that even though the scaffold might have scored 10/10, it could still fail to complete a scaffold print of 100%. Consequently, the visual judgement is just as important as the grading methods.

6 Parameter optimisation index

The parameter optimisation index (POI) was calculated for each individual set of parameters (6) according to Webb and Doyle (2017) and Lewicki *et al*. (2019). The POI describes the relationship between the variables of shear rate.

$$POI = \frac{1}{t_{line} \cdot D_G \cdot p} \quad [5]$$

$$POI_i = \frac{POI_i}{POI_{MAX,n}} \quad [6]$$

Where t_{line} = printed line width, D_G = needle gauge, p = extrusion pressure, POI_i = POI for an individual set of parameter, POI_{MAX} = maximum POI of the range tested, n = total number of parameter combinations. The POI_i can assume values between 0 (worst) to 1 (best) (Webb & Doyle, 2017; Lewicki *et al*., 2019).

7 Cross-linking of scaffold

Cross-linking of the scaffolds was conducted with a 4% (w/v) $CaCl_2$ cross-linking solution that was heated to the printing temperature of 37ºC, as this concentration was deemed sufficient during the hydrogel formulation study. Cross-linking of the scaffold had to occur after the scaffold base (8-12%) was printed to ensure the scaffold did not move around on the petri dish from its printing/calibration point. The cross-linker was dripped into the petri dish, around the 8 to 12% printed scaffold, as they were continuing to print, being careful not to have submerged the entire scaffold under the cross-linking solution as this resulted in the top layer cross-linking before the next layer of bioink could be extruded onto it to form the subsequent layer. After 100% print completion, the petri dish containing the scaffold was filled with the cross-linking solution to completely submerge the scaffold. It was left on the heated printbed for 1min, where after it was tilted to allow the excess cross-linking solution to flow out of the petri dish.

The petri dish was rotated to face the ground, leaving the scaffold turned upside-down, while the scaffolds first layer remained stuck to the dish. It was thereafter submerged into a beaker filled to the brim with the cross-linking solution. The scaffold was left upside down, with its first layer still stuck to the petri dish, inside the cross-linker for 2min. It was subsequently lifted out the cross-linking solution, still keeping it over the beaker filled with the cross-linker it was lifted out of, and using a dripper, the cross-linking solution was gently gushed into the base and sides of the scaffold to loosen its first layer from the petri dish without compromising the integrity of the semi cross-linked scaffold. This was done on each side of the scaffold until it gently slid off to the side of the petri dish and fell into the beaker filled with cross-linker solution. The free/loosened scaffold was left submerged in the cross-linker for 24h at 37ºC to ensure complete cross-linking of the entire scaffold.

8 Swelling ratio of scaffold

The swelling response was investigated by calculating the equilibrium swelling ratio (SR). Twelve 10mm x 10mm x 10mm scaffolds were printed to 100% completion and cross-linked with 4% (w/v) $CaCl_2$ cross-linking solution. After successful and complete cross-linking of the scaffolds (24h in 4% (w/v) $CaCl_2$ at 37ºC), they were left to dry for 24h on a paper towel and consequently weighed again and submerged into dH_2O and 2% (w/v) $CaCl_2$ for 24h at 4ºC and 37ºC to determine how

a lower pH and temperature difference influenced the swelling ratio. The aim of the $CaCl_2$ solution, that the scaffolds were submerged into after being dried during the swelling ratio characterisation, was not to cross-link the scaffolds any further and was only used to alter the pH of the dH_2O. It is known that $CaCl_2$ lowers the pH of water when in solution. The scaffolds were weighed a last time after being patted dry with a paper towel to remove the excess aqueous solution it was submerged in (Mulakkal *et al*., 2018; Mazi & Surmelihindi, 2021).

The SR was calculated as follows:

$$SR = \left(\frac{W_s - W_d}{W_d}\right) \quad [7]$$

Where W_s is the weight of the swollen hybrid hydrogel and W_d the weight of the dried hybrid hydrogel (Mulakkal *et al*., 2018). All tests were conducted in triplicate.

9 Statistical analysis

The data was analysed by GraphPad Prism™ version 9 (GraphPad Software, LLC, San Diego, CA, USA). Statistical significance was determined with two-way analysis of variance (ANOVA), with Tukey's multiple comparison tests. Data is presented as mean ± standard deviation (SD) and significance was set at $p \leq 0.05$. Correlations between the POI and the print score were analysed with Spearman's rank correlation.

10 Results and discussion

10.1 Bioink formulation

Hydrogels are used as bioinks when working with printing methods such as pneumatic-based extrusion (Roehm, 2018) and the hybrid hydrogel formulation study had shown that a hybrid hydrogel with an alginate (A) concentration of 4 and 6% (w/v) was deemed the most successful in cross-linking with the ionic 2% (w/v) $CaCl_2$ cross-linker. The combination with PF127 in concentrations of 40, 46 and 50% (w/v) mixed in a 2:1 A:PF127 ratio resulted in smooth gels with good homogeneity and no phase separation after cross-linking (results shown in Annexure A).

10.2 Characterisation of hybrid hydrogel bioink

10.3 Line test

Line tests were conducted on all hybrid hydrogel formulations excluding hybrid hydrogel 1 (4%A:40%PF127), following an adaptation from the extrusion fibre test described by Trachtenberg *et al*. (2016). All line test results are presented in Annexure B. Figure 3-5 illustrates

representative photographs of line test results of the different hybrid hydrogels. Figure 3-5(A) represents a line print with weak line width, integrity and line volume, before and (B) after cross-linking. Figure3-5(C) signifies a line print with a good line width, average integrity and an average line volume, before and (D) after cross-linking. Figure 3-5(E) portray a line print that is too wide, has good line integrity and too much line volume, before and (F) after cross-linking. Figure3-5(G) indicates a line print with a good line width, integrity and volume, before and (H) after cross-linking.

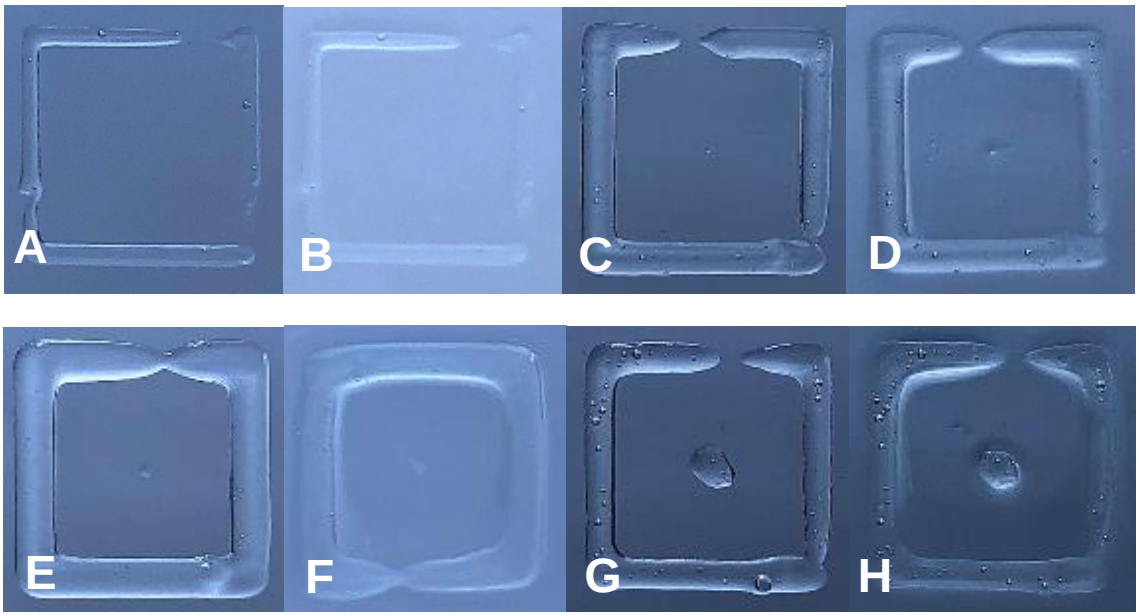

Figure 3-5: Representative photographs of the line test of different hybrid hydrogels

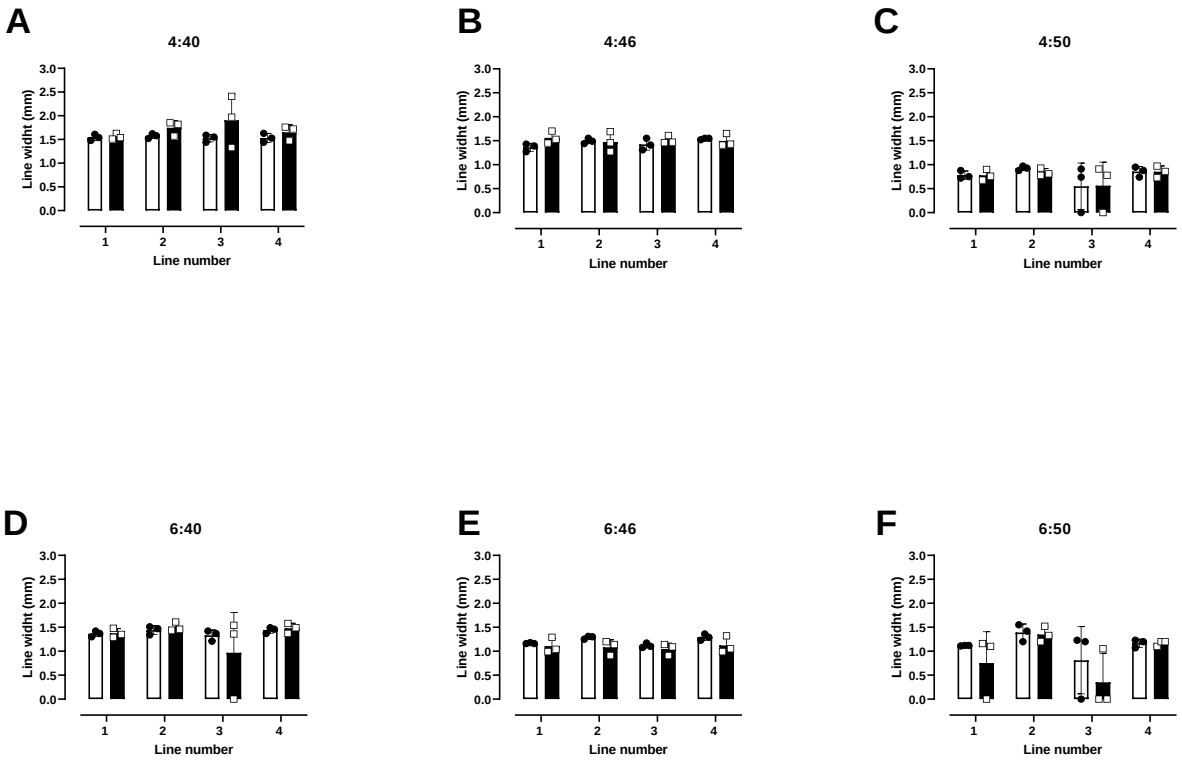

Figure 3-6: **Line test results presented as line width (mm) at four different positions of the different alginate (A) and PF127 hybrid hydrogel bioinks before (white bars) and after (black bars) cross-linking with 4% (w/v) $CaCl_2$, A) 4%A:40%PF127 (w/v), B) 4%A:46%PF127 (w/v), C) 4%A:50%PF127 (w/v), D) 6%A:40%PF127 (w/v), E) 6%A:46%PF127 (w/v) and F) 6%A:50%PF127 (w/v). Results are presented as mean ± standard deviation (SD), n=3**

Considering the line width measurement as well as the internal diameter (Figure 3-1) provided information regarding the hybrid hydrogels printing and cross-linking capabilities. Thicker line widths could be attained with the hybrid hydrogels viscosity before cross-linking and a more viscous gel would result in thinner line widths. The line width measurement taken after cross-linking provided information regarding the cross-linking capabilities of the alginate concentration within the hybrid hydrogel. If the alginate concentration was too low, the line width would increase post cross-linking, since the hybrid hydrogel is incapable of holding its line volume and would flatten. The optimal hybrid hydrogel would display an insignificant increase in line width, which was represented by the hydrogel that was capable of holding its printed structure.

There were no significant differences between the line widths measured before or after cross-linking (Figure 3-6). During the line test study, hybrid hydrogel 1 (4%A:40%PF127) (Figure 3-6A)

was eliminated as successful cross-linking of the alginate did not occur. It was concluded that the formulation had an alginate concentration too low to be successfully cross-linked with the 4% (w/v) $CaCl_2$ cross-linker and was eliminated as a potential hybrid hydrogel bioink formulation. Hybrid hydrogel 4 (4%A:50%PF127) had displayed significantly thinner line widths comparatively ($p \leq 0.05$). Hybrid hydrogel 5 (6%A:46%PF127) showed line width measurements with the least variability and was overall the closest to the ideal value of 1mm (Figure 3-6E).

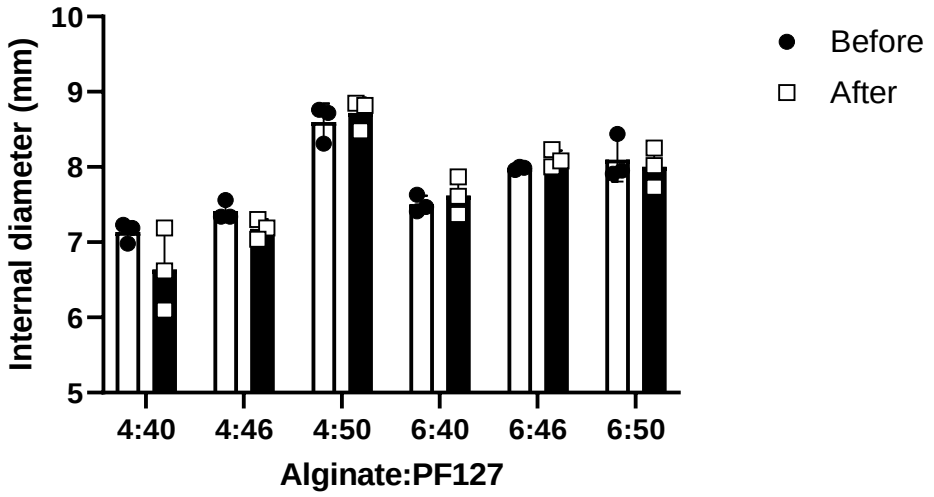

Figure 3-7: Line test results presented as internal diameter (mm) of the different alginate (A) and PF127 hybrid hydrogel bioinks. Results are presented as mean ± standard deviation (SD), n=3

There were also no significant differences in the internal diameter for all the hybrid hydrogel formulations before and after cross-linking (Figure 3-7). Hybrid hydrogel 3 (4%A:50%PF127) revealed a significantly larger internal diameter compared to hybrid hydrogels 1 (4%A:40%PF127), 2 (4%A:46%PF127) and 4 (6%A:40%PF127) ($p \leq 0.05$). Similar to the results of the line width, hybrid hydrogel 5 (6%A:46%PF127) displayed the least variability and was the closest to the ideal internal diameter of 7.99mm.

10.4 Degradation/stability

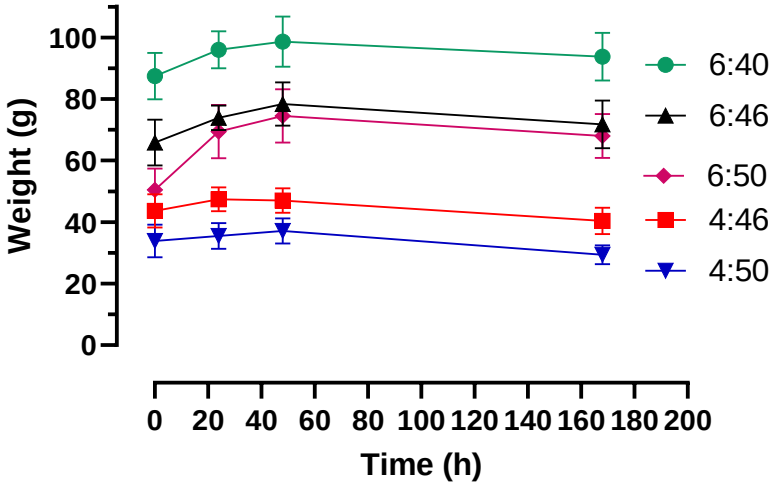

Figure 3-8: Degradation presented as weight change (g) of the different hybrid hydrogel bioinks containing alginate and PF127 at 24, 48 and 168h. Results are presented as mean ± standard deviation (SD), n=12

Hybrid hydrogel 1 (4%A:40%PF127) did not successfully cross-link into a disc as described and was disqualified from the degradation study (results not shown). The hybrid hydrogels containing 6% (w/v) alginate weighed significantly more than the hybrid hydrogels containing 4% (w/v) alginate as seen in Figure 3-8 ($p \leq 0.05$). The degradation study of the hybrid hydrogel discs formed by means of cross-linking, concluded that almost no degradation occurred over the time period, confirming the stability of hydrogels. These results have also been found in previous studies (Kuo, 2002; Roehm, 2018).

The weight gained can be attributed to the porosity of the hydrogel that allows fluid to be absorbed into the discs. It could also be due to the hydrogel's ability to maintain large amounts of fluid (Roehm, 2018) and the discs possibly maintaining their water even after being patted dry and left on a paper towel for 10min.

10.5 Porosity

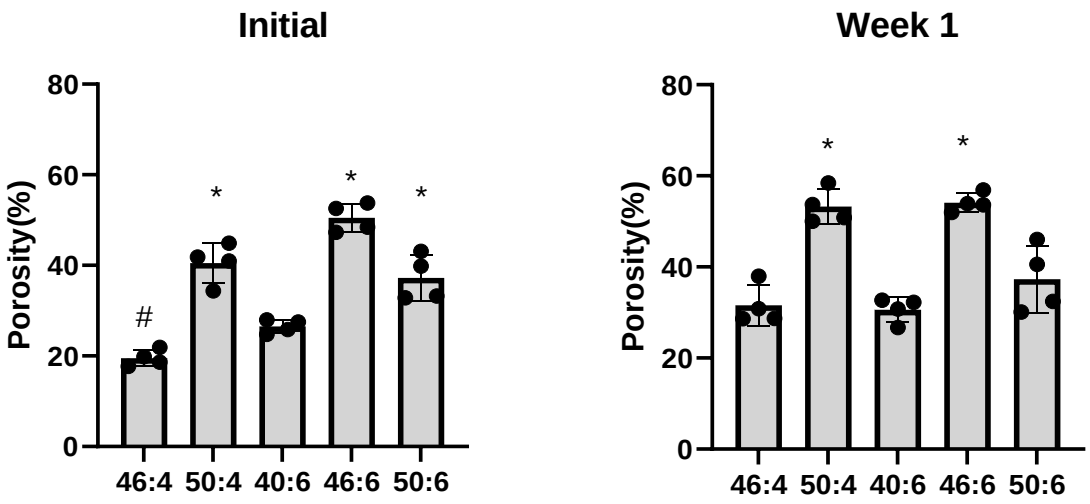

Figure 3-9: Porosity (%) of the different alginate and PF127 hybrid hydrogel bioinks initially and after one week. Results are presented as mean ± standard deviation (SD), n=3. * p≤0.05 significantly higher compared to all the other formulations

From the results obtained during the porosity study, it was clear that hybrid hydrogel 5 (6%A:46%PF127) had depicted the highest percentage porosity of 50.5±3.1% initially; and 54.1±2.1% after one week (Figure 3-9). This is regarded as an important property that a bioink should have since the porosity will contribute to all nutrients and waste products to be moved within the construct (Calejo *et al*., 2018). Hybrid hydrogel 3 (4%A:50%Pf127) and 5 (6%A:46%PF127) differed and had significantly higher porosity initially and after one week (p≤0.05) compared to the other hybrid hydrogels. From the hybrid hydrogel formulation studies it could thus be concluded that a hybrid hydrogel with a concentration of 6% (w/v) alginate and 46% (w/v) PF127 was the optimal formulation to start optimising the print parameters.

10.6 Viscosity

The apparent viscosity decreased as the shear rate increased from 0 to 100 (results shown in Annexure B). This result proved that the formulated hybrid hydrogel 5 (6%A:46%PF127) can be regarded as a non-Newtonian fluid because of the apparent viscosity that decreased as the shear rate increased (Chimene *et al*., 2020).

10.7 Print parameter optimisation

All print parameter optimisation results including the visual representations, line width, corner drag and print scores are listed in Annexure C. Scaffolds printed with both the 22G and 25G nozzle sizes were not successful at any of the extrusion pressures, print speeds or temperatures investigated, with most print scores below 8/10. Scaffolds printed with the 27G nozzle size at print pressures of 30, 35 or 40kPa were most successful with print scores above 9/10; however, they did not yield a 100% complete and successful scaffold print.

It was clear that both the visual observation of the printing process as well as the grading methods used in this study are needed to determine which parameters will be able to yield a successful scaffold print to 100% completion. Optimal printing parameters for hybrid hydrogel 5 (6%A:46%PF127) were determined as an extrusion pressure of 70kPa, a printing speed of 30mm/s at a temperature of 37ºC using a 27G nozzle size. These parameters physically yielded a 100% complete scaffold print. Additionally, this printed scaffold illustrated a print score of 7.9/10, which is evidently lower than other scaffolds scores. Therefore, from these results, it is evident that using only one grading or characterisation method could not accurately determine the optimised print parameters.

Interestingly, in the study by Webb and Doyle (2017) where they tested a 7% (w/v) alginate and 8% (w/v) gelatine hydrogel, it was concluded that a nozzle gauge of 30G, a printing pressure of 100kPa and print speed of 4mm/s could be considered optimised print parameters. Another study by Lewicki *et al*. (2019) used a 2% (w/v) alginate hydrogel and described optimised print parameters of 86kPa, a print speed of 8mm/s, as well as a nozzle gauge of 30G could be deemed. Both of these groups used pneumatic extrusion-based printing; however, two different models of 3D bioprinters were employed. This again emphasises the importance of establishing optimised printing parameters for each bioink on a specific 3D bioprinter.

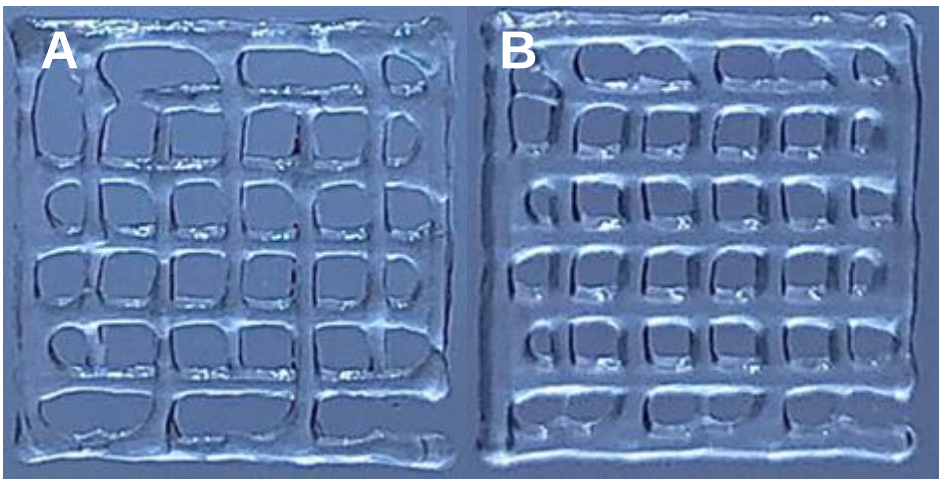

Figure 3-10: Representative photographs of 8–12% printed base of scaffold using a 27G nozzle at A) 37ºC and B) 35ºC with a printing speed of 30mm/s and extrusion pressure of 70kPa

10.8 Parameter optimisation index

Webb and Doyle (2017) developed a parameter optimisation index (POI) that is a measure of the printing accuracy represented by the geometry of the printed lines and the shear stress associated with the fluid mechanics of extruding the hydrogel through a thin nozzle. The POI equations described using average line width values interpolated to 10mm, were calculated for each individual set of parameters as presented in Annexure C.

For the 22G nozzle at 35ºC and 37ºC, it was the scaffold with an extrusion pressure of 20kPa and a printing speed of 15mm/s that had a POI_i of 1. For the 25G nozzle at 35ºC and 37ºC, the scaffold that obtained a POI_i of 1, had a printing speed of 15mm/s and an extrusion pressure of 25kPa. For the 27G nozzle at 35ºC and 37ºC, the scaffold that had a POI_i of 1, had a printing speed of 10mm/s and an extrusion pressure of 30kPa. Figure 3-11 is a visual representation of the printed scaffold bases with the highest POI_i scores.

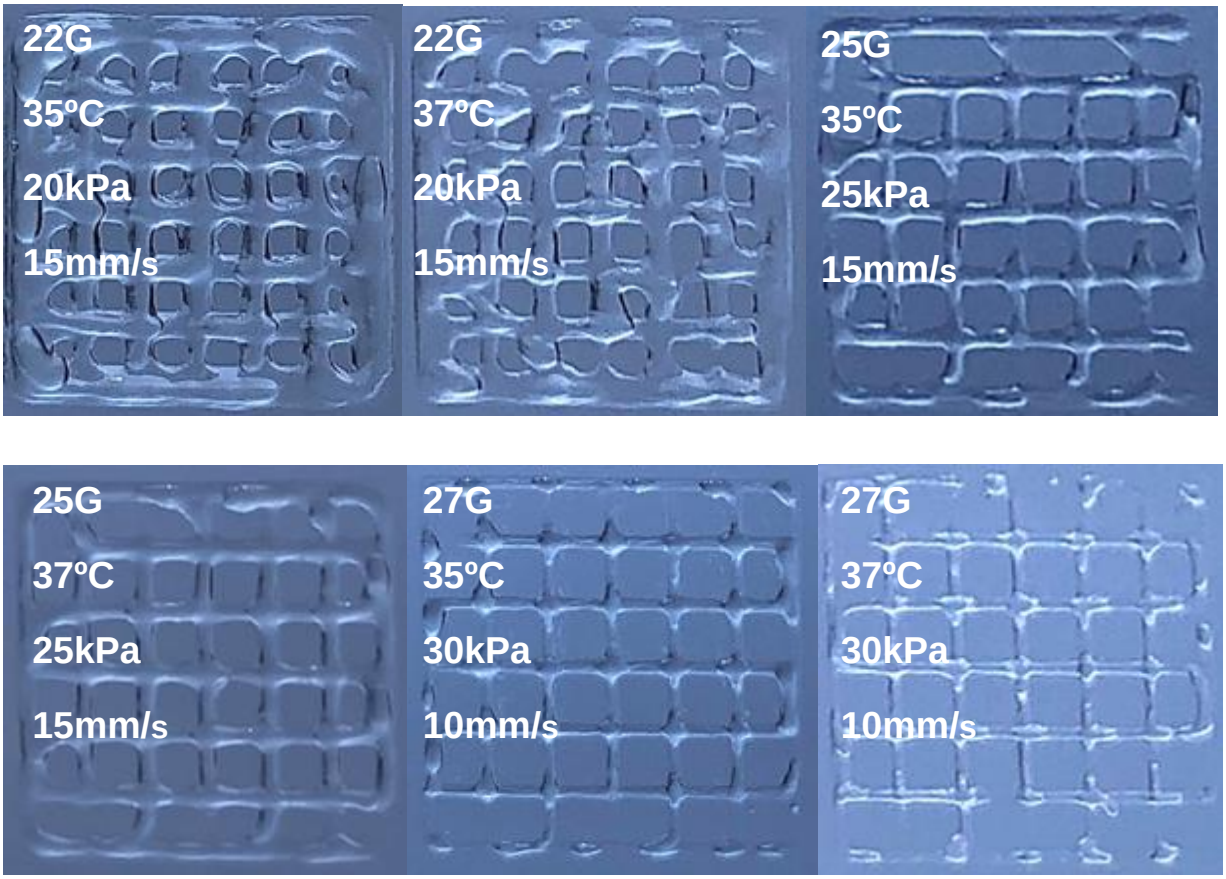

Figure 3-11: Scaffolds that scored 1 in the POI_i calculation of each group

Figure 3-10 visually displays the scaffold base with the highest POI_i score of 1. The line widths are consistent in contrast to Figure 3-11, where it can be seen that the hydrogel did not print a solid line from the one side of the scaffold to the other. This means that these base scaffolds' parameters are not sufficient to maintain the rest of the scaffold, and continuing to print on a compromised scaffold base will lead to a lack in structural integrity. From Figure 3-11, it can be visually observed that the scaffolds that scored 1 during the POI_i calculation do indeed display a good line width.

However, they do not necessarily display scaffolds that have printed the most accurately from visual observations. This confirmed the importance of measuring the corner drag in addition to the line width in scaffolds. It was important to determine whether the print score proposed in this study compared to the POI. Spearman's rank correlations, confirmed a strong correlation between the print score and the POI, with *r*-values of above 0.8 for all the printing parameters (result in Annexure C).

The visual appearance of the scaffold during the printing process was observed at all times as it was deemed indispensable to establish whether the scaffold would print to 100% completion. The most recent layer of the extruded bioink on top of the scaffold appeared to be wetter than the rest of the scaffold. This was attributed to the decrease in temperature of the hybrid hydrogel once it was extruded from the temperature controlled syringe/cartridge. This layer needed to be warmed to 37ºC (that only took a few seconds) before the following layer could be extruded. In the event that the extrusion pressure and printing speed were not optimal, the scaffolds top layer appeared to start to melt, and this caused the scaffold to self-collapse (Figure 3-13, A).

Figure 3-13B visually displays a scaffold that was able to be printed to 100% completion, before cross-linking occurred. The scaffold appeared to have a more solid colour after cross-linking with a 4% (w/v) $CaCl_2$ solution in comparison to the scaffold colour prior to cross-linking. It was likewise observed that the scaffold size decreased after cross-linking (Figure 3-13, D) and that it decreased even more after being patted dry with a paper towel (Figure 3-13, E). Noentheless, this was attributed to the hybrid hydrogel's ability to retain large amounts of fluids (Roehm, 2018).

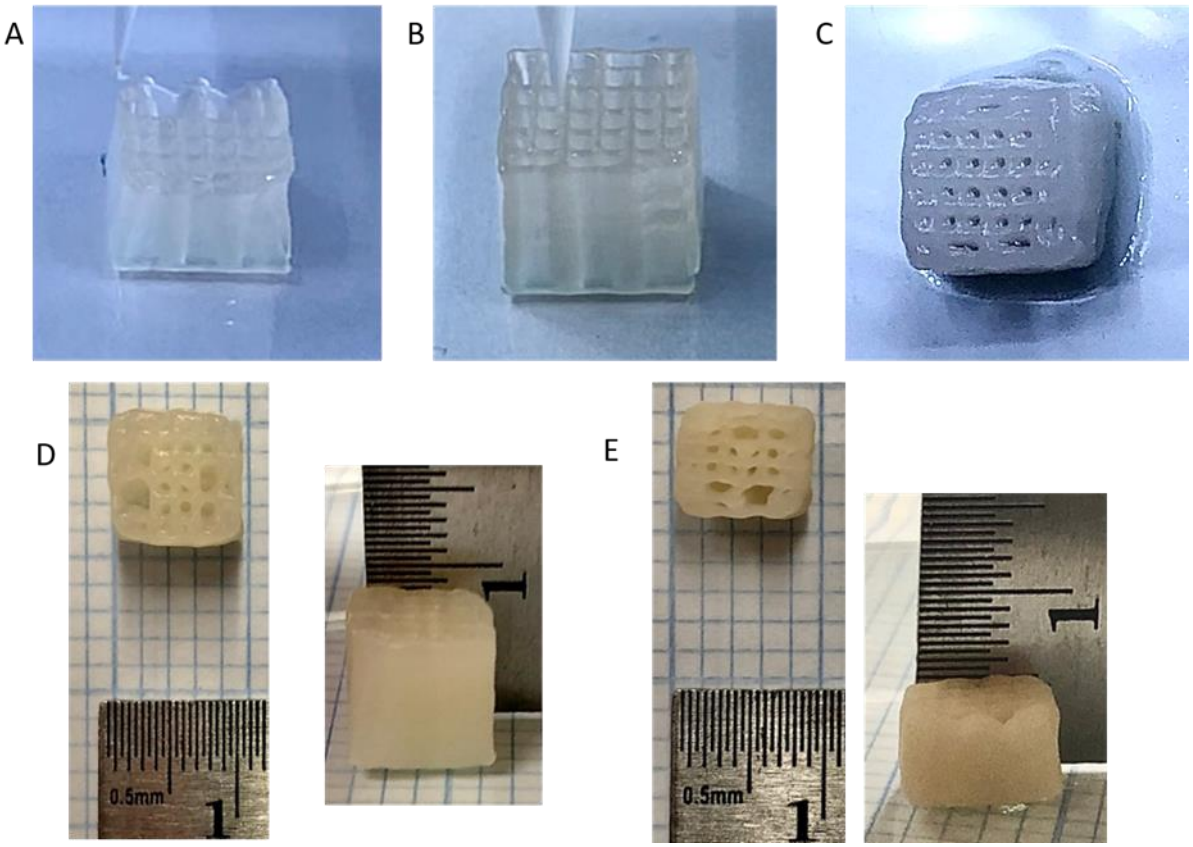

Figure 3-12: **Representative photographs of the scaffold illustrating A) self-collapsing of the structure, B) the scaffold during the printing process at 85-99% completion, C) the effect of cross-linking with 4% $CaCl_2$, D) the scaffold saturated with water and E) the mass loss after drying**

10.9 Swelling ratio

Table 3-1: **Swelling ratio of scaffolds in $CaCl_2$ and dH_2O at 4ºC and 37ºC.**

	SR±SD at 4ºC	*SR±SD at 37ºC*
2% $CaCl_2$	0.697±0.02	0.987±0.04
dH_2O	0.684±0.01	0.958±0.02

The scaffold depicted an average weight of 63.5±13.9mg after being dried for 24h and a swollen mass of 116±26.5mg after 24h in a liquid swelling solution. From Table 3-1 it can clearly be seen that the scaffolds displayed a slightly higher ratio of swelling when submerged in 2% (w/v) $CaCl_2$ in comparison to dH_2O. However, a significant difference was observed between different

temperatures ($p \leq 0.05$). At 4ºC the SR was an average of 0.691±0.04, whereas it was 0.973±0.05 at 37ºC, which was a 70% increase from 4ºC. A study conducted by Mulakkal *et al*. (2018), determined swelling ratios of their formulations with values between 0.82 and 2.6, though, the formulations they used all contained cellulose and were not composed of alginate or PF127. This emphasises the fact that all hydrogels will be characterised differently owing to the unique properties hydrogels could possess.

11 Conclusion

During the printability testing, hybrid hydrogel 1 (4%A:40%PF127) was disqualified from further studies due to too low concentrations of either or both components, and the line volume could also not be maintained after cross-linking. It was also found that the hybrid hydrogel formulation containing only 4% (w/v) alginate did not cross-link sufficiently with the 4% (w/v) $CaCl_2$ cross-linking solution with significantly increased line widths compared to the line widths before cross-linking. It was found that nearly no degradation of any of the hybrid hydrogel discs occurred. This could possibly be ascribed to the addition of the synthetic biopolymer PF127. In a study conducted by Kuo (2002), alginate lyase was added to the hybrid hydrogel formulation to accelerate the degradation rate.

Porosity studies have shown hybrid hydrogel 5 (6%A:46%PF127) portrayed the highest percentage of 50.50%, which is essential in transporting nutrients and waste products in the structure. The selected hybrid hydrogel with concentrations of 4% (w/v) alginate and 46% (w/v) PF127 was determined to be a non-Newtonian fluid. Non-Newtonian fluids display a decrease in viscosity as the shear rate increases, resulting in a lower chance of cell death in the event that live cells are incorporated.

Parameters optimised during this study using hybrid hydrogel 5 (6%A:46%PF127), were extrusion pressure (kPa), printing speed (mm/s), nozzle size (G) and extrusion temperature (ºC). The POI depicted that with an extrusion temperature of 35ºC and 37ºC, using a 22G nozzle, an extrusion pressure of 20kPa and a 15mm/s printing speed, an index value of 1 was attained. For the 25G nozzle at both temperatures, a POI_i of 1 was calculated when a 25kPa extrusion pressure and a 15mm/s printing speed were engaged. The 27G nozzle presented an index value of 1 at an extrusion temperature of 35ºC and 37ºC, with an extrusion pressure of 30kPa and a printing speed of 10mm/s. There was a strong correlation between the print score developed in this study and the POI as developed by Webb and Doyle (2017).

Since the 27G nozzle produced 33 successful prints, according to the printing score for both extrusion temperatures, this nozzle size was concluded to print the hybrid hydrogel the most

accurately. It resulted in the higher number of successful prints when compared to the other nozzle sizes, where some had less than half this number of successful prints. The POI of the 27G nozzle at both temperatures pointed to parameters of 30kPa and 10mm/s being the most optimal. However, from the visual differences observed in Figure 3-10 and 3-11, an extrusion pressure of 70kPa and a printing speed of 30mm/s have produced more accurate scaffold bases after visual inspection and concluding that they will print a scaffold successfully to 100% completion. The swelling ratio demonstrates improved results when it was resubmerged into a swelling medium with a lower pH than dH_2O and at a temperature closer to body temperature (37ºC) than it does when left in the fridge at 4ºC.

This was also confirmed during the optimisation study, where these parameters were the most successful in producing a 10mm x 10mm x 10mm completely printed scaffold. Other parameters tested did not yield a 100% complete print of the scaffolds as they printed less accurately and in some cases too fast, resulting in a significant corner drag, or at other times, too slow; causing the scaffold to self-collapse as it cannot maintain its structure until cross-linking could commence. It can therefore be concluded that the hybrid hydrogel containing 6% (w/v) alginate and 46% (w/v) PF127, mixed in a 2:1 ratio, displayed the most desirable characterisation results and will yield a 100% successfully 3D bioprinted scaffold that will hold its structure until after ionic cross-linking with 4% (w/v) $CaCl_2$, when using a 27G nozzle, 70kPa extrusion pressure and a printing speed of 30mm/s at 37ºC.

Optimisation with smaller nozzle sizes could have a more positive effect on the printing accuracy of the scaffolds and therefore should be considered; however, it should also be kept in mind that decreasing the nozzle size could lead to an increase in shear stress that ultimately has a negative effect on cell proliferation. Previous studies used 30G nozzle sizes successfully to 3D print bioinks into scaffolds that are seeded with live cells, nevertheless, the bioink formulation will play a vital role in the fluid mechanics of the extrusion process.

Acknowledgements

The viscosity measurements were supported in part by the National Research Foundation of South Africa (grant number 105700). The study was funded in part by the National Research Foundation of South Africa (grant numbers 85297 and 129244). Any opinion, finding, and conclusion or recommendation expressed in this material is that of the authors. The South African National Research Foundation does not accept any liability in this regard.

References

1. Berg, J., Hiller, T., Kissner, M.S., Qazi, T.H., Duda, G.N., Hocke, A.C., Hippenstiel, S., Elomaa,L., Weinhart, M., Fahrenson, C. & Kurreck, J. 2018. Optimization of cell-laden bioinks for 3D bioprinting and efficient infection with influenza A virus. *Scientific Reports*, 8:13877.

2. Calejo, M.T., Ilmarinen, T., Skottman, H. & Kellomäki, M. 2018. Breath figures in tissue engineering and drug delivery: State-of-the-art and future perspectives. *Acta Biomaterialia*, 66:44–66.

3. Cao, D., Zhang, Y., Cui, Z., Du, Y. & Shi, Z. 2017. New strategy for design and fabrication of polymer hydrogel with tunable porosity as artificial corneal skirt. *Materials Science & Engineering C*, 70:665–672.

4. Chimene, D., Kaunas, R. & Gaharwar, A.K. 2020. Hydrogel Bioink Reinforcement for Additive Manufacturing: A Focused Review of Emerging Strategies. *Advanced Material Science*, 32:1902026.

5. Choi, H.G., Lee, M.K. & Kim, M.N., 1999. Oxidation Behavior of Hot-pressed Si_3N_4 with Re_2O_3 (Re=Y, Yb, Er, La). *Journal of the European Ceramic Society*, 19:2757–2762.

6. Datta, P., Barui, A., Wu, Y., Ozbolat, V., Moncal, K.K. & Ozbolat, I.T. 2018. Essential steps in bioprinting: From pre- to post-bioprinting. *Biotechnology Advances*, 36:1481–1504.

7. Herrera, C. 2019. The pre-clinical toolbox of pharmacokinetics and pharmacodynamics: *in vitro* and *ex vivo* models. *Frontiers in Pharmacology*, 10:578.

8. Koçak, E., Yıldız, A. & Acartürk, F. 2021. Three dimensional bioprinting technology: Applications in pharmaceutical and biomedical area. *Colloids and Surfaces B: Biointerfaces*, 197:111396

9. Kuo, C.K. 2002. Ionically cross-linked alginate hydrogels as scaffolds for tissue engineering. United States of America: The University of Michigan (Thesis – PhD).

10. Lewicki, J., Bergman, J., Kerins, C. & Hermanson, O. 2019. Optimization of 3D bioprinting of human neuroblastoma cells using sodium alginate hydrogel. *Bioprinting*, 16:e00053.

11. Li, T., Bao, Q., Shen, J., Lalla, R.V. & Bergess, D.J. 2020. Mucoadhesive *in situ* forming gel for oral mucositis pain control. *International Journal of Pharmaceutics*, 580:119238.

12. Ma, X., Liu, J., Zhu, W., Tang, M., Lawrence, N., Yu, C., Gou, M. & Chen, S. 2018. 3D bioprinting of functional tissue models for personalized drug screening and *in vitro* disease modelling. *Advanced Drug Delivery Reviews*, 132:235–251.

13. Mazi, H. & Surmelihindi, B. 2021. Temperature and pH-sensitive Super absorbent Polymers based on Modified Maleic Anhydride. *Journal of Chemical Science*, 133:10.

14. Mironov, V., Trusk, T., Kasyanov, V., Little, S., Swaja, R. & Markwald, R. 2009. Biofabrication: a 21st century manufacturing paradigm. *Biofabrication 1*, 022001.

15. Montalbano, G., Toumpaniari, S., Popov, A., Duan, P., Chen, J., Dalgarno, K., Scott III, W.E. & Ferreira, A.M. 2018. Synthesis of bioinspired collagen/alginate/fibrin based hydrogels for soft tissue engineering. *Materials Science & Engineering C,* 91:236–246.

16. Mulakkal, M., Trask, R., Ting, V. & Seddon, A. 2018. Responsive cellulose-hydrogel composite ink for 4D printing. *Materials and Design,* 160:108–118.

17. Roehm, K. 2018. Bioprinting cell laden structures with chitosan-gelatin for neural tissue applications. United States of America: New Jersey Institute of Technology (Thesis – PhD).

18. O'Brien, F.J. 2011. Biomaterials & scaffolds for tissue engineering. *Materials Today*, 14(3):88-95.

19. Ozbolat, I. & Hospodiuk, M. 2016. Current advances and future perspectives in extrusion-based. *Biomaterials,* 76:321–343.

20. Parak, A., Pradeep, P., Du Toit, L.C., Kumar, P., Choonara, Y.E. & Pillay, V. 2019. Functionalizing bioinks for 3D bioprinting applications. *Drug Discovery Today,* 24:198205.

21. Peng, W., Datta, P., Ayan, B., Ozbola, V., Sosnoski, D. & Ozbolat, I.T. 2017. 3D bioprinting for drug discovery and development in pharmaceutics. *Acta Biomaterialia,* 57:26–46.

22. Trachtenberg, J.E, Placone, J.K., Smith, B.T., Fisher, J.P. & Mikos, A.G. 2017. Extrusion-based 3D printing of poly(propylene fumarate) scaffolds with hydroxyapatite gradients. *Journal of Biomaterial Science: Polymer Edition.,* 28(6):532–554.

23. Tytgat, L., Van Damme, L., Arevalo, M.D.P.O., Declarcq, H., Thienpont, H., Otteveare, H., Blondeel, P., Dubruel, P. & Van Vlierberghe, S. 2019. Extrusion-based 3D printing of photo-cross-linkable gelatin and κ-carrageenan hydrogel blends for adipose tissue regeneration. *International Journal of Biological Macromolecules*, 140:929–938.

24. Vijayavenkataraman, S., Yan, W.C., Lu, W.F., Wang, C.H. & Fuh, J.Y.H. 2018. 3D bioprinting of tissues and organs for regenerative medicine. *Advanced Drug Delivery Reviews,* 32:296–332.

25. Wang, Q.Q., Liu, Y., Zhang, C.J., Zhang, C. & Zhu, P. 2019. Alginate/gelatin blended hydrogel fibers cross-linked by Ca2+ and oxidized starch: Preparation and properties. *Materials Science & Engineering C,* 99:1469–1476.

26. Webb, B. & Doyle, B. 2017. Parameter optimization for 3D bioprinting of hydrogels. *Bioprinting*, 8:8–12.

27. Zhu, W. 2016. 3D printing of functional biomaterials for tissue modeling. San Diego, CA: University of California. (Thesis – PhD).

CHAPTER 4: CONCLUSIONS AND FUTURE RECOMMENDATIONS

4.1 Concluding discussion

In drug discovery and drug delivery research there is a continuing need for valid and reliable alternatives for *in vitro* drug efficacy and toxicity testing (Herrera, 2019). Classic tissue engineering methods have several disadvantages as they lack the ability to fabricate complex biometric structures. This leads to over-simplified tissue constructs that are inaccurate with unrealistic cell microenvironments (Vijayavenkataraman *et al*., 2018). 3D bioprinting allows cell-cell and cell-extracellular matrix interaction, whereas this is absent in 2D tissue constructs (Wu *et al*., 2018). According to Webb and Doyle (2017), there is currently no standard method of comparing bioprint results, and recent papers published focus mainly on the final tissue construct rather than the process. The aim of this study was to establish the optimal printing parameters to successfully 3D print a sustainable scaffold from a preformulated hybrid hydrogel.

Additional to this aim, a suitable hybrid hydrogel had to be formulated as the bioink during the printing process. A hybrid hydrogel was formulated containing alginate, which is a natural biopolymer, and PF127, which is classified as a synthetic biopolymer (Gyles *et al*., 2017). A preliminary hydrogel formulation study was conducted with alginate to determine the optimal alginate concentration needed (Annexure A). PBS was used as aqueous solution wherein the alginate was dissolved. This ensured that the pH would not change and it also assisted in controlling the gelation process that alginate undergoes when being ionically cross-linked.

Alginate gels were made in various concentrations according to Webb & Doyle, (2017). During the preliminary formulation study, the concentration of the ionic cross-linker $CaCl_2$ was also tested and determined. Various studies have used alginate in combination with various polymers in tissue engineering and pneumatic extrusion (Ma *et al*., 2018; Zhang *et al.,* 2020). However, alginate alone does not provide the required shape fidelity to support tissue scaffolds. It was important to have a homogenous gel, with high shape fidelity to be able to investigate the print parameters with pneumatic extrusion.

It was observed that the increasing concentrations of the $CaCl_2$ cross-linker resulted in a firmer, less transparent and non-homogenous alginate gel. Alginate was determined to display the most optimal cross-linking capabilities at 4 and 6% (w/v) after being cross-linked with a 2% (w/v) $CaCl_2$ cross-linking solution. It was concluded that cross-linking prior to the printing process was not possible and had to occur during, and post printing (Chapter 3, Annexure A).

A hybrid hydrogel formulation study was conducted, and PF127 was added into 4 and 6% alginate (A) solutions in concentrations of 40, 46 and 50% (w/v) in a 2:1 (A:PF127) ratio. Degradation/stability and porosity tests, described by Montalbano *et al.* (2018) and Cao *et al*. (2017), were adapted and conducted on the proposed formulations. Hybrid hydrogel 5 (6%A:46%PF127) was proved to be the most successful hybrid hydrogel formulation. It was a stable hybrid hydrogel as it did not degrade within a week and possessed an average porosity of 50.5% (Annexure B, Chapter 3).

Rheological studies were done on an ARES-G2 Rheometer (TA instruments, New Castle, DE), where viscosity and stress were tested over an increasing shear rate while temperature and step time were kept constant. The apparent viscosity of the selected hybrid hydrogel formulation decreased as the shear rate increased, characterising the hybrid hydrogel formulation as being a non-Newtonian fluid. This hybrid hydrogel formulation was used in the print parameter optimisation study (Annexure B, Chapter 3).

The hybrid hydrogel composed of 6% (w/v) alginate and 46% (w/v) PF127, was concluded to be the most optimal for printing parameter optimisation with the BioX™ pneumatic bioprinter from Cellink® (Gothenburg, Sweden). Pneumatic-based extrusion allows for the air pressure to be controlled and subsequently it has a higher success rate when printing with cell-laden bioinks (Roehm, 2018; Vijayavenkataraman *et al*., 2018). The original cross-linking concentration of 2% (w/v) $CaCl_2$, was ultimately disregarded as a higher concentration of at least 4% (w/v) $CaCl_2$ was needed for successful cross-linking of the hybrid hydrogel. This could be attributed to the addition of the PF127, which does not participate in ionic cross-linking.

The aforementioned bioprinter is equipped with intelligent printhead mounts and a printbed that allows for temperature control between 4 and 250ºC. Subsequently, the printing process could occur at 35 and 37ºC. The hybrid hydrogel was loaded into the pneumatic syringes (that also act as the print cartridge) using an adapter that has a connection for a simple mechanical syringe to be inserted into, that screwed onto the nozzle connection point of the syringe. The cartridge was placed into the intelligent printhead mounts, tightened and heated to the required temperature.

A preselected CAD model with dimensions of 10mm x10mm x 10mm, was used for the line tests as well as the print parameter optimisation study. It was printed without a grid infill and stopped after the first layer was extruded and photographed. For the print parameter optimisation study, the CAD model was printed with a grid infill pattern (Figure 3-1) between 8 to 12% completion, where after it was also photographed (Annexure A, Annexure C).

An adaptation of the single fibre extrusion test, described by Trachtenberg *et al.* (2016), was conducted on six proposed hybrid hydrogel formulations to determine the optimal concentrations of each respective hybrid hydrogel component. During the line test study, the printing parameters, as described, were all kept constant to ensure that the formulations could be compared (Annexure B).

Printing parameters that were taken into consideration for optimisation were as follows: nozzle size (G), extrusion pressure (kPa), extrusion time (mm/s) and extrusion temperature (ºC). Parameters were divided into six groups, where extrusion temperature and nozzle size were kept as constants, and extrusion time and pressure values were compared within these parameters. It was determined that hybrid hydrogel 5 (6%A:46%PF127) was 3D printed into a scaffold more accurate and successfully with an extrusion temperature of 37ºC, using a nozzle size of 27G. The parameter optimisation index (POI) that explains how the parameters influence each other (Webb & Doyle, 2017; Lewicki *et al*., 2019) was utilised in combination with a newly formulated grading method that allowed for scaffolds to be compared although they were created using differentiating parameters (Annexure C).

These parameters were used for further experimentation, including extrusion time and pressure optimisation. A wide range of each of these parameters was tested and it was concluded that a range between 25 and 35mm/s and 65 and 75kPa, respectively, could be successfully printed up to 70 to 80% completion. Within these ranges tested, it was discovered that a printing speed of 30mm/s and a 70kPa extrusion pressure yielded a 100% successfully 3D printed scaffold. The cross-linking solution used to cross-link the scaffold also had to be optimised. A 4% (w/v) $CaCl_2$ cross-linking solution was determined to be the optimal concentration for successful cross-linking. The cross-linking solution was heated before it was dripped over the printed scaffold to ensure it will hold its structure during the cross-linking process. The scaffold was then completely submerged within the heated $CaCl_2$ solution and placed in an incubator for 24h to ensure complete cross-linking ensued (Annexure C).

After complete cross-linking, it was found that PF127 forms part of the scaffold structure as it does not weigh less after being placed in the fridge for 24h to determine whether PF127 melts out of the structure or not. Swelling ratio and viscosity studies were conducted with cross-linked scaffolds, as described by Wang *et al*. (2019). Hydrogels have the ability to retain large amounts fluid (Rashid *et al*., 2019; Gyles *et al*., 2017) and this could be seen in the SR study results (Annexure C, Chapter 3).

The specific research question of this study was to systematically optimise the printing parameter required to successfully 3D print a preselected CAD model to 100% completion using a

preformulated hybrid hydrogel. It was, therefore, concluded that the optimal printing parameters for the 10mm x 10mm x 10mm preselected CAD model, to print a scaffold to 100% completion with a grid infill pattern, were a printing speed of 30mm/s with an extrusion pressure of 70kPa, while the extrusion temperature and print bed were kept at 37ºC and a 27G nozzle was used.

Utilising a combination of the POI and newly formulated scoring method contributed immensely to the selection process to determine the optimal printing parameters; however, the visual appearance of the scaffolds has shown to be just as an important to consider when selecting optimal printing parameters, since the highest scoring scaffolds within the groups failed to yield a 100% successful print. This newly formulated scoring method can subsequently not be used alone to determine the optimal printing parameters and should therefore be utilised with the visual appearance and other grading methods, such as the POI.

These results have yielded optimal printing parameters that allowed for a scaffold to be 100% completely and successfully 3D printed and cross-linked, which could contribute to further tissue engineering scaffold models to be utilised in the field of alternative drug efficacy and toxicity testing whenever an alginate and PF127 (or similar poloxamers) hybrid hydrogel have to be used as bioink.

4.2 Limitations and recommendations

Preliminary hydrogel formulation included alginate gels in various concentrations being cross-linked with an ionic cross-linker, namely $CaCl_2$ to determine the optimal concentration alginate needed, in combination with gelatine. However, gelatine cross-linking was unsuccessful and consequently removed from the formulation. This component could have possibly contributed to a more positive outcome on structural integrity (Berg *et al*., 2017), and should be investigated for further parameter optimisation with regards to gelatine-containing hydrogels. This would therefore ensure a more natural bioink with fewer negative effects on live cells when they are included into a formulation.

Alginate did not degrade as fast as was hypothesised, which proved the stability of the hybrid hydrogel, which could lead to a delay in the degradation process of the alginate, which is necessary in the event that tissue constructs are printed. In a study conducted by Kuo (2002), it was observed that the alginate lyase enzyme can be added to the solution to increase the degradation time of the alginate scaffold. When working with live cells and tissue, this important factor should be taken into consideration, and a hybrid hydrogel containing this enzyme should possibly be formulated and tested.

The SR of the 3D printed scaffolds were conducted in dH_2O and a 2% (w/v) $CaCl_2$ solution which yielded significant results, however, these solutions' pH values are lower than that of the humans natural physiology. Thus, evaluating the SR in a phosphate buffer with a pH that is more relevant to the human physiology would yield results of higher value in the event that live cells are incorporated into the hybrid hydrogel. Physicomechanical studies could also be conducted in the future for example studies to determine the deformation energy and tensile strength, which could possibly elevate the results and characteristics of the printed scaffolds.

A very specific hybrid hydrogel was formulated containing predetermined amounts of each respective component, and therefore, these optimised parameters are only of value if a similar hybrid hydrogel is to be formulated for further studies. Print parameter optimisation for various hybrid hydrogels could be tested in the future, as they should all have differences in optimal printing parameters, which all contribute different characteristics within the hybrid hydrogels. This would ensure that optimal printing parameters could be found for different biopolymers available for bioink formulation studies, and could therefore be used for further studies, biomedical applications, or as drug efficacy and toxicity 3D models.

The formulated hybrid hydrogel contained PF127, used in high concentrations (30% (w/v) and higher), which can have a negative effect on cell proliferation, and therefore it can be recommended that future studies should consider using a lower concentration to better the chances of cell growth within the structure. Although PF127 can be used to establish print parameters, especially when new 3D bioprinters are being developed, there is clear need for the design and development of other polymer support materials.

4.3 References

1. Berg, J., Hiller, T., Kissner, M.S., Qazi, T.H., Duda, G.N., Hocke, A.C., Hippenstiel, S., Elomaa, L., Weinhart, M., Fahrenson, C. & Kurreck, J. 2018. Optimization of cell-laden bioinks for 3D bioprinting and efficient infection with influenza A virus. *Scientific Reports*, 8:13877.

2. Cao, D., Zhang, Y., Cui, Z., Du, Y. & Shi, Z. 2017. New strategy for design and fabrication of polymer hydrogel with tunable porosity as artificial corneal skirt. *Materials Science & Engineering C*, 70:665–672.

3. Gyles, D.A., Castro, L.D., Silva, J.O.C. Jnr. & Ribeiro-Costa, R.M. 2017. A review of the designs and prominent biomedical advances of natural and synthetic hydrogel formulations. *European Polymer Journal*, 88:373–392.

4. Herrera, C. 2019. The pre-clinical toolbox of pharmacokinetics and pharmacodynamics: *in vitro* and ex vivo models. *Frontiers in Pharmacology*, 10:578.

5. Kuo, C.K. 2002. Ionically cross-linked alginate hydrogels as scaffolds for tissue engineering. United States of America: The University of Michigan (Thesis – PhD).

6. Lewicki, J., Bergman, J., Kerins, C. & Hermanson, O. 2019. Optimization of 3D bioprinting of human neuroblastoma cells using sodium alginate hydrogel. *Bioprinting*, 16:e00053.

7. Ma, X., Liu, J., Zhu, W., Tang, M., Lawrence, N., Yu, C., Gou, M. & Chen, S. 2018. 3D bioprinting of functional tissue models for personalized drug screening and *in vitro* disease modelling. *Advanced Drug Delivery Reviews*, 132:235–251.

8. Montalbano, G., Toumpaniari, S., Popov, A., Duan, P., Chen, J., Dalgarno, K., Scott III, W.E. & Ferreira, A.M. 2018. Synthesis of bioinspired collagen/alginate/fibrin based hydrogels for soft tissue engineering. *Materials Science & Engineering C*, 91:236–246.

9. Rashid, F., Albayati, M. & Dodou, K. 2019. Studies on Novel Methods for Formulating Novel Cross-Linked Hydrogel Films of Hyaluronic Acid. *Cosmetics*, 6(59):2–19.

10. Roehm, K. 2018. Bioprinting cell laden structures with chitosan-gelatin for neural tissue applications. United States of America: New Jersey Institute of Technology (Thesis – PhD).

11. Trachtenberg, J.E., Placone, J.K., Smith, B.T., Fisher, J.P. & Mikos, A.G. 2017. Extrusion-based 3D printing of poly(propylene fumarate) scaffolds with hydroxyapatite gradients. *Journal of Biomaterial Science*: *Polymer Edition*, 28(6):532–554.

12. Wu, Y., Lin, Z.Y.W., Wenger, A.C., Tam, K.C. & Tanga, X.S. 2018. 3D bioprinting of liver-mimetic construct with alginate/cellulose nanocrystal hybrid bioink. *Bioprinting*, 9:1–6.

13. Vijayavenkataraman, S., Yan, W.C., Lu, W.F., Wang, C.H. & Fuh, J.Y.H. 2018. 3D bioprinting of tissues and organs for regenerative medicine. *Advanced Drug Delivery Reviews*, 32:296–332.

14. Wang, Q.Q., Liu, Y., Zhang, C.J., Zhang, C. & Zhu, P. 2019. Alginate/gelatin blended hydrogel fibers cross-linked by Ca2+ and oxidized starch: Preparation and properties. *Materials Science & Engineering C,* 99:1469–1476.

15. Webb, B. & Doyle, B. 2017. Parameter optimization for 3D bioprinting of hydrogels. *Bioprinting*, 8:8–12.

16. Zhang, S., Gao, H., Guo, P., Li,T., Lin, T., Ding, R., Wang, Z. & He, P. 2020. Fabrication and extrusion of the PAAm-SAlg hydrogels with magnetic particles. *Colloids and Surfaces A*, 603:125280.

ANNEXURE A: FORMULATION AND EVALUATION OF HYBRID HYDROGEL BIOINK

A.1 Introduction

The first important step in the 3D bioprinting process is the formulation of a bioink that is suited for a tissue scaffold. In this study it was decided to formulate a hybrid hydrogel bioink from biomaterials. Hydrogels are defined as 3D porous networks of hydrophilic polymers that are cross-linked and capable of retaining large amounts of biological fluids. Owing to their high biocompatibility, they demonstrate a similar structure to the extracellular matrix (ECM) (Wang *et al*., 2018). Moreover, due to these properties, hydrogels are the ideal candidate for bioink formulation when working with live cells or soft tissue (Vijayavenkataraman *et al*., 2018). Characterisation and optimisation of a formulated hybrid hydrogel is of importance because this influences the viability/possibility of successful printing as well as the integrity and properties of the printed scaffold (Chimene *et al.,* 2018)

The aim of formulating and optimising a suitable hybrid hydrogel/bioink is to ensure that it is capable of retaining its structure while in printing as well as during the post printing process when cross-linking is transpiring. Controlling the properties of the hyrbid hydrogel formulation before cross-linking, during the printing process and after cross-linking are important aspects to investigate in the optimisation process of a bioink. Cross-linking the scaffold after the printing process causes the existing polymer chains to cross-link together, forming more chains and resulting in a stiffer network. Conventional hydrogels are typically liquid polymer solutions prior to cross-linking, and therefore they cannot hold a subsequent layer as they lack the intrinsic fracture energy and mechanical dissipation capabilities needed to provide a structurally sound scaffold. Cross-linking is consequently vital for the polymer network structure to form (Chimene *et al*., 2020).

Hydrogels can have a wide range of applications such as drug delivery systems, skin burn treatment and cosmetic uses. The end product to be produced from the hydrogel will therefore determine what properties the hydrogel should possess. The characteristics of conventional hydrogels allow them to mimic the ECM as well as their highly porous network and permeability allow for rapid nutrient and oxygen diffusion throughout the scaffold, rendering them nearly the universal choice for 3D printing. The limitation of conventional hydrogels is that they are unable to sustain a subsequent layer since most of these gels are liquid polymer solutions (Chimene *et al.,* 2020). However, polymers can be added to increase certain desired characteristics, since hydrogel properties should be tailored to the specific bioprinting method that is going to be applied (Hölzl *et al*., 2016; Panwar & Tan, 2016).

A.2 Experimental design

The planned methods for this study were based on the three phases of the bioprinting process (Vijayavenkataraman *et al*., 2018; Varkey *et al*., 2019) as outlined in Figure 1-2 in Chapter 1 section 1.2.3, namely pre-processing, processing and post-processing. The formulation and evaluation of the hybrid hydrogel formed part of the pre-processing phase to create a suitable bioink with desirable characteristics that ensured successful printing.

A.3 Materials

The materials used for this study fell into the category of a natural biopolymer and a synthetic, nontoxic poloxamers. The formulation used in the study can therefore be regarded as a hybrid hydrogel, which has slowly been replacing natural hydrogels as they provide a higher gel strength and water absorption capacity (Gyles *et al*., 2017; Chimene *et al*., 2020). Alginic acid sodium salt (powder, 180947), phosphate buffered saline (PBS) (powder, P3813), anhydrous calcium chloride (granules, C1016) and Pluronic F-127 (powder, P2443) were purchased from Sigma-Aldrich (Merck, Darmstadt, Germany). They are discussed in Chapter 2 section 2.6 and 2.8.

A.4 Composition of bioink

The initial bioink was formulated using the biopolymer alginate, in various combinations, ionically cross-linked to enable gelling. Concentrations of 2, 4, 6 and 8% (w/v) were prepared and their cross-linking capabilities with various cross-linker concentrations including 0.5, 1.0, 1.5, and 2.0% (w/v) were evaluated. PF127 was added after evaluation of the alginate, in concentrations of 40, 46 and 50% (w/v). Cross-linking the alginate/PF127 hybrid hydrogel with 2% (w/v) $CaCl_2$ was found to be unsuccessful and the cross-linking concentration was increased to 4% (w/v). These materials are discussed in Chapter 2 sections 2.6 and 2.8.

A.5 Biopolymer cross-linking

Alginate had to undergo ionic cross-linking with a $CaCl_2$ solution for polymer chains to be formed that resulted in a stiff and rigid gel. This ensured that the bioink/hybrid hydrogel maintained the 3D scaffold form it was printed into. Cations, such as Ca^{2+}, have been found to cause rapid gelation of alginate; nonetheless, it was also discovered that thereafter the viscosity could possibly be too high. In this same study, it was proven that alginate was furthermore cross-linked by submerging it in a $CaCl_2$ solution (Berg *et al*., 2018). Although alginate undergoes ionic cross-linking with $CaCl_2$, it typically leads to rapid and poorly controlled gelation. Subsequently, PBS was used as a buffer to slow and control the gelation, because the phosphate groups compete with the carboxylate groups of alginate in the reaction with the calcium ions (Lee & Mooney, 2012).

A.5.1 Cross-linker $CaCl_2$ preparation

$CaCl_2$ was prepared by dissolving 40g into room temperature dH_2O (at approximately 22–24ºC) to create 1l of a 4.0% (w/v) solution. The solution was kept overnight at room temperature (22–24ºC) to ensure the solution had reached equilibrium. The 4.0% (w/v) $CaCl_2$ was diluted to a 0.5, 1.0, 1.5 and a 2.0% (w/v) (Paxton *et al*., 2019) solution by adding dH_2O. The 4% (w/v) $CaCl_2$ was only used for the hybrid hydrogel cross-linking, as 2% (w/v) $CaCl_2$ was deemed insufficient during the line test conduction.

A.6 Alginate formulation method

Alginate solutions were prepared in 30ml PBS at concentrations 2, 4, 6 and 8% (w/v) as described by Berg *et al*. (2017). PBS was prepared according to the manufacturer's instructions. The PBS was heated to 40ºC before the alginate powder was gradually added and stirred for 10min at 40ºC. After the alginate powder had dissolved it had the consistency of syrup. The solution was left in the fridge at 4ºC for 24h which allowed the solution to settle and air bubbles to escape. After 24h at 4ºC, the alginate had no bubbles and had a higher consistency/viscosity as when it does when warmed.

Alginate was tested to determine how successful cross-linking with various $CaCl_2$ concentrations including 0.5, 1.0, 1.5 and 2.0% (w/v) was. $CaCl_2$ (approximately 10ml) was gradually added to each respective concentration of alginate mixture and mixed thoroughly with a spatula tool. This resulted in non-uniform, lumpy cross-linking of the alginate that resulted in a non-homogenous gel. The severity of non-uniform lumps forming after cross-linking was dependent on the respective concentrations of the alginate and $CaCl_2$ and was caused by the disruption of the polymer chains that formed during cross-linking (Chimene *et al*., 2020). Alginate could not be cross-linked before being printed. The cross-linking capabilities of the respective amounts of alginate and $CaCl_2$ were determined during this part of the study.

A.6.1 Gelling properties of the alginate solution

Each formulation was photographed with an iPhone 8 plus equipped with a 12-megapixel wide-angle and telephoto lens and the vial-tilt test was used to describe the gelling properties of the alginate. This method was adapted from Marwan *et al*. (2017). The alginate was prepared as described previously and after 24h refrigeration at 4ºC, the beakers were removed and left at room temperature (22–24ºC) for 30min. After the alginate solutions were at room temperature (22–24ºC), they were inverted to monitor their ability to flow.

The alginate solutions were photographed before and after cross-linking with 0.5, 1.0, 1.5 and 2.0% (w/v) $CaCl_2$ concentrations. Each cross-linker concentration was tested in each

concentration of the alginate solutions (2, 4, 6, and 8% w/v) and was tilted after cross-linking to display how easily the solutions flowed, whether two phases could be observed, and whether complete cross-linking had taken place. Complete cross-linking for this part of the formulation study was a visible phase change from a complete liquid to a semi-solid. The visual display of a semi-solid complete cross-linked solution can be observed in Table A.1, 6% (w/v) alginate after 2% (w/v) $CaCl_2$ cross-linking. If the semi-solid phase and the liquid phase were present in one alginate solution, it was assumed that complete cross-linking of the alginate did not yet occur.

A.6.2 Results

Important requirements in the formulation of a hybrid hydrogel that is used as bioink, are that the materials used in combination should result in a vicious enough liquid that could be loaded into the print cartridges (syringes) for pneumatic extrusion (Chimene *et al.,* 2020) which is displayed in Figures 1-1 and 2-1. The ideal alginate solution had to have the same viscosity as syrup. It had to present with the capacity to still flow (less than water) when it was tilted sideways as seen in Table A-1, before cross-linking.

Successful cross-linking was regarded as when the entire content of the beaker was cross-linked with the predetermined amount of a certain concentration of the cross-linker as seen in Table A-1, under 6% (w/v) alginate after 2% (w/v) $CaCl_2$ cross-linking. Two phases could be observed when alginate was not completely/successfully cross-linked (Table A.1, 2% (w/v) alginate after 2% (w/v) $CaCl_2$ cross-linking), while only non-uniform semi-solid lumps were visible when the alginate was completely cross-linked (Table A.1, 6 and 8% (w/v) alginate after 2% (w/v) cross-linking). Stirring the cross-linker into the alginate caused a disruption of the polymer chains that had formed during cross-linking (Chimene *et al*., 2020), which resulted in a very lumpy gel as can be seen in Table A-1.

Table A-1: Visual representation of alginate solutions with concentrations from 2 to 8% (w/v) before cross-linking and cross-linked with 0.5–2.0% (w/v) $CaCl_2$

	2% alginate	*4% alginate*	*6% alginate*	*8% alginate*
Before cross-linking				
After 0.5% $CaCl_2$ cross-linking				
After 1.0% CaCl2 cross-linking				
After 1.5% CaCl2 cross-linking				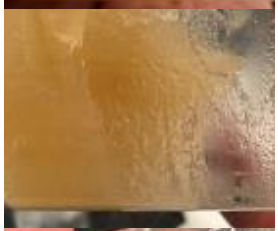
After 2.0% CaCl2 cross-linking				

From the images presented in Table A.1, it was observed that the increasing concentrations of the $CaCl_2$ cross-linker resulted in a firmer, less transparent and non-homogenous gel. Cross-linking started taking place the moment the cross-linker came into contact with the alginate. During the cross-linking process, the solution was continuously stirred and this resulted in the polymer chains that were formed during cross-linking to be disrupted or broken. This meant that alginate could not be reformed into a new structure after the cross-linking process, since it led to a lumpy and non-homogeneous solution/semi-solid as seen in Table A-1. Cross-linking of alginate had to take place after printing it into the 3D scaffold.

Alginate concentrations below 6% (w/v) led to unsuccessful cross-linking, which can be seen in the pictures in Table A.1. After cross-linking with the highest concentration $CaCl_2$ solution, the

alginate still appeared to have a liquid phase present in the 2 and 4% (w/v) alginate where there was no liquid phase visible in the 6 and 8% (w/v) alginate. Another biopolymer was added as alginate alone was not a firm enough hydrogel by itself to be printed into a scaffold before the cross-linking process and could not be used alone to fabricate a new scaffold (Chimene *et al*., 2020). The 2% (w/v) alginate gel was disqualified since they did not result in complete cross-linking. The 8% (w/v) alginate gel resulted in an unusually thick gel and was also disqualified. According to the study conducted by Webb and Doyle (2017), a 7% (w/v) concentration of alginate within an alginate-gelatine hydrogel was successfully 3D printed using optimised parameters.

A.7 Alginate/PF127 hybrid hydrogel

PF127 was subsequently introduced into the alginate base hydrogel as this compound shows reverse thermoresponsive properties in aqueous solutions that have various applications in gelling systems (Grassi *et al*., 2006; Rarokar *et al*., 2018). It had to be prepared using the 'cold method' as PF127's gelation process started as the temperature increased and the flakes only dissolved in water at 4ºC. This synthetic poloxamer is described as being chemically inert, and therefore it did not participate in ionic cross-linking like alginate (Rarokar *et al*., 2018; Yap & Yang, 2016). This compound gave the gel the structural integrity at 37ºC while the printing process was happening, before the alginate could be cross-linked, and held the structure as is while cross-linking transpired. After the scaffold was cross-linked with 4% (w/v) $CaCl_2$ solution, it was left in the fridge at 4ºC to determine whether the PF127 separated out of the cross-linked structure, as the PF127 did not react with the cross-linker. During the line test conduction, it was discovered that cross-linking of the lines printed with a 2% (w/v) $CaCl_2$ solution was deemed unsuccessful since it did not cross-link the alginate component fast or efficiently enough to maintain the printed line. This caused the samples to become unusable since no measurements could be taken after 2% (w/v) $CaCl_2$ cross-linking. This led to the increase in the cross-linker solution concentration to 4% (w/v) $CaCl_2$.

A.7.1 Alginate/Pluronic F-127 formulation method

Distilled H_2O was refrigerated to 4ºC before PF127 was dissolved. The respective amounts of 40g, 46g and 50g PF127 were placed into containers and were made up to volume with 4ºC dH_2O (100ml). The containers were sealed and shaken for 5 minutes. The mixture was left in the fridge at 4ºC to ensure that the PF127 crystals had completely dissolved into the dH_2O. After 24h in the fridge at 4ºC, some of the crystals had still not dissolved and the mixture was shaken daily and left in the fridge until no more crystals or lumps were visible. This process took two to four days, the highest concentration taking longer to completely dissolve.

Six proposed alginate and PF127 formulations were prepared. Alginate and PF127 were mixed together in a 2:1 ratio (Grassi *et al*., 2006), respectively, to ensure that more than 50% of the hybrid hydrogel consisted of alginate for successful cross-linking:

Hybrid hydrogel 1: 4% (w/v) Alginate + 40% (w/v) PF127

Hybrid hydrogel 2: 4% (w/v) Alginate + 46% (w/v) PF127

Hybrid hydrogel 3: 4% (w/v) Alginate + 50% (w/v) PF127

Hybrid hydrogel 4: 6% (w/v) Alginate + 40% (w/v) PF127

Hybrid hydrogel 5: 6% (w/v) Alginate + 46% (w/v) PF127

Hybrid hydrogel 6: 6% (w/v) Alginate + 50% (w/v) PF127

A.7.2 Characterisation of alginate/PF127 hybrid hydrogel

Drops of each formulation were made onto a petri dish and photographed before and after gelation occurred. Gelation of these hybrid hydrogels was temperature dependent as the PF127 gelation is temperature and concentration dependent, and therefore the petri dish was heated to 37ºC. The visual appearance of each formulation was observed and compared to one another. The ideal hybrid hydrogel should completely gel at 37ºC as this was cause by the PF127 component, and should not have flowed at all if it was tilted. Hybrid hydrogels that flowed easily while tilted were labelled unstable, whereas gels that had no flow and remained intact with the shape of the petri dish were labelled stable (Marwan *et al*., 2017).

A.7.3 Results

Table A-2: Characterisation of alginate (A) and PF127 hybrid hydrogel bioink formulations

	Hybrid hydrogel 1 ***(4%A:40%PF127)***	*Hybrid hydrogel 2* ***(4%A:46%PF127)***	*Hybrid hydrogel 3* ***(4%A:50%PF127)***	*Hybrid hydrogel 4* ***(6%A:40%PF127)***	*Hybrid hydrogel 5* ***(6%A:46%PF127)***	*Hybrid hydrogel 6* ***(6%A:50%PF127)***
Physical appearance before gelation						
Physical appearance after gelation *(held at an angle)*						
Transparency	Translucent	Greenish translucent, turning opaque after gelation	Greenish translucent, turning opaque after gelation	Greenish translucent, turning opaque after gelation	Greenish translucent, turning opaque after gelation	Greenish translucent, turning opaque after gelation
Texture	Smooth	Smooth, with an uneven surface after gelation	Smooth	Smooth, with an uneven surface after gelation	Smooth, with an uneven surface after gelation	Smooth, with an uneven surface after gelation
Homogeneity	No crystals/ bubbles	No crystals, bubbles caused by mixing.	No crystals/ bubbles	No crystals, bubbles caused by mixing	No crystals, bubbles caused by mixing.	Small crystals, bubbles caused by mixing.
Stability	Phase separation	Phase separation	Phase separation	Phase separation	Phase separation	Phase separation

Table A-2 provides a summary of the physical characteristics of the hybrid hydrogel bioinks. Hybrid hydrogel 1 (4%A:40%PF127) had a lower amount of PF127 and alginate, which resulted in a less stiff gel that can be observed in Table A-2, and when tilted the hybrid hydrogel had started to flow. This placed hybrid hydrogel 1 (4%A:40%PF127) in the category of being an unstable gel (Marwan *et al.*, 2017). All the other hybrid hydrogels had sufficient amounts and ratios of the alginate and PF127 combined to produce stiff hybrid hydrogels after gelation.

According to a study conducted by Webb and Doyle (2017), they had made successful hybrid hydrogels with alginate concentrations of up to 7% (w/v).

Alginate hybrid hydrogels will always have a greenish-brown appearance, since this is its natural color, while PF127, when in solution alone, provides a crystal clear gel. These two combined will still result in a greenish-brown coloured gel. The hybrid hydrogel was semi-transparent before cross-linking, but the tight polymer chains formed during cross-linking resulted in the gel turning opaque, as seen in Table A.1. The texture should be smooth and homogenous. Phase separation doe occur between alginate and PF127 before cross-linking, but a thorough stir resulted in a homogenous mixture again. There was no phase separation of the alginate and PF127 after gelation and cross-linking.

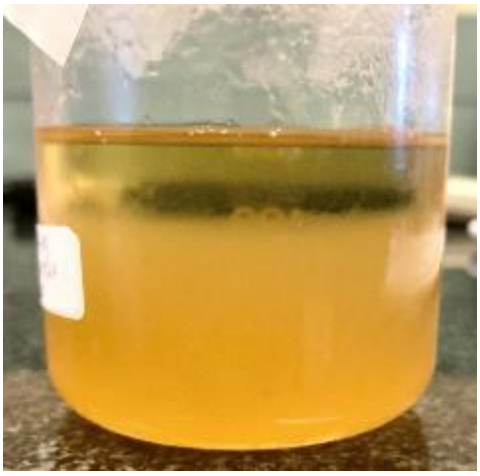

Figure A-1: Phase separation of alginate and PF127 as described in Table A-2

A.8 Conclusion

It was concluded that a $CaCl_2$ concentration of 4% (w/v) was required for successful cross-linking of the hybrid hydrogel. Alginate concentrations of 4 and 6% (w/v) were deemed successful to continue further studies in combination with 40, 46, and 50% (w/v) PF127. Concentrations of 50% (w/v) PF127 are regarded as too high for this study as it resulted in a lower degree of alginate cross-linking.

A.9 References

1. Berg, J., Hiller, T., Kissner, M.S., Qazi, T.H., Duda, G.N., Hocke, A.C., Hippenstiel, S., Elomaa, 488 L., Weinhart, M., Fahrenson, C. & Kurreck, J. 2018. Optimization of cell-laden bioinks for 3D 489 bioprinting and efficient infection with influenza A virus. *Scientific Reports,* 8:13877.

2. Chimene, D., Kaunas, R. & Gaharwar, A.K. 2020. Hydrogel Bioink Reinforcement for Additive Manufacturing: A Focused Review of Emerging Strategies. *Advanced Material Science*, 32:1902026.

3. Grassi, G., Crevatin, A., Farra, R., Guarnieri, G., Pascotto, A., Rehimers, B., Lapasin, R. & Grassi, M. 2006. Rheological properties of aqueous Pluronic-alginate systems containing liposomes. *Journal of Colloid and Interface Science*, 301:282–290.

4. Gyles, D.A., Castro, L.D., Silva, J.O.C. Jnr. & Ribeiro-Costa, R.M. 2017. A review of the designs and prominent biomedical advances of natural and synthetic hydrogel formulations. European Polymer Journal, 88:373–392.

5. Hölzl, K., Lin, S., Tytgat, L., Van Vlierberghe, S., Gu, L. & Ovsianikov, A. 2016. Bioink properties before, during and after 3D bioprinting. *Biofabrocation*, 8:032022.

6. Lee, K.Y. & Mooney, D.J. 2012. Alginate: Properties and biomedical applications. *Progress in Polymer Science*, 37:106–126.

7. Marwan, A.I., Williams, S.M., Bardill, J.R, Gralla, J., Abdul-Aziz, N.M. & Park, D. 2017. Reverse Thermal Gel for In Utero Coverage of Spina Bifida Defects: An Innovative Bioengineering Alternative to Open Fetal Repair. *Macromolecular Bioscience*, 17:1600473.

8. Panwar, A. & Tan, L. 2016. Current status of bioinks for micro-extrusion-based 3D bioprinting. *Molecules,* 1:2–26.

9. Paxton, N.C., Allenby, M.C., Lewis, P.M. & Woodruff, M.A. 2019. Biomedical applications of polyethylene. *European Polymer Journal*, 118:412–428.

10. Rarokar, N.R., Saoji, S.D. & Khedekar, P.B. 2018. Investigation of effectiveness of some extensively used polymers on thermoreversible properties of Pluronic tri-block copolymers. *Journal of Drug Delivery Science and Technology*, 44:220–230.

11. Varkey, M., Visscher, D.O., Van Zuijlen, P.P.M., Atala, A. & Yoo, J.J. 2019. Skin bioprinting: the future of burn wound reconstruction?. *Burns & Trauma.* 7(4):3.

12. Vijayavenkataraman, S., Yan, W.C., Lu, W.F., Wang, C.H. & Fuh, J.Y.H. 2018. 3D bioprinting of tissues and organs for regenerative medicine. *Advanced Drug Delivery Reviews*, 32:296–332.

13. Wang, L., Neumann, M., Fu, T., Li, W., Cheng, X. & Su, B.L, 2018. Porous and responsive 581 hydrogels for cell therapy. *Colloid & Interface Science,* 38:135–157.

14. Webb, B. & Doyle, B. 2017. Parameter optimization for 3D bioprinting of hydrogels. *Bioprinting*, 8:8–12.

15. Yap, L.S. & Yang, M.C. 2016. Evaluation of hydrogel composing of Pluronic F127 and carboxymethyl hexanoyl chitosan as injectable scaffold for tissue engineering applications. *Colloids and Surfaces B: Biointerfaces*, 146:204–211.

ANNEXURE B: PRINTABILITY OF ALGINATE PF127 HYBRID HYDROGEL

B.1 Introduction

3D printing can be defined as the stacking and assembling of organic materials containing living cells and other biological inks (bioinks) in spatial patterns by using a computer-aided layer-by-layer deposition approach creating a well-arranged 3D structure. The 3D structure can be any design, but most tissue constructs use a scaffold architecture in a geometric pattern (grid with different pore sizes) (Datta *et al*., 2018; O'Brien, 2011; Ozbolat & Hospodiuk, 2016). Bioinks are extruded by means of mechanical or pneumatic forces through a nozzle (Bishop, 2017).

Successful 3D bioprinting relies on two characteristics: cell viability and geometric accuracy. Both these characteristics depend on the properties of the biomaterial being used, and are both influenced by the bioprinting parameters (Webb & Doyle, 2017). The printability of the bioink/hybrid hydrogel should present with structural precision and accuracy post printing, withstand forces during the printing process, and possess characteristics that render the bioink printable.

Furthermore, the bioink should be biocompatible, presenting a high cell viability post printing, be porous enough to allow nutritional transport and encourage cell adhesion and growth (Parak *et al*., 2019). When printing with hydrogels, considerable effort is required to determine the optimum printing parameters to ensure successful printing. These parameters include extrusion temperature, nozzle diameter, printing time and speed, and dispensing pressure. These are often optimised and established in the absence of cells. These parameters also directly influence cell viability, since the parameters determine the shear forces within the bioinks when printing (Webb & Doyle, 2017).

This study primarily focused on the printability and biocompatibility of the bioinks. Line test photographs and line width measurements taken from them, as described by Figure 3-1 in Chapter 3, are presented in this annexure, while the statistical analyses of the line widths are presented in Chapter 3.

B.2 Experimental design

The planned methods for this study are based on the three phases of the bioprinting process (Vijayavenkataraman *et al*., 2018; Varkey *et al*., 2019), as outlined in Chapter 1 section 1.2.3,

namely pre-processing, processing and post-processing. This part of the study falls into the pre-processing phase, as the hybrid hydrogel for print parameter optimisation was being formulated

B.3 Materials

The materials used for this study fall into the category of natural biopolymers and synthetic, nontoxic poloxamers. The formulation used in the study can therefore be regarded as a hybrid hydrogel, which has slowly been replacing natural hydrogels as they provide a higher gel strength and water absorption capacity (Gyles *et al*., 2017; Chimene *et al*., 2020). Alginic acid sodium salt (powder, 180947), phosphate buffered saline (PBS) (powder, P3813), Pluronic F-127 (powder, P2443) and anhydrous calcium chloride (granules, C1016) were purchased from Sigma-Aldrich (Merck, Darmstadt, Germany), 3ml pneumatic syringe/cartridges and 22, 25 and 27G high-precision conical bioprinting nozzles were purchased from Cellink® (Gothenburg, Sweden). These materials are discussed in Chapter 2 in sections 2.6 and 2.8.

B.4. Methods

Alginate and PF127 were prepared as described in Annexure A. They were subsequently mixed into six variations of concentrations into different formulations. Concentrations of 4 and 6% (w/v) alginate and 40, 46 and 50% (w/v) PF127 were used. Line tests were conducted to test the printability of each formulation.

B.4.1 Print process

The non-cellularised hybrid hydrogel used as bioink underwent printing parameter optimisation with the BioX™ 3D bioprinter from Cellink® (Gothenburg, Sweden) with a HeartOS operating system. This bioprinter is equipped with intelligent printhead mounts capable of temperature control between 4 and 250ºC and a printbed capable of controlling temperatures between 4 and 60ºC. This feature allowed for temperature control at 35 and 37ºC during the printing process. Before each printing session, these printhead mounts had to be calibrated to align the nozzle with the surface onto which the scaffold was printed, on top of the printbed.

The bioprinter has clean chamber technology (shield covering the printing mechanisms) that helps control the temperature used during the printing process and for working sterile in the event that it is required. It is also equipped with multiple UV curing systems that allow for chamber sterilisation as well as UV curing of scaffolds. All tests were conducted using 3ml pneumatic syringes with sterile high precision conical 22G (410µm inner diameter), 25G (250µm inner diameter) and 27G (200µm inner diameter) nozzles (Cellink®, Gothenburg, Sweden) that can be screwed onto the pneumatic syringes, as seen in Figure 1-1 in Chapter 1. These pneumatic

syringes are regarded as the cartridges where the bioink was loaded into. An easy to use adapter was screwed onto the pneumatic syringe nozzle connection point (Figure 1-1, Chapter 1), wherein a simple mechanical syringe was inserted and then the bioink was extruded out of the simple mechanical syringe and loaded into the pneumatic syringe/cartridge.

The filled 3ml pneumatic syringe was inserted into one of the intelligent printhead mounts, where after it was connected to the pneumatic airflow inlet using the pneumatic airflow adapter (Figure 1-1, Chapter 1), tightened using the cartridge fastener (Figure 2-1 in Chapter 2), and heated to the required temperature of 35 or 37ºC for this study. A layer height of 0.2 to 0.3mm was printed, depending on the nozzle size used, with a grid infill pattern (Figure 3-1) and no supporting material. The extrusion pressure and printing speed were constantly changed as they were part of the printing parameter optimisation process (BioX™ printer manual). For the line test conduction, the same CAD model was used for the line test as well as the printing parameter optimisation process. The printing process was selected to print without a grid infill pattern and was stopped after extruding only the first layer of the CAD model had been printed.

B.4.2 Line test

An adaptation from the single fibre extrusion test described by Trachtenberg *et al.* (2016) was performed on all six proposed formulations stated in Appendix A. A single line was printed into a 10x10 mm rectangle without infill with a 25G nozzle at 35ºC with an extrusion pressure of 30kPa and printing speed of 10mm/s. Photographs were taken with an iPhone 8 Plus equipped with a 12-megapixel wide-angle and telephoto lens. The line test method is described in Chapter 3 section 4, and the line width measurement locations can be seen in Figure 3-1. All line width results obtained through the printing parameter optimisation study were calculated according to an extrapolation value of 52mm: they had to be interpolated back to 10mm as this is the physical line width value. Inserting the extrapolated values into the parameter optimisation index (POI) equations resulted in extremely low and unusable values.

B.5 Hybrid hydrogel characterisation

There are various standardised and non-standardised methods available to determine the properties of hybrid hydrogels: however, only characterisation methods relevant to 3D bioprinting were considered, including porosity, degradation or stability and viscosity. The SR of the hybrid hydrogel was only evaluated after print parameter optimisation as a complete scaffold had to be used

B.5.1 Porosity

The porosity of a hydrogel is of importance since this property is responsible for transporting nutrients and waste products throughout the scaffold and is directly related to the hybrid hydrogel's ability to retain large amounts of fluid (Roehm, 2018; Calejo *et al*., 2018; Cao *et al*., 2017; Rashid *et al*., 2019; Gyles *et al*., 2017). The porosity was calculated using the Archimedes principle described in Chapter 2 section 2.9.1.

B.5.2 Degradation

Since alginate scaffolds used for tissue engineering purposes are not meant to be permanent, they should degrade within a predetermined time into non-toxic by products while the ECM replaces the alginate (Roehm, 2018; Calejo *et al*., 2018; Cao *et al*., 2017). The degradation rate was determined using an adaptation from Montalbano *et al*., (2018) and is described in Chapter 2 section 2.9.2.

B.5.3 Viscosity

The hybrid hydrogel formulation had to be classified as a non-Newtonian fluid that display a decrease in viscosity as the shear rate increases. Rheological studies were conducted on an ARES-G2 Rheometer (TA instruments, New Castle, DE) and viscosity and stress were tested over an increasing shear rate, while temperature and step time were kept constant. The rheometer is equipped with a 40mm steel cone plate with a 2º angle and a 30µm truncation gap and a sample size of approximately 6ml was used.

B.6 Results

B.6.1 Line test

Cross-linking of the lines printed with 2% (w/v) $CaCl_2$ was deemed unsuccessful since it did not cross-link fast or efficiently enough to maintain the printed line. This led to the fact that these samples were unusable because they could not be measured as the hybrid hydrogel line disappeared into the cross-linking solution where lower w/v concentration hybrid hydrogels were used or had no visual appearance of cross-linking. This led to the increase in cross-linker solution to 4% (w/v) $CaCl_2$.

Table B-1: Hybrid hydrogel 1 (4%A:40%PF127) line test photographs before and after cross-linking

	Line test 1	*Line test 2*	*Line test 3*
Before cross-linking: *Appearance visualisation*			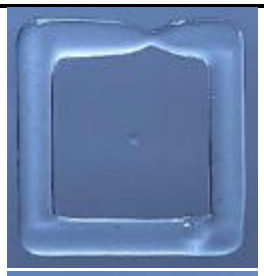
After 4.0% $CaCl_2$ cross-linking: *Appearance visualisation*			
Before cross-linking: *Used for line width measure-ments*	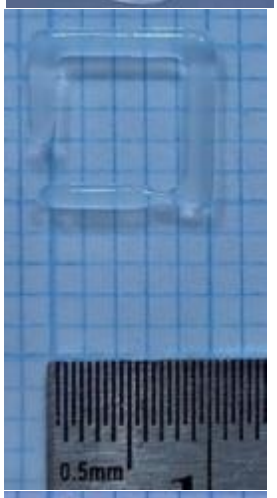		
After 4.0% $CaCl_2$ cross-linking: *Used for line width measure-ments*			

It can be seen from Table B-1 that the hybrid hydrogel 1 (4%A:40%PF127) formulation printed a line width with a larger volume in comparison to other formulations. This larger volume did not

visually seem to be maintained after cross-linking with 4% (w/v) $CaCl_2$. This could be ascribed to the low concentrations of both biopolymers in comparison with the other formulations. The line width measurements taken from the photographed images, as described above, are presented in Table B-2.

Table B-2: Hybrid hydrogel 1 (4%A:40%PF127) line width measurements as described by Figure 3-1

Hybrid hydrogel 1: 4%A:40%P						
	Before cross-linking line width (mm)			*After cross-linking line width (mm)*		
1	1.48	1.61	1.54	1.63	1.54	1.51
2	1.52	1.58	1.62	1.85	1.82	1.57
3	1.44	1.59	1.55	2.41	1.97	1.33
4	1.44	1.63	1.53	1.47	1.72	1.76
Int*	7.19	6.98	7.23	6.10	6.62	7.19
	Average	*Before*	*After*	**Internal*	*Before*	*After*
	line width:	1.54	1.72	*diameter:*	7.13	6.64

From Table B-2, it can be seen that hybrid hydrogel 1 (4%A:40%PF127) had an average line width of 1.54mm and 1.72mm before and after cross-linking. This was the largest line width measurement taken from all the line tests conducted. The internal diameter measured 7.13mm and decreased by 0.49mm after cross-linking. This could have been due to the lower concentrations of both components that were present, which caused the lines to lose their volume during the cross-linking process, and resulted in a bigger line width measurement since the line was ‘flatter’ than it was originally after printing.

Table B-3: Hybrid hydrogel 2 (4%A:46%PF127) line test photographs before and after cross-linking

	Line test 1	*Line test 2*	*Line test 3*
Before cross-linking: *Appearance visualisation*			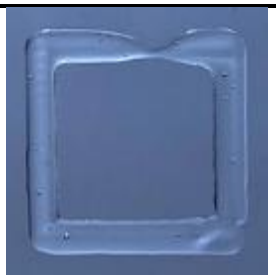
After 4.0% $CaCl_2$ cross-linking: *Appearance visualisation*			
Before cross-linking: *Used for line width measure-ments*			
After 4.0% $CaCl_2$ cross-linking: *Used for line width measure-ments*			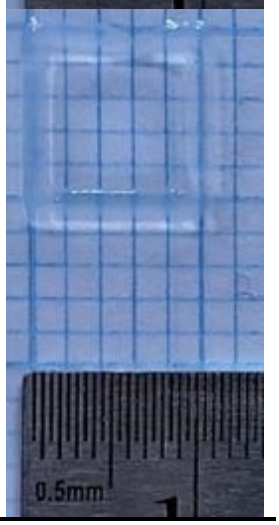

It can be seen from Table B-3 that hybrid hydrogel 2 (4%A:46%PF127) printed a line width that visually looked like it had a similar line volume as hybrid hydrogel 1 (4%A:40%PF127). After 4% (w/v) $CaCl_2$ cross-linking, the border of the printed line could be visually observed, where this was not possible for some of the other formulations. This could have been due to the lower concentration of alginate in ratio to PF127 in comparison with the other hybrid hydrogel formulations. The line width measurements taken from the photographed images as described above, are represented in Table B-4.

Table B-4: Hybrid hydrogel 2 (4%A:46%PF127) line width measurements as described by Figure 3-1

Hybrid hydrogel 2: 4%A:46%P						
	Before cross-linking line width (mm)			*After cross-linking line width (mm)*		
1	1.43	1.39	1.27	1.70	1.53	1.45
2	1.55	1.44	1.49	1.69	1.46	1.27
3	1.55	1.31	1.41	1.47	1.46	1.61
4	1.55	1.52	1.55	1.65	1.41	1.43
Int*	7.34	7.56	7.34	7.30	7.19	7.04
	Average	*Before*	*After*	**Internal*	*Before*	*After*
	line width:	1.46	1.51	*diameter:*	7.41	7.17

From Table B-4, it can be seen that hybrid hydrogel 2 (4%A:46%PF127) had an average line width of 1.46mm and 1.51mm before and after cross-linking. The internal diameter measured 7.41mm and decreased by 0.24mm after cross-linking. This could have been due to the lower concentration of alginate in ratio to the PF127 that resulted in less alginate to be cross-linked and the line width to lose some of its volume.

Table B-5: Hybrid hydrogel 3 (4%A:50%PF127) line test photographs before and after cross-linking

	Line test 1	*Line test 2*	*Line test 3*
Before cross-linking: *Appearance visualisation*			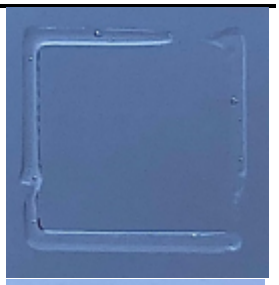
After 4.0% $CaCl_2$ cross-linking: *Appearance visualisation*	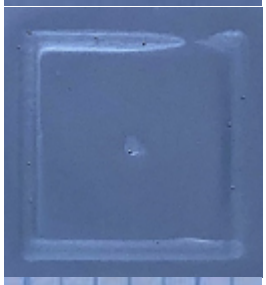		
Before cross-linking: *Used for line width measure-ments*			
After 4.0% $CaCl_2$ cross-linking: *Used for line width measure-ments*			

From Table B-5, it is very clearly seen that hybrid hydrogel 3 (4%A:50%PF127) printed thin lines with a small line volume. After 4% (w/v) $CaCl_2$ cross-linking, the scaffold was hardly visible and

the borders of the printed line visually looked indistinguishable when compared to other hybrid hydrogel formulations. This could again be due to the lower concentration of alginate in ratio to the PF127 that resulted in a bioink formulation that contained a higher concentration of PF127. The line width measurements taken from the photographed images, as described above, are represented in Table B-6.

Table B-6: Hybrid hydrogel 3 (4%A:50%PF127) line width measurements as described by Figure 3-1

Hybrid hydrogel 3: 4%A:50%P						
	Before cross-linking line width (mm)			*After cross-linking line width (mm)*		
1	0.88	0.75	0.72	0.90	0.68	0.76
2	0.97	0.88	0.93	0.93	0.81	0.78
3	0.91	0.74	0.00	0.91	0.78	0.00
4	0.88	0.74	0.95	0.97	0.73	0.86
Int*	8.31	8.76	8.72	8.48	8.85	8.82
	Average	*Before*	*After*	**Internal*	*Before*	*After*
	line width:	0.85	0.83	*diameter:*	8.60	8.72

From Table B-6, it can be seen that hybrid hydrogel 3 (4%A:50%PF127) had an average line width of 0.85mm and 0.83mm before and after cross-linking This average line width was the smallest of all line tests conducted with the pre-formulated hybrid hydrogels. The internal diameter measured 8.06mm and increased by 0.12mm after cross-linking. This could have been due to the lower concentration of alginate in ratio to the PF127 that resulted in a viscosity too high to extrude successfully.

Table B-7: Hybrid hydrogel 4 (6%A:40%PF127) line test photographs before and after cross-linking

	Line test 1	*Line test 2*	*Line test 3*
Before cross-linking: *Appearance visualisation*			
After 4.0% $CaCl_2$ cross-linking: *Appearance visualisation*		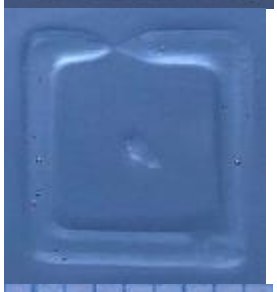	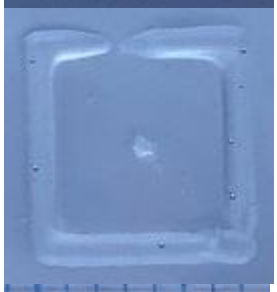
Before cross-linking: *Used for line width measure-ments*		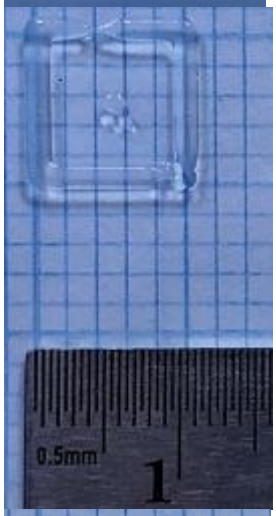	
After 4.0% $CaCl_2$ cross-linking: *Used for line width measure-ments*			

It can be seen from Table B-7 that hybrid hydrogel 4 (6%A:40%PF127) printed a line width with a larger line volume in comparison with hybrid hydrogel 3 (4%A:50%PF127), but still smaller than hybrid hydrogel 1 (4%A:40%PF127). After 4% (w/v) $CaCl_2$ cross-linking, the borders of the printed line could still be visually observed, but seemed to be visually less distinguishable when compared to the other hybrid hydrogel formulations. This could have been attributed to the higher concentrations of alginate in comparison to the PF127, which resulted in better cross-linking in comparison with the formulations containing a lower concentration. The line width measurements taken from the photographed images, as described above, are represented in Table B-8.

Table B-8: Hybrid hydrogel 4 (6%A:40%PF127) line width measurements as described by Figure 3-1

Hybrid hydrogel 4: 6%A:40%P						
	Before cross-linking line width (mm)			*After cross-linking line width (mm)*		
1	1.30	1.42	1.37	1.35	1.48	1.29
2	1.34	1.47	1.51	1.44	1.61	1.46
3	1.21	1.37	1.42	0.00	1.54	1.36
4	1.37	1.49	1.46	1.37	1.58	1.49
Int*	7.63	7.41	7.47	7.87	7.37	7.61
	Average	*Before*	*After*	**Internal*	*Before*	*After*
	line width:	1.39	1.45	*diameter:*	7.50	7.62

From Table B-8, it can be seen that hybrid hydrogel 4 (6%A:40%PF127) had an average line width of 1.39mm and 1.45mm before and after cross-linking. The internal diameter measured 7.50mm and increased by 0.12mm after cross-linking. This could have been due to the lower concentration of PF127 in ratio to the alginate that resulted in successful cross-linking of the alginate within the hybrid hydrogel mixture, which resulted in stiff lines that maintained their volume during the cross-linking process.

Table B-9: Hybrid hydrogel 5 (6%A:46%PF127) line test photographs before and after cross-linking

	Line test 1	*Line test 2*	*Line test 3*
Before cross-linking: *Appearance visualisation*			
After 4.0% $CaCl_2$ cross-linking: *Appearance visualisation*	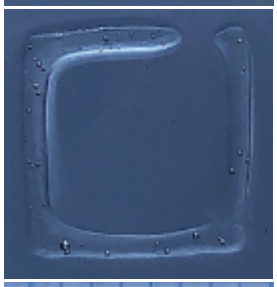		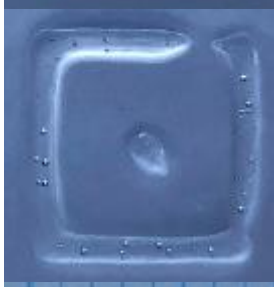
Before cross-linking: *Used for line width measure-ments*		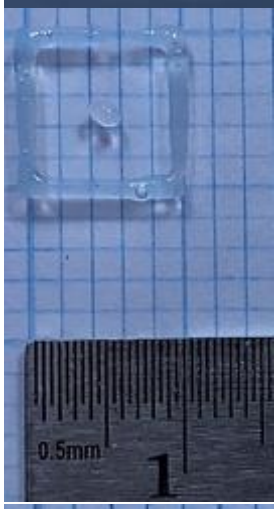	
After 4.0% $CaCl_2$ cross-linking: *Used for line width measure-ments*			

From Table B-9, it was observed that hybrid hydrogel 5 (6%A:46%PF127) printed a line width with a smaller volume in comparison to hybrid hydrogel 4 (6%A:40%PF127), but still larger than hybrid hydrogel 3 (4%A:50%PF127). After 4% (w/v) $CaCl_2$ cross-linking, the line printed visually looks the same as it did before cross-linking. This could have been the result of a good balance between the two hybrid hydrogel components. The line width measurements taken from the photographed images, as described above, are represented in Table B-10.

Table B-10: Hybrid hydrogel 5 (6%A:46%PF127) line width measurements as described by Figure 3-1

Hybrid hydrogel 5: 6%A:46%P						
	Before cross-linking line width (mm)			*After cross-linking line width (mm)*		
1	1.16	1.18	1.16	1.04	1.29	0.99
2	1.25	1.30	1.31	0.91	1.20	1.14
3	1.08	1.10	1.17	0.91	1.09	1.14
4	1.29	1.23	1.36	0.99	1.32	1.05
Int*	8.00	7.99	7.96	8.23	8.00	8.08
	Average	*Before*	*After*	**Internal*	*Before*	*After*
	line width:	1.22	1.09	*diameter:*	7.99	8.10

From Table B-10, it can be seen that hybrid hydrogel 5 (6%A:46%PF127) had an average line width of 1.22mm and 51.09mm before and after cross-linking. The internal diameter measured 7.99mm and increased by 0.11mm after cross-linking. This could have been due to the successful cross-linking of the alginate within the hybrid hydrogel mixture, which resulted in stiff lines that have maintained their volume during the cross-linking process.

Table B-11: Hybrid hydrogel 6 (6%A:50%PF127) line test photographs before and after cross-linking

	Line test 1	*Line test 2*	*Line test 3*
Before cross-linking: *Appearance visualisation*			
After 4.0% $CaCl_2$ cross-linking: *Appearance visualisation*	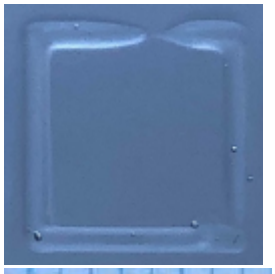	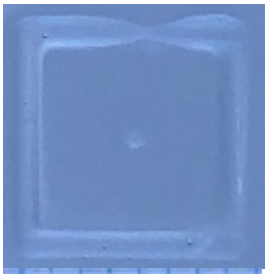	
Before cross-linking: *Used for line width measure-ments*			
After 4.0% $CaCl_2$ cross-linking: *Used for line width measure-ments*			

It can be seen from Table B-11 that hybrid hydrogel 6 (6%A:50%PF127) printed a line width with a larger volume in comparison to hybrid hydrogel 3 (4%A:50%PF127) containing the same concentration of PF127. After 4% (w/v) $CaCl_2$ cross-linking, the border of the printed line visually looked to be less distinguishable when compared to other hybrid hydrogel formulations. This could still be attributed to the higher concentration of PF127 in comparison with the other hybrid hydrogel formulations. The line width measurements taken from the photographed images, as described above, are represented in Table B-12.

Table B-12: Hybrid hydrogel 6(6%A:50%PF127) line width measurements as described by Figure 3-1

Hybrid hydrogel 6: 6%A:50%P						
	Before cross-linking line width (mm)			*After cross-linking line width (mm)*		
1	1.12	1.12	1.11	1.16	1.10	0.00
2	1.20	1.42	1.55	1.20	1.33	1.52
3	1.20	1.23	0.00	1.05	0.00	0.00
4	1.07	1.23	1.20	1.10	1.20	1.20
Int*	7.95	7.91	8.44	8.02	8.25	7.73
	Average	*Before*	*After*	**Internal*	*Before*	*After*
	line width:	1.22	1.21	*diameter:*	8.10	8.00

From Table B-12, it can be seen that hybrid hydrogel 6 (6%A:50%PF127) had an average line width of 1.22mm and 1.21mm before and after cross-linking. The internal diameter measured 8.10mm and decreased by 0.1mm after cross-linking. This was in contrast to hybrid hydrogel 5 (6%A:46%PF127) and could have been due to the higher concentration PF127 in ratio to the alginate as in the previous hybrid hydrogels that could have possibly led to a lower degree of alginate cross-link, which allowed the line to ‘flatten’, losing its volume and increasing the line width.

B.6.2 Degradation

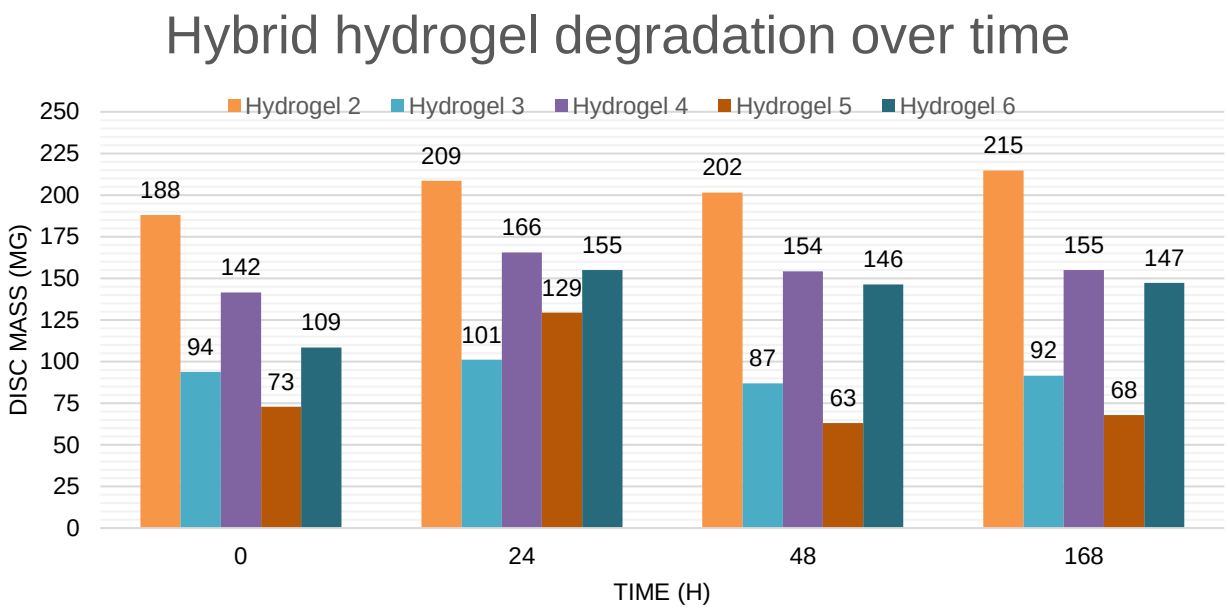

Figure B-1: Hybrid hydrogel formulations degradation rate measured over 168 hours

From Table B-1, it can be observed that the formulations did not degrade as expected. This could be because PF127 was incorporated into the alginate gel that decreased the degradation of the alginate. It also proved the stability of the hybrid hydrogel.

B.6.3 Porosity

Table B-13: Hybrid hydrogel porosity

	Disc 1	*Disc 2*	*Disc 3*	*Disc 4*	*Average*
Hybrid hydrogel 2 (4%A:46%PF127)	18.60%	19.82%	31.26%	17.71%	21.85%
Hybrid hydrogel 3 (4%A:50%PF127)	34.35%	41.81%	44.93%	40.96%	40.51%
Hybrid hydrogel 4 (*6%A:40%PF127)*	27.50%	24.79%	25.80%	27.96%	26.51%
Hybrid hydrogel 5 (6%A:46%PF127)	48.43%	47.28%	53.74%	52.58%	50.50%
Hybrid hydrogel 6 (6%A:50%PF127)	32.83%	33.26%	39.82%	43.07%	37.25%

From Table B-13, it can clearly be observed that hybrid hydrogel 5 (6%A:46%PF127) had displayed the highest percentage of porosity. This was an important factor to take into consideration as this property will allow for nutrients to move within the structure (Roehm, 2018).

B.6.4 Viscosity

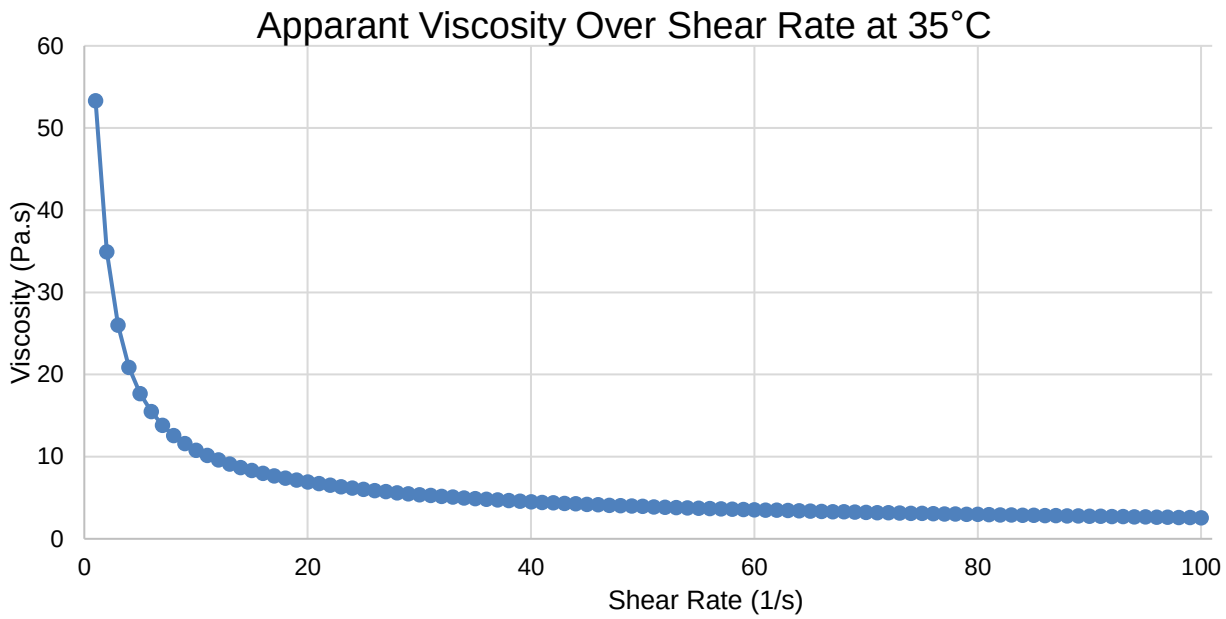

Figure B-2: Apparent viscosity of hybrid hydrogel 5 (6$A:46%PF127) measured at 35ºC over an increasing shear rate

Figure B-2 shows how the apparent viscosity decreases as the shear rate increases from 0 to100. From Figure B-2, it can be seen that hybrid hydrogel 5 (6%A:46%PF127) can be regarded as a non-Newtonian fluid because of the apparent viscosity that decreased as the shear rate increased (Chimene *et al*., 2020).

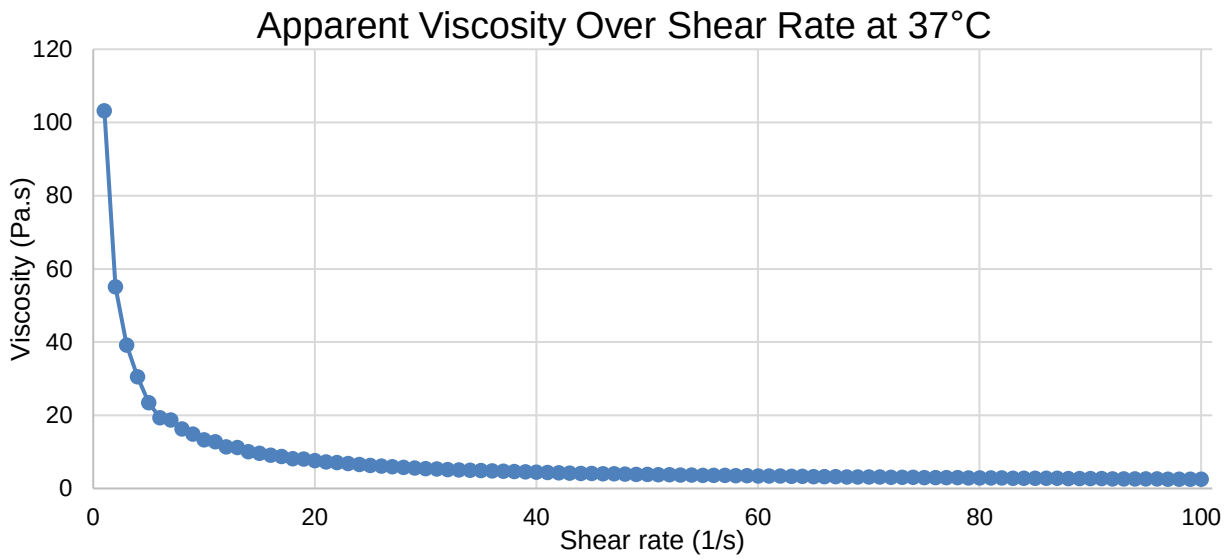

Figure B-3: Apparent viscosity of hybrid hydrogel 5 (6$A:46%PF127) measured at 37ºC over an increasing shear rate

Figure B-3 shows how the apparent viscosity decreases as the shear rate increases from 0 to 100. From Figure B-3, it can be seen that hybrid hydrogel 5 (6%A:46%PF127) can be regarded as a non-Newtonian fluid because of the apparent viscosity that decreased as the shear rate increased (Chimene *et al*., 2020).

B.7 Conclusion

Form the line tests conducted on the six hybrid hydrogel formulations, hybrid hydrogel 5 (6%A:46%PF127) was visually observed to print more successful lines where they mostly maintained their line volumes resulting in a smaller increase in line width after cross-linking when compared to the other hybrid hydrogel formulations. A concentration of 50% (w/v) PF127 has been deemed too high as it seems to negatively influence the cross-linking capabilities of the alginate within the hybrid hydrogel, even though PF127 is described as being inert and does not participate in the cross-linking process alginate undergoes when exposed to $CaCl_2$ (Roehm, 2018). Hybrid hydrogel 5 (6%A:46%PF127) had shown almost no degradation, proving its stability, the highest percentage of porosity and was also classified as being a non-Newtonian fluid, which is ideal for bioink formulations.

B.8 References

1. Bishop, E.S., Mostafa, S., Pakvasa, M., Luu, H.H., Lee, M.J., Moriatis Wolf, J., Ameer, G.A., He, T.C. & Reid, R.R. 2017. 3-D bioprinting technologies in tissue engineering and regenerative medicine: Current and future trends*. Genes & Diseases*, 4(4):185-195.

2. Calejo, M.T., Ilmarinen, T., Skottman, H. & Kellomäki, M. 2018. Breath figures in tissue engineering and drug delivery: State-of-the-art and future perspectives. *Acta Biomaterialia*, 66:44–66.

3. Cao, D., Zhang, Y., Cui, Z., Du, Y. & Shi, Z. 2017. New strategy for design and fabrication of polymer hydrogel with tunable porosity as artificial corneal skirt. *Materials Science & Engineering C*, 70:665–672.

4. Chimene, D., Kaunas, R. & Gaharwar, A.K. 2020. Hydrogel Bioink Reinforcement for Additive Manufacturing: A Focused Review of Emerging Strategies. *Advanced Material Science*, 32:1902026.

5. Datta, P., Barui, A., Wu, Y., Ozbolat, V., Moncal, K.K. & Ozbolat, I.T. 2018. Essential steps in bioprinting: From pre- to post-bioprinting. *Biotechnology Advances*, 36:1481-1504.

6. Gyles, D.A., Castro, L.D., Silva, J.O.C. Jnr. & Ribeiro-Costa, R.M. 2017. A review of the designs and prominent biomedical advances of natural and synthetic hydrogel formulations*. European Polymer Journal*, 88:373-392.

7. Montalbano, G., Toumpaniari, S., Popov, A., Duan, P., Chen, J., Dalgarno, K., Scott III, W.E. & Ferreira, A.M. 2018. Synthesis of bioinspired collagen/alginate/fibrin based hydrogels for soft tissue engineering. *Materials Science & Engineering C*, 91:236–246.

8. O'Brien, F.J. 2011. Biomaterials & scaffolds for tissue engineering. *Materials Today*, 14(3):88-95.

9. Ozbolat, I. & Hospodiuk, M. 2016. Current advances and future perspectives in extrusion-based. *Biomaterials,* 76:321-343.

10. Parak, A., Pradeep, P., Du Toit, L.C., Kumar, P., Choonara, Y.E. & Pillay, V. 2019. Functionalizing bioinks for 3D bioprinting applications. *Drug Discovery Today,* 24:198-205.

11. Rashid, F., Albayati, M. & Dodou, K. 2019. Studies on Novel Methods for Formulating Novel Cross-Linked Hydrogel Films of Hyaluronic Acid. *Cosmetics*, 6(59):2–19.

12. Roehm, K. 2018. Bioprinting cell laden structures with chitosan-gelatin for neural tissue applications. United States of America: New Jersey Institute of Technology (Thesis – PhD).

13. Trachtenberg, J.E., Placone, J.K., Smith, B.T., Fisher, J.P. & Mikos, A.G. 2017. Extrusion-based 3D printing of poly(propylene fumarate) scaffolds with hydroxyapatite gradients. *Journal of Biomateral Science*: *Polymer Edition*, 28(6):532-554.

14. Varkey, M., Visscher, D.O., Van Zuijlen, P.P.M., Atala, A. & Yoo, J.J. 2019. Skin bioprinting: The future of burn wound reconstruction? *Burns & Trauma,* 7(4):3.

15. Vijayavenkataraman, S., Yan, W.C., Lu, W.F., Wang, C.H. & Fuh, J.Y.H. 2018. 3D bioprinting of tissues and organs for regenerative medicine. *Advanced Drug Delivery Reviews,* 32:296–332.

16. Webb, B. & Doyle, B. 2017. Parameter optimization for 3D bioprinting of hydrogels. *Bioprinting*, 8:8-12.

ANNEXURE C: PRINT PARAMETER OPTIMISATION

C.1 Introduction

The print parameter optimisation process was conducted on the BioX™ 3D bioprinter from Cellink® (Gothenburg, Sweden) with a HeartOS operating system. A newly formulated grading method was formulated during this study, which was utilised in combination with the parameter optimisation index (POI) as described by Webb and Doyle (2017). The visual appearance of the scaffold while it was being printed was a similarly important factor to consider. The parameters that were optimised include: nozzle size, extrusion pressure, printing speed and temperature.

C.2 Experimental design

The planned methods for this study are based on the three phases of the bioprinting process (Vijayavenkataraman *et al*., 2018; Varkey *et al*., 2019), as outlined in Figure 1-1 in Chapter 1 section 1.2.3, namely pre-processing, processing and post-processing. This part of the study falls into the processing phase as printing parameters were optimised.

C.3 Materials

Alginic acid sodium salt (powder, 180947), phosphate buffered saline (PBS) (powder, P3813), Pluronic F-127 (powder, P2443) and anhydrous calcium chloride (granules, C1016) were purchased from Sigma-Aldrich (Merck, Darmstadt, Germany), 3ml pneumatic syringe/cartridges and 22, 25 and 27G high-precision conical bioprinting nozzles were purchased from Cellink® (Gothenburg, Sweden). The materials are discussed in Chapter 2 section 2.6 and 2.8.

C.4 Method

A grading system was formulated to enable scaffolds within the same temperature and nozzle size groups to be compared to each other. Scaffolds were only printed to 8 to 12% completion where after they were photographed with an iPhone 8 plus equipped with a 12-megapixel wide-angle and telephoto lens. They were extrapolated to 52mm and the line widths and corner drags were measured and a score out of ten was allocated to them based on these measurements, with ten being the best score. This score was labelled the print score. The grading method is thoroughly explained in Chapter 3 section 5.

C.4.1 Printing process

The BioX™ bioprinter is equipped with intelligent printhead mounts as well as a printbed that allows for temperature control between 4 and 250ºC. This allowed for the bioink to be heated to 35 and 37ºC before it was extruded and for the surface it was extruded onto to be heated to the same temperature. The bioink was drawn up by a simple mechanical syringe out of the beaker it was mixed in, and extruded into the pneumatic syringe (that doubled as the printing cartridge) using a small adapter that screwed into the pneumatic syringe and nozzle connection point.

After the pneumatic syringe was filled, it was placed into the intelligent printhead mounts, fastened and heated to the required temperature. A CAD model with the dimensions of 10mm x 10mm x 10mm was preselected and only printed to 8 to 12% completion, where after it was photographed and measured according to its line width and corner drag values. A layer height of 0.2 to 0.3mm was printed, depending on the nozzle size used, with a grid infill pattern (Figure 3-1) and no supporting material. The extrusion pressure and printing speed were constantly changed as they were part of the printing parameter optimisation process (BioX™ printer manual).

C.4.2 Print parameter optimisation scaffold number allocation

Each parameter tested was given a number within that nozzle size and temperature parameter. There were six groups of parameters: (1) 22G at 35ºC; and (2) at 37ºC; (3) 25G at 35ºC; and (4) at 37ºC; (5) 27G at 35ºC; and (6) at 37ºC. A red cross indicates an unsuccessful print. These parameters did not contribute to the final results nor were they investigated further.

Table C-1: Scaffold number allocation to 22G nozzle at 35ºC

22G at 35ºC

Extrusion pressure (kPa) \ *Extrusion speed (mm/s)*	10	15	20	25	30	35	40	45
20	1	2						
25	X	3	4					
30		X	5	6	7	8		
35			X	X	X	9	10	
40				X	X	X	11	
45					X	X	X	X

From Table C-1, it can be seen that a total of 23 parameter combinations within the 22G at 35ºC group were, where 12 of them were unsuccessful and 11 of them contributed to the printing parameter optimisation process.

Table C-2: Scaffold number allocation to 22G nozzle at 37ºC

22G at 37ºC

Extrusion pressure (kPa) \ *Extrusion speed (mm/s)*	10	15	20	25	30	35
20	1	2				
25	3	4	5			
30	X	6	7	8		
35	X	9	10	11		
40		X	12	13	14	
45			X	15	16	17

From Table C-2, it can be seen that a total of 21 parameter combinations within the 22G at 37ºC group were found, where four of them were unsuccessful and 17 of them contributed to the printing parameter optimisation process.

Table C-3: Scaffold number allocation to 25G nozzle at 35ºC

25G at 35ºC

Extrusion pressure (kPa) \ *Extrusion speed (mm/s)*	10	15	20	25	30
20	X	X			
25	1	2			
30	3	4			
35	5	6	7		
40	X	8			
45		9	10	11	
50			12	13	14
55			X	X	15

From Table C-3, it can be seen that a total of 20 parameter combinations within the 25G at 35ºC group were found, where five of them were unsuccessful and 15 of them contributed to the printing parameter optimisation process.

Table C-4: Scaffold number allocation to 25G nozzle at 37ºC

25G at 37ºC

Extrusion pressure (kPa)	*Extrusion speed (mm/s)*					
	10	15	20	25	30	35
20	X	X				
25	1	2				
30	3	4				
35	5	6	7			
40	X	8	9	10		
45		X	11	12	13	
50		X	X	14	15	16
55			X	X	17	18

From Table C-4, it can be seen that a total of 26 parameter combinations within the 25G at 37ºC group were found, where eight of them were unsuccessful and 18 of them contributed to the printing parameter optimisation process.

Table C-5: Scaffold number allocation to 27G nozzle at 35ºC

27G at 35ºC

Extrusion pressure (kPa)	*Extrusion speed (mm/s)*							
	10	15	20	25	30	35	40	45
20	X							
25	X							
30	1							
35	X							
40	2	3						
45	4	5						
50	6	7	8	9				
55	10	11	12	13	14			
60	X	15	16	17	18	19		
65		X	20	21	22	23	24	
70			25	26	27	28	29	30
75				X	31	32	33	

From Table C-7 it can be seen that a total of 39 parameter combinations within the 27G at 37ºC group were found, where six of them were unsuccessful and 33 of them contributed to the printing parameter optimisation process.

Table C-6: Scaffold number allocation to 27G nozzle at 37ºC

27G at 37ºC

Extrusion pressure (kPa)	*Extrusion speed (mm/s)*					
	10	15	20	25	30	35
20	X					
25	X					
30	1					
35	2	3				
40	4	5				
45	6	7	8			
50	9	10	11	12		
55	X	13	14	15	16	
60	X	17	18	19	20	
65	X	21	22	23	X	
70		X	24	25	26	
75		X	27	28	29	X
80		X	30	31	32	33

From Table C-6, it can be seen that a total of 43 parameter combinations within the 27G at 37ºC group were found, where ten of them were unsuccessful and 33 of them contributed to the printing parameter optimisation process.

C.5.2 Parameter optimisation index

The POI described by Webb and Doyle (2017) was utilised in combination with the newly-formulated grading method and the visual observation thereof, to determine the optimal printing parameters. The POI describes the relationship between the parameters and how they directly influence each other. The POI is thoroughly described in Chapter 2, section 2.11.1.

C.6 Results

Below are the results for the parameter groups described in Chapter 3, section 5: within them was a constant change in extrusion pressure (kPa) and extrusion time (mm/s).

Table C-7: Scaffold line and corner measurements using a 22G nozzle at 35ºC

22G at 35ºC Line width/Corner drag measurement (mm) (AVE±SD)

Extrusion pressure (kPa) \ Extrusion speed (mm/s)	10	15	20	25	30	35	40
20	**4.40±0.3** **2.62±0.3**	**4.09±0.7** **2.53±0.3**					
25		**4.41±0.6** **2.90±0.2**	**3.38±0.6** **2.95±0.4**				
30			**4.99±0.6** **2.71±0.5**	**4.65±0.4** **2.84±0.3**	**3.95±0.4** **2.51±0.3**	**3.76±0.3** **2.41±0.2**	
35						**4.92±0.3** **3.04±0.2**	**4.94±0.3** **2.95±0.5**
40							**4.85±0.5** **2.76±0.2**

An average line width of 4.4±0.5mm and corner drag of 2.7±0.2mm were calculated from Table C-7. The corresponding score allocations using the equations described in Chapter 3 are displayed in Table C-8.

Table C-8: Printing parameter score allocation using a 22G nozzle at 35ºC

22G at 35ºC Line width/Corner drag score

Extrusion pressure (kPa) \ Extrusion speed (mm/s)	10	15	20	25	30	35	40
20	1.5 4.4	2.3 4.5					
25		0.7 2.8	4.6 2.8				
30			0 4.1	0.9 3.7	3.0 4.6	3.6 5.0	
35						0 2.8	0 3.2
40							0 3.8

It can be observed from this table that these parameters did not score very high with average scores of 1.5/10 for kPa (extrusion pressure) and 3.8/10 for mm/s (corner drag) being calculated, resulting in an overall score of 2.7/10 for the 22G nozzle at 35ºC.

Table C-9: Scaffold line and corner measurements using a 22G nozzle at 37ºC

22G at 37ºC Line width/Corner drag measurement (mm) (AVE±SD)

Extrusion pressure (kPa) \ Extrusion speed (mm/s)	10	15	20	25	30	35
20	**2.79±0.2** **1.81±0.1**	**2.14±0.6** **2.11±0.3**				
25	**3.23±0.2** **2.29±0.4**	**2.77±0.4** **2.99±0.5**	**2.69±0.2** **3.08±0.2**			
30		**4.28±0.2** **2.78±0.2**	**2.88±0.3** **3.00±0.6**	**3.27±0.4** **2.72±0.2**		
35		**4.39±0.4** **3.15±0.2**	**4.13±0.7** **2.93±0.4**	**3.99±0.7** **2.34±0.4**		
40			**5.04±0.3** **3.23±0.2**	**4.45±0.3** **2.50±0.2**	**3.70±0.4** **2.36±0.3**	
45				**5.00±0.7** **3.18±0.3**	**4.74±0.2** **2.54±0.2**	**5.07±0.3** **2.74±0.5**

An average line width of 3.8±0.9mm and corner drag of 2.7±0.4mm were calculated from Table C-9. The corresponding score allocations using the equations described in Chapter 3 are displayed in Table C-10.

Table C-10: Printing parameter score allocation using a 22G nozzle at 37ºC

22G at 37ºC Line width/Corner drag score

Extrusion pressure (kPa) \ Extrusion speed (mm/s)	10	15	20	25	30	35
20	6.9 7.0	9.4 6.2				
25	5.4 5.3	7.0 2.9	7.4 2.7			
30		1.9 3.7	6.7 3.0	5.5 4.0		
35		1.6 2.5	2.6 3.3	2.9 5.3		
40			0 2.7	1.6 4.8	4.2 5.4	
45				0 2.4	0 4.3	0 4.2

An average score of 3.7/10 for kPa (extrusion pressure) and 4.1/10 for mm/s (corner drag) were calculated, resulting in an overall score of 3.9/10 for the 22G nozzle at 37ºC.

Table C-11: Scaffold line and corner measurements using a 25G nozzle at 35ºC

25G at 35ºC Line width/Corner drag measurement (mm) (AVE±SD)

Extrusion pressure (kPa) \ Extrusion speed (mm/s)	10	15	20	25	30
25	**2.61±0.6** 2.02±0.2	**2.52±0.2** 2.15±0.5			
30	**3.22±0.5** 2.42±0.4	**2.55±0.3** 2.45±0.4			
35	**4.23±0.7** 2.61±0.2	**3.29±0.5** 2.79±0.1	**2.37±0.2** 2.25±0.4		
40		**3.11±0.4** 2.29±0.3			
45		**5.01±1.2** 2.95±0.5	**4.27±0.5** 2.52±0.4	**3.65±0.9** 2.63±0.4	
50			**4.96±1.2** 3.56±0.7	**4.01±1.0** 3.36±0.5	**3.58±0.8** 2.56±0.5
55					**4.19±1.0** 2.61±0.2

An average line width of 3.6±0.9mm and corner drag of 2.6±0.4mm were calculated from Table C-11. The corresponding score allocations using the equations described in Chapter 3 are displayed in Table C-12.

Table C-12: Printing parameter score allocation using a 25G nozzle at 35ºC

25G at 35ºC Line width/Corner drag score

Extrusion pressure (kPa) \ Extrusion speed (mm/s)	10	15	20	25	30
25	7.5 6.3	7.9 5.9			
30	5.3 4.8	7.7 4.7			
35	1.6 4.0	5.0 3.4	8.5 5.5		
40		6.0 5.5			
45		0 3.2	2.0 4.7	4.0 4.2	
50			0 1.1	3.2 2.0	4.2 4.4
55					1.9 3.9

An average score of 4.3/10 for kPa (extrusion pressure) and 4.2/10 for mm/s (corner drag) were calculated, resulting in an overall score of 4,3/10 for the 25G nozzle at 35ºC.

Table C-13: Scaffold line and corner measurements using a 25G nozzle at 37ºC

25G at 37ºC Line width/Corner drag measurement (mm) (AVE±SD)

Extrusion pressure (kPa) \ Extrusion speed (mm/s)	10	15	20	25	30	35
25	**2.95±0.5** 2.41±0.4	**2.76±0.1** 1.83±0.5				
30	**3.53±0.5** 2.28±0.3	**2.95±0.8** 2.14±0.3				
35	**4.59±0.9** 2.94±0.5	**3.66±0.3** 2.35±0.3	**3.08±1.0** 3.26±0.8			
40		**4.93±1.5** 3.88±0.8	**3.87±0.8** 3.24±0.4	**3.83±1.3** 2.85±0.4		
45			**4.61±2.0** 2.73±0.4	**4.23±1.5** 3.26±0.8	**4.20±1.3** 3.12±0.7	
50				**5.38±1.9** 3.69±0.7	**4.55±1.5** 3.46±0.5	**4.24±1.2** 2.99±0.7
55					**5.65±2.5** 4.12±0.7	**5.11±2.3** 3.43±0.5

An average line width of 4.1±0.9mm and corner drag of 3.0±0.6mm were calculated from Table C-13. The corresponding score allocations using the equations described in Chapter 3 are displayed in Table C-14.

Table C-14: Printing parameter score allocation using a 25G nozzle at 37ºC

25G at 37ºC Line width/Corner drag score

Extrusion pressure (kPa) \ Extrusion speed (mm/s)	10	15	20	25	30	35
25	6.8 5.3	7.1 7.0				
30	4.8 5.7	6.7 6.1				
35	0.7 3.1	4.0 5.2	6.3 2.4			
40		0 0	3.4 2.2	3.5 3.5		
45			0.7 3.9	1.4 1.6	1.7 2.2	
50				0 0	1.3 1.7	2.3 3.2
55					0 0	0 1.6

An average score of 2.8/10 for kPa (extrusion pressure) and 3/10 for mm/s (corner drag) were calculated, resulting in an overall score of 2.9/10 for the 25G nozzle at 37ºC.

Table C-15: Scaffold line and corner measurements using a 27G nozzle at 35ºC

27G at 35ºC Line width/Corner drag measurement (mm) (AVE±SD)

Extrusion pressure (kPa) \ Extrusion speed (mm/s)	10	15	20	25	30	35	40	45
30	1.43±0.2 1.35±0.1							
35								
40	2.01±0.2 1.78±0.4	2.19±0.2 1.61±0.3						
45	2.45±0.4 1.39±0.2	3.27±0.6 1.28±0.3						
50	2.17±0.3 2.21±0.3	2.74±0.5 1.78±0.6	2.78±0.3 1.79±0.4	2.21±0.5 1.93±0.8				
55	4.89±0.9 2.54±0.4	4.13±0.6 2.45±0.7	3.04±0.2 2.22±0.3	2.84±0.5 1.80±0.5	2.48±0.5 1.88±0.5			
60		4.70±0.7 2.90±0.4	3.45±0.6 2.61±0.5	2.62±0.3 1.90±0.5	2.66±0.9 2.05±0.7	2.60±0.6 2.02±0.3		
65			3.82±0.3 2.57±0.3	3.30±0.7 2.40±0.5	3.18±0.7 2.45±0.4	2.57±0.5 1.85±0.04	2.78±0.7 2.48±0.3	
70			4.63±0.8 3.06±0.1	4.03±0.5 3.00±0.4	3.26±0.8 2.27±0.4	2.92±0.6 2.48±0.4	2.78±0.7 2.07±0.3	2.49±0.6 2.28±0.4
75					3.89±0.4 2.71±0.3	2.90±0.6 2.45±0.3	2.91±0.7 2.39±0.5	

An average line width of 3.0±0.8mm and corner drag of 2.2±0.5mm were calculated from Table C-15. The corresponding score allocations using the equations described in Chapter 3 are displayed in the table below.

Table C-16: Printing parameter score allocation using a 27G nozzle at 35ºC

27G at 35ºC Line width/Corner drag score

Extrusion pressure (kPa) \ Extrusion speed (mm/s)	10	15	20	25	30	35	40	45
30	11.8 8.7							
40	9.7 7.2	9.1 7.8						
45	8.1 8.5	5.4 8.9						
50	9.4 5.9	7.2 7.2	7.3 7.3	9.2 6.8				
55	0 4.6	2.4 4.9	6.1 5.6	6.7 7.0	7.9 6.7			
60		0.7 3.5	4.9 4.5	7.7 6.8	7.5 6.2	7.8 6.5		
65			3.2 4.3	5.2 5.0	5.5 4.8	7.6 6.8	7.0 4.7	
70			0.6 2.7	2.9 3.1	5.5 5.5	6.7 4.9	7.2 6.3	8.1 5.5
75					3.0 3.8	6.7 4.9	6.5 5.0	

An average score of 6.2/10 for kPa (extrusion pressure) and 5.8/10 for mm/s (corner drag) were calculated, resulting in an overall score of 6/10 for the 27G nozzle at 35ºC.

Table C-17: Scaffold line and corner measurements using a 27G nozzle at 37ºC

27G at 37ºC Line width/Corner drag measurement (mm) (AVE±SD)

Extrusion pressure (kPa) \ *Extrusion speed (mm/s)*	10	15	20	25	30	35
30	**1.80±0.2** **1.59±0.2**					
35	**1.92±0.3** **1.56±0.5**	**1.90±0.1** **1.24±0.4**				
40	**2.52±0.3** **1.93±0.2**	**1.95±0.2** **1.73±0.2**				
45	**2.93±0.7** **1.8±0.2**	**2.59±0.3** **1.73±0.2**	**2.33±0.4** **1.51±0.2**			
50	**3.95±0.6** **2.37±0.2**	**3.01±0.4** **2.34±0.3**	**2.44±0.2** **1.71±0.3**	**3.67±0.7** **1.53±0.2**		
55		**3.74±0.6** **2.24±0.2**	**2.93±0.3** **1.94±0.4**	**2.70±0.5** **1.97±0.6**	**2.47±0.2** **2.02±0.3**	
60		**3.34±0.8** **2.32±0.6**	**2.62±0.5** **1.74±0.2**	**2.62±0.7** **1.80±0.1**	**2.07±0.5** **2.13±0.7**	
65		**3.85±0.8** **2.48±0.4**	**3.48±0.6** **2.20±0.4**	**2.75±0.6** **2.43±0.04**		
70			**3.46±1.1** **2.37±0.4**	**2.99±0.6** **2.35±0.4**	**2.50±0.7** **1.77±0.3**	
75			**3.19±0.7** **2.28±0.1**	**2.67±0.4** **2.10±0.3**	**3.03±0.8** **2.50±0.6**	
80			**4.10±1.2** **2.39±0.6**	**3.36±1.1** **2.39±0.6**	**2.93±0.3** **1.91±0.6**	**2.62±0.8** **1.83±0.3**

An average line width of 2.8±0.6mm and corner drag of 2.0±0.3mm were calculated from Table C-17. The corresponding score allocations using the equations described in Chapter 3 are displayed in Table C-18.

Table C-18: Printing parameter score allocation using a 27G nozzle at 37ºC

27G at 37ºC Line width/Corner drag score

Extrusion pressure (kPa)	*Extrusion speed (mm/s)*					
	10	15	20	25	30	35
30	10.6 7.9					
35	10.1 8.0	10.2 9.1				
40	8.2 6.8	9.9 7.3				
45	6.5 7.1	7.8 7.4	8.7 8.1			
50	3.3 5.3	6.4 5.4	8.3 7.5	4.3 8.2		
55		3.6 5.6	6.7 6.7	7.6 6.7	8.2 6.4	
60		5.1 5.3	7.5 7.3	7.5 7.0	9.5 5.9	
65		3.4 4.8	4.7 5.8	7.2 4.9		
70			4.7 5.1	6.3 5.2	7.9 7.1	
75			5.4 5.3	7.3 6.0	6.4 4.8	
80			2.5 5.1	4.8 4.9	6.4 6.7	7.7 7.1

An average score of 6.8/10 for kPa (extrusion pressure) and 6.4/10 for mm/s (corner drag) were calculated, resulting in an overall score of 6.6/10 for the 27G nozzle at 37ºC.

From this, it was concluded that the optimal parameters for further testing would be with a 27G nozzle at 37ºC, as these parameters scored the highest out of the six groups. Parameters that were taken into consideration for further testing were 65 to 75kPa and 25 to 35mm/s. Complete scaffolds (100% scaffolds) were to be printed within these parameters, using a 27G nozzle at 37ºC. Photographic results are available in supplementary photographs.

C.6.2 Parameter optimisation index

Table C-19: POI individual score for each scaffold measured

Parameter optimisation index individual score

	22G		*25G*		*27G*	
Scaffold number:	*35ºC*	*37ºC*	*35ºC*	*37ºC*	*35ºC*	*37ºC*
1.	0,9495	0,7463	0,9565	0,9644	1,0000	1,0000
2.	1,0000	1,0000	1,0000	1,0000	0,5283	0,7908
3.	0,7180	0,5147	0,6413	0,6713	0,4880	0,8060
4.	0,9530	0,6002	0,8114	0,7989	0,3830	0,5381
5.	0,5614	0,6283	0,4148	0,4273	0,2896	0,6790
6.	0,6053	0,3269	0,5372	0,5366	0,4055	0,3978
7.	0,7007	0,4873	0,7620	0,6592	0,3114	0,4562
8.	0,7341	0,4328	0,5128	0,3568	0,3147	0,5080
9.	0,4809	0,2757	0,2813	0,4488	0,3936	0,2739
10.	0,4815	0,2946	0,3325	0,4514	0,1599	0,3575
11.	0,4260	0,3023	0,3832	0,3320	0,1872	0,4370
12.		0,2185	0,2571	0,3464	0,2541	0,2956
13.		0,2407	0,3244	0,3541	0,2688	0,2551
14.		0,2908	0,3497	0,2516	0,3054	0,3325
15.		0,1869	0,2690	0,3107	0,1537	0,3646
16.		0,1914		0,3325	0,2088	0,3922
17.		0,1904		0,2271	0,2727	0,2637
18.				0,2468	0,2667	0,3315
19.					0,2764	0,3322
20.					0,1680	0,4230
21.					0,1976	0,2118
22.					0,2034	0,2350
23.					0,2503	0,2960
24.					0,2334	0,2175
25.					0,1310	0,2523
26.					0,1530	0,2969
27.					0,1879	0,2154
28.					0,2101	0,2600
29.					0,2211	0,2363
30.					0,2449	0,1614
31.					0,1433	0,1932
32.					0,1970	0,2232
33.					0,1934	0,2555

From Table C-19, it can be observed that the scaffold, with a parameter optimisation index of 1 for the 22G nozzle at 35ºC and 37ºC, was the scaffold printed with an extrusion pressure of 20kPa and a printing speed of 15mm/s. For the 25G nozzle at 35ºC and 37ºC, a printing speed of 15mm/s and an extrusion pressure of 25kPa had a POI of 1. For the 27G nozzle at 35ºC and 37ºC, a printing speed of 10mm/s and an extrusion pressure of 30kPa had a POI of 1.

C.6.3 Spearman's rank correlations

The Spearman's rank correlations were calculated as a non-parametric measure of rank correlations between the print score and the POI. It assessed how close the relationship was between the two parameters and whether there was statistical dependence between the pairs of observations. A perfect Spearman positive correlation has an *r* of 1, values close to 1 therefore indicate a strong dependence and correlation between the variables. The Spearman's rank correlations were calculated with GraphPad Prim version 9 (GraphPad Software, LLC, San Diego, CA, USA).

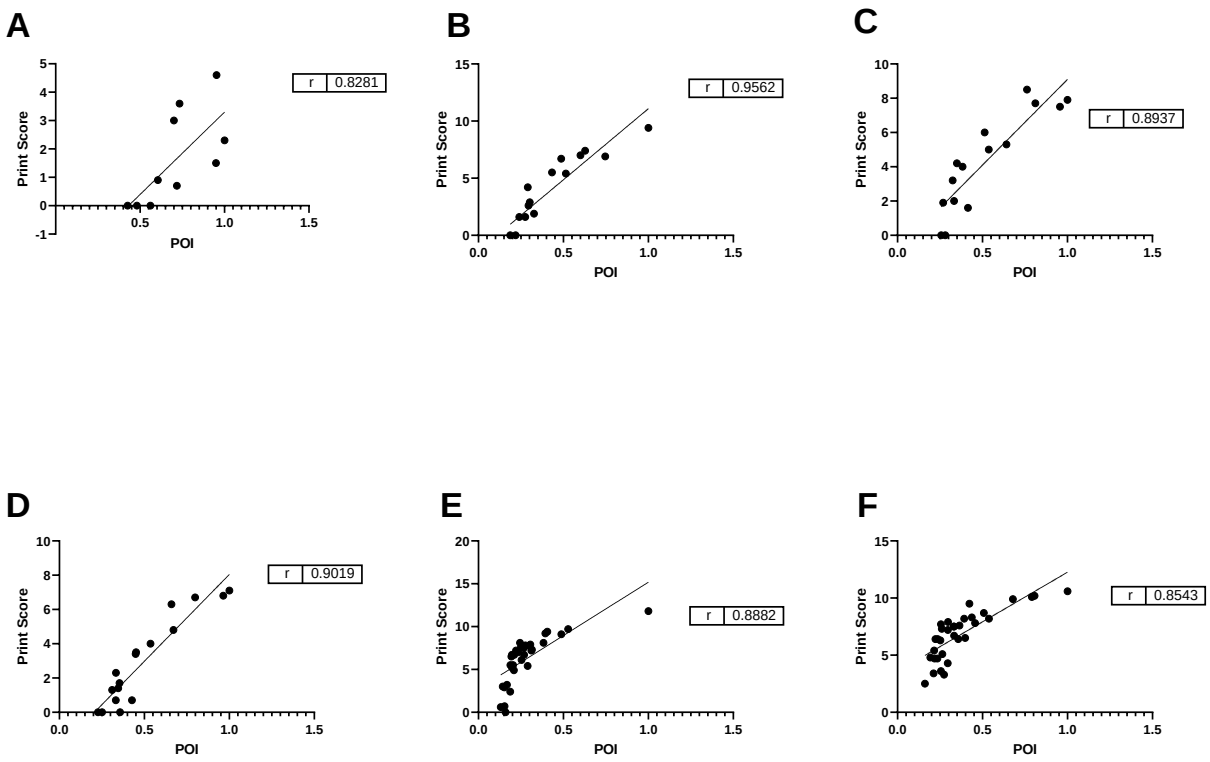

Figure C-1: Spearman's rank correlation graphs between the print score and the POI with the respective *r*-values. A) 22G at 35ºC, B) 22G at 37ºC, C) 25G at 35ºC, D) 25G at 35ºC, E) 27G at 35ºC, F) 27G at 35ºC

C.6.4 Visual appearance of scaffold

It can be seen from Figure C-2 that the scaffold's newest layers appeared wetter than the rest of the scaffold. This can possibly be attributed to the hybrid hydrogel slightly lowering in temperature after it has been extruded through the nozzle onto the previous scaffold layer. As only the surface

of the print bed and the mechanism keeping the syringe system in place can be heated to 37ºC (in place for thermosensitive PF127 component), the environment around the scaffold could possibly be at a slightly lower temperature than this.

The new layer extruded hybrid hydrogel had to be given a second or two to warm up to 37ºC and to be set in place and ready for the next layer. In the event that a new layer hybrid hydrogel was extruded onto the previous layer before this had happened, the integrity of the scaffold started to decline as the small temperature difference within that surrounding scaffold environment causes the scaffold's top layer to start to melt and the entire scaffold then started to collapse before reaching a 100% complete print. An adjustment to the printing speed (mm/s) and/or extrusion pressure (kPa) can resolve this issue.

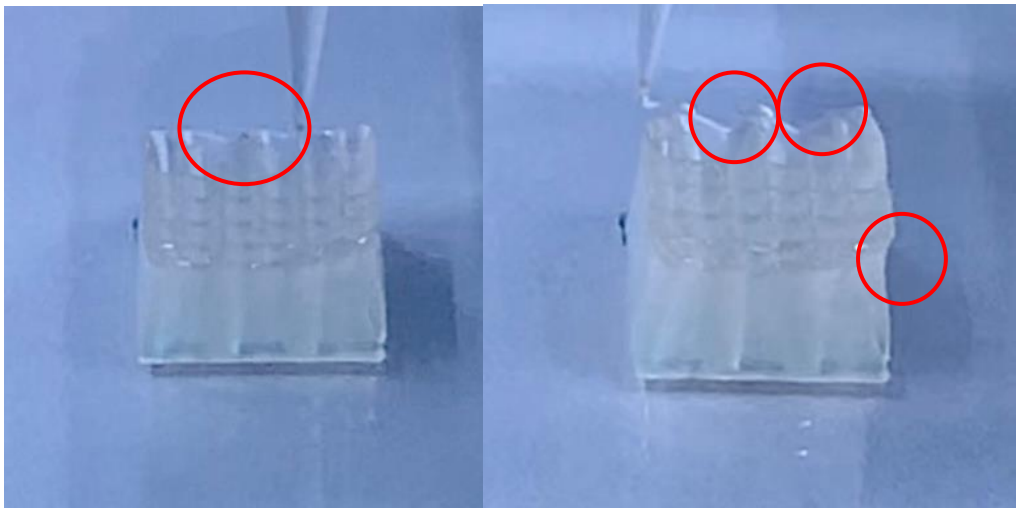

Figure C-2: Photographs taken of the self-collapsing effect on a scaffold caused by insufficient pressure or printing speed

From the parameters tested for printing a 100% complete scaffold, 27G and 37ºC have been identified as the optimal parameters and a range between a printing speed of 30mm/s and extrusion pressure of 70kPa has been successful.

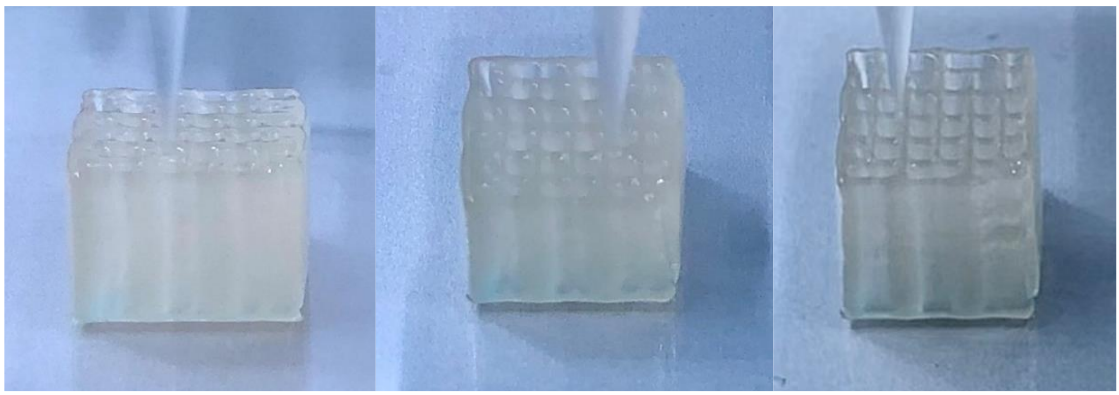

Figure C-3: Photographs taken during the printing process at 85 to 99% completion. Parameters include a 27G nozzle at 37˚C with an extrusion pressure of 70kPa and an extrusion speed of 30mm/s.

C.6.5 Cross-linking of scaffold

Post printing cross-linking is what gave the scaffold its integrity and ability to maintain its structure when the temperature fell below 37ºC and PF127 no longer had the capacity to sustain the scaffold. Ionically cross-linking the alginate component within the hybrid hydrogel caused an irreversible covalent bond to be formed between the ions and the alginate, which caused the gel to be more rigid (Gyles *et al*., 2017).

Cross-linking directly after printing with a 4% (w/v) $CaCl_2$ cross-linking solution that had also been heated up to 37ºC was deemed the most successful method, as cross-linking with cold $CaCl_2$ caused the same self-collapsing effect as described in Figure C-2. Cross-linking of the entire scaffold during the printing process was not a possibility, as the cross-linker is a watery solution and caused the first layer of the scaffold's hybrid hydrogel layer not to stick to the petri dish it was printed inside of and move around, resulting in accurate printing positions. Printing precision contributes to the structural integrity, and a lack in foundation integrity within the first printed layer would lead to each layer printed thereafter to start printing at random positions since the foundation is moving. This led to a failure in precision, which, in turn, led to a weak scaffold (Figure C-2). Figure C-3 represents parameters that yielded a 100% successful scaffold print.

Cross-linking of the entire scaffold could not take place during the printing process, as the cross-linking of the top layer influenced how the following layer binds to the printed structure, which could lead to different bindings within each layer. This caused a lack in structural integrity that led to a weak scaffold. Cross-linking therefore had to take place partially and carefully during the printing process and after the printing process had occurred. The heated 4% (w/v) $CaCl_2$ was

dripped around the printing scaffold with a dripper, ensuring not to allow any cross-linker to come in contact with the newest extruded bioink layer. After 100% completion of the scaffold printing, the cross-linking solution was dripped all over the scaffold. Thereafter, the petri dish was tilted to remove any excess cross-linking solution from the petri dish, then it was rotated to face the ground, leaving the scaffold upside-down to be entirely submerged within a beaker filled to the brim with heated $CaCl_2$, resting the petri dish sides on the brim of the beaker, on top of the heated printbed for 1min.

After 1min, the scaffold was removed from the cross-linking solution and the petri dish was tilted, still facing downwards. A dripper filled with heated $CaCl_2$ was used to carefully remove the scaffold by gently gushing the cross-linking solution to the scaffolds sides, careful not to compromise the integrity of the 3D printed scaffold. After doing this about three times on each side of the scaffold, it gently came loose and slid to the side of the petri dish where it fell back into the cross-linking solution in the beaker. The submerged scaffold in the cross-linking solution was kept at 37ºC for 24h to ensure that complete cross-linking of the entire scaffold took place.

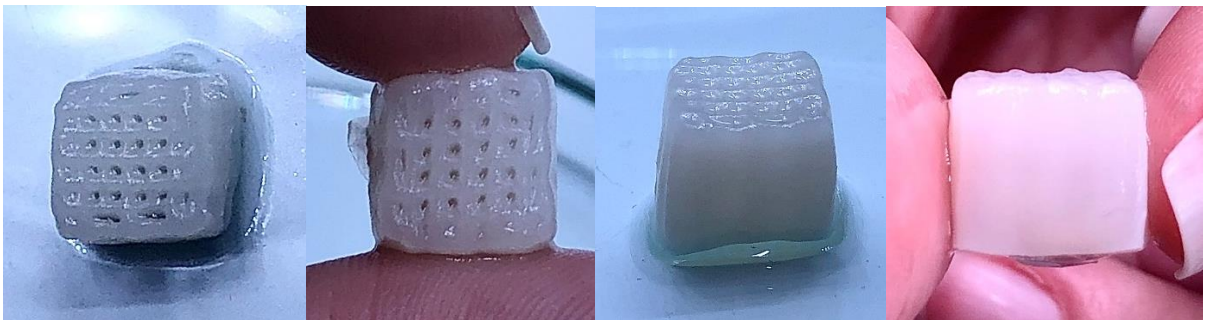

Figure C-4: Photographs taken after 4% $CaCl_2$ cross-linking for 24h at 4ºC.

These scaffolds were then removed from the $CaCl_2$ and placed in beakers filled with 4ºC dH_2O and placed inside the fridge (4ºC) for 24h to try and determine whether the PF127 component of the hybrid hydrogel would undergo phase separation. Six of these scaffolds were printed to 100% completion and weighed directly after printing, cross-linking and refrigeration at 4ºC. Results are displayed in Table C-20:

Table C-20: Scaffold mass after printing, after cross-linking and after refrigeration

Scaffold number	*Mass directly after printing (g)*	*Mass after 24h $CaCl_2$ cross-linking at 37ºC (g)*	*Mass after 24h at 4ºC (g)*
1	1.130	1.055	1.038
2	1.006	0.909	0.894
3	1.398	1.044	1.093
4	1.167	0.993	1.070
5	0.983	0.870	0.979
6	1.096	0.990	1.057
AVE±SD	**1.13±0.15**	**0.98±0.07**	**1.02±0.07**

From these results, it can be seen that the scaffold loses mass after it has been cross-linked. This can possibly be contributed to water loss within the scaffold as it does shrink between 0.5 and 1.5mm after cross-linking still saturated with dH_2O, and between 1 and 5mm after being completely dried with a paper towel.

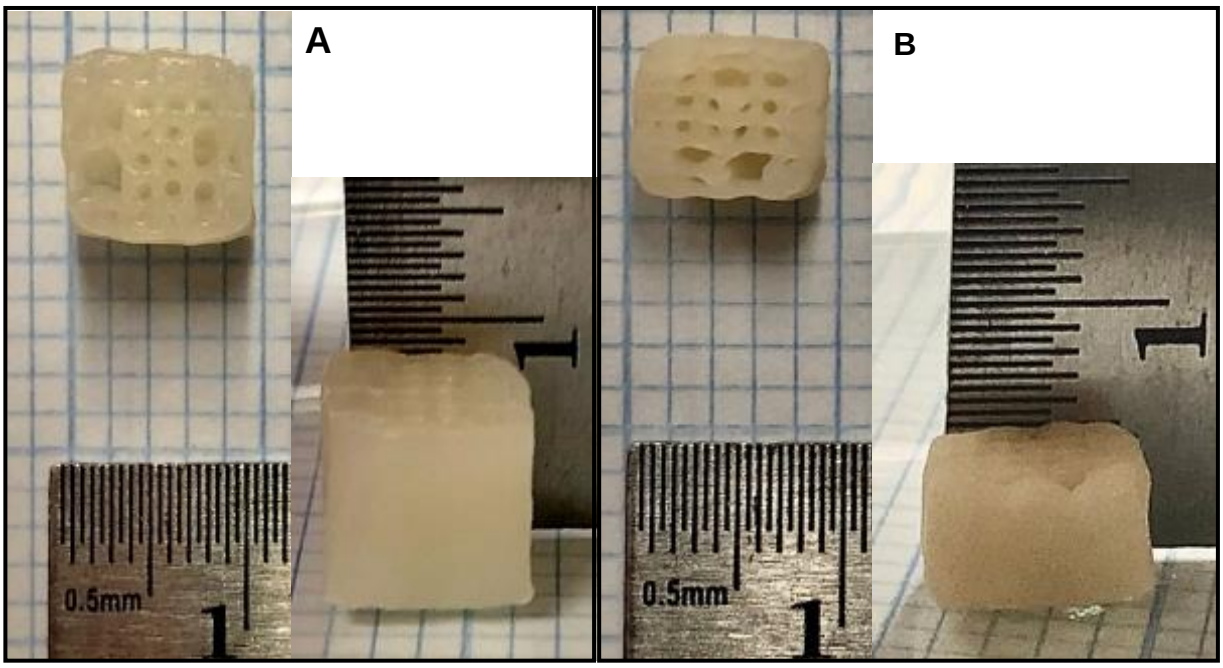

Figure C-5: **$CaCl_2$ cross-linked scaffolds visibly showing mass loss (a) saturated with dH_2O and (b) completely dried with a paper towel.**

Since the loss of mass after cross-linking can be attributed to water loss and the overall mass seems to have slightly increased (again attributed to water gain/porosity) after 24h at 4ºC and 1/3 of the hybrid hydrogel consists of PF127, it can be concluded that the PF127 does not separate after alginate cross-linking has taken place. PF127 entangles within the polymer chains formed by the alginate after cross-linking and therefore forms part of the final scaffold (Chimene *et al*., 2020; Rarokar *et al*., 2018).

C.7 Conclusion

The printing parameters selected to be optimal for the printing of a hybrid hydrogel formulation, consisting of 6% (w/v) alginate and 46% (w/v) PF127 mixed in a 2:1 ratio, are a printing speed of 30mm/s with an extrusion pressure of 70kPa, while using a 27G nozzle at 37ºC. It was found that PF127 does not separate from the cross-linked alginate and forms part of the final structure.

C.8 References

1. Chimene, D., Kaunas, R. & Gaharwar, A.K. 2020. Hydrogel Bioink Reinforcement for Additive Manufacturing: A Focused Review of Emerging Strategies. *Advanced Material Science*, 32:1902026.

2. Gyles, D.A., Castro, L.D., Silva, J.O.C. Jnr. & Ribeiro-Costa, R.M. 2017. A review of the designs and prominent biomedical advances of natural and synthetic hydrogel formulations*. European Polymer Journal*, 88:373-392.

3. Rarokar, N.R., Saoji, S.D. & Khedekar, P.B. 2018. Investigation of effectiveness of some extensively used polymers on thermoreversible properties of Pluronic tri-block copolymers. *Journal of Drug Delivery Science and Technology*, 44:220-230.

4. Varkey, M., Visscher, D.O., Van Zuijlen, P.P.M., Atala, A. & Yoo, J.J. 2019. Skin bioprinting: the future of burn wound reconstruction? *Burns & Trauma,* 7(4):3.

5. Vijayavenkataraman, S., Yan, W.C., Lu, W.F., Wang, C.H. & Fuh, J.Y.H. 2018. 3D bioprinting of tissues and organs for regenerative medicine. *Advanced Drug Delivery Reviews*, 32:296–332.

6. Webb, B. & Doyle, B. 2017. Parameter optimization for 3D bioprinting of hydrogels. *Bioprinting*, 8:8-12.

C.9 Supplementary photographs used for line width and corner drag score calculations

C.9.1 35ºC 22G

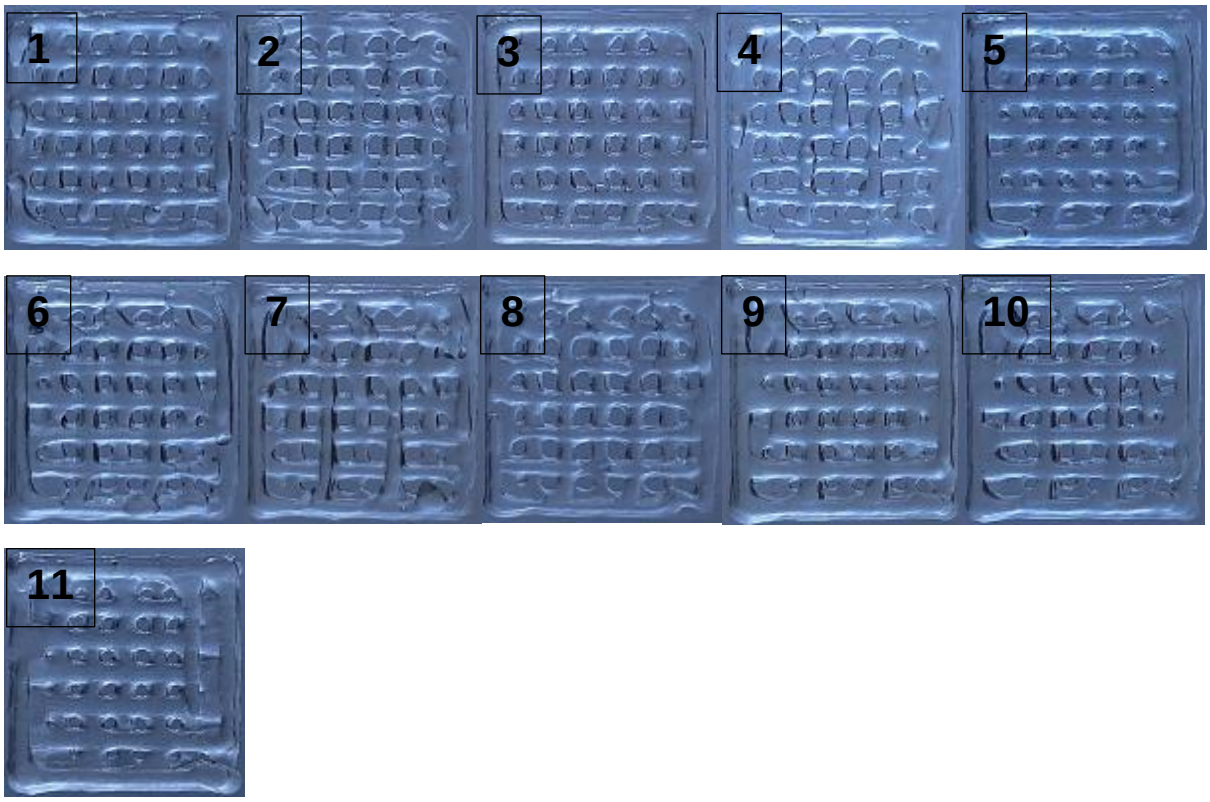

C.9.2 35ºC 25G

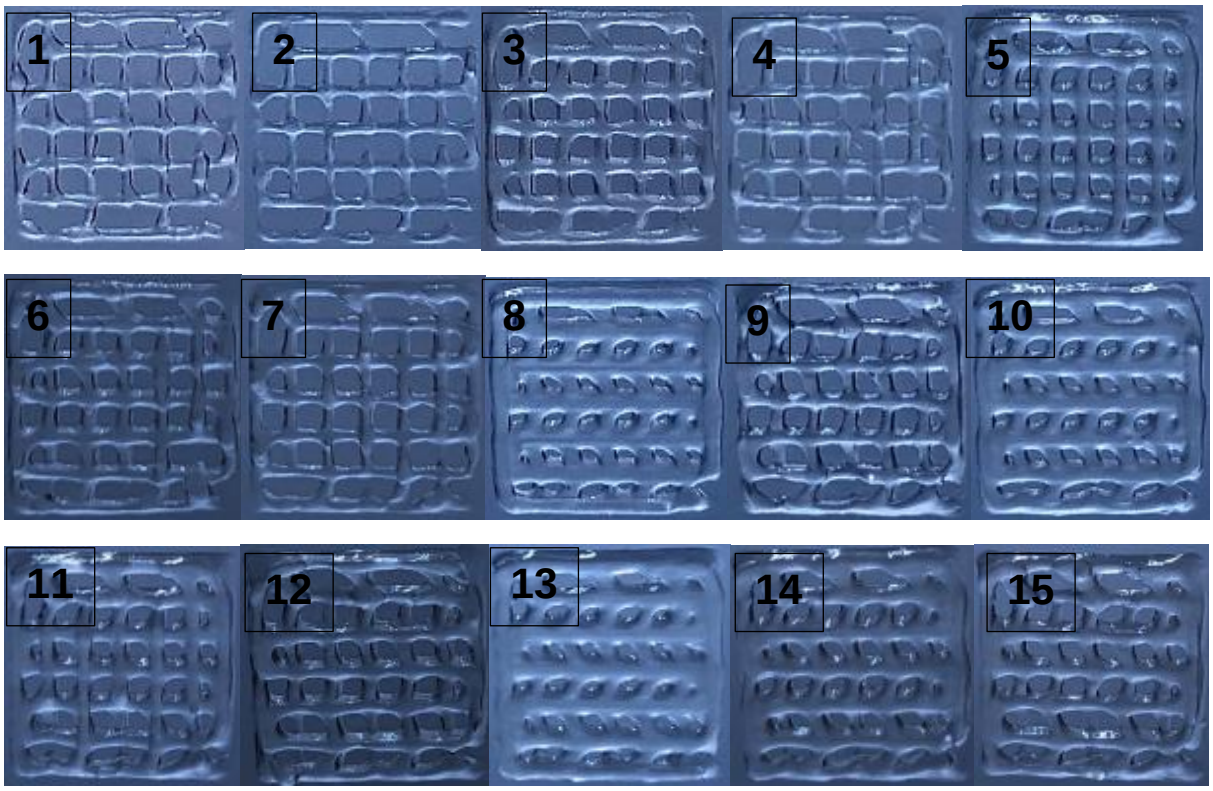

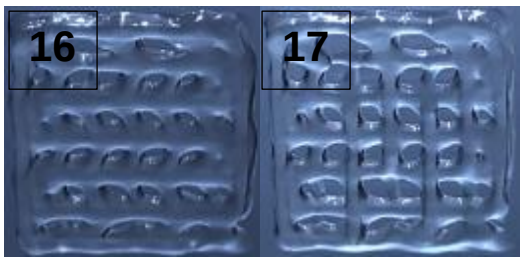

C.9.3 35ºC 27G

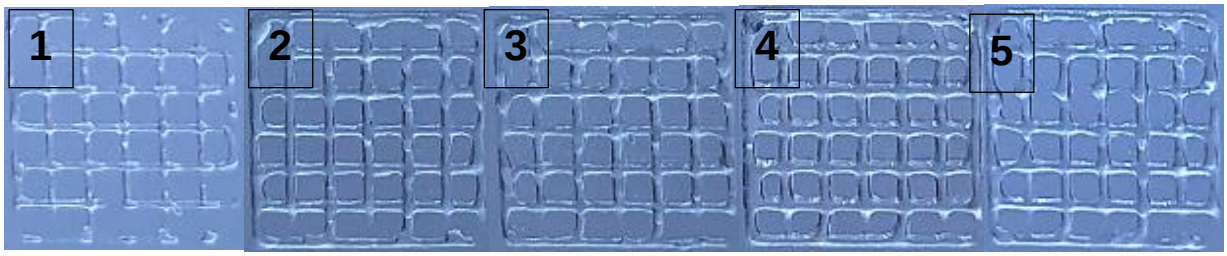

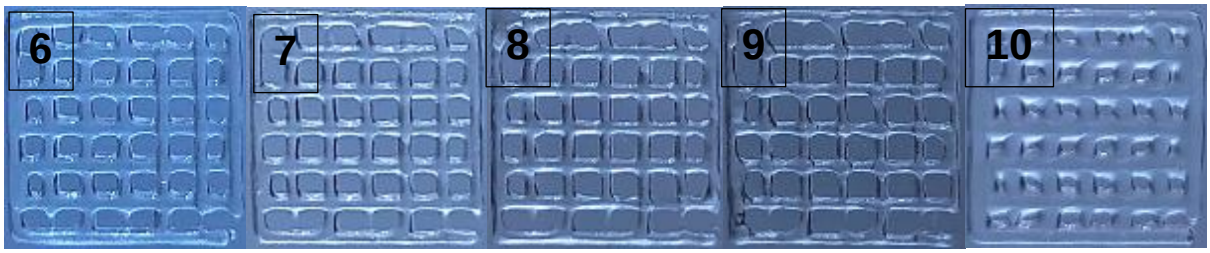

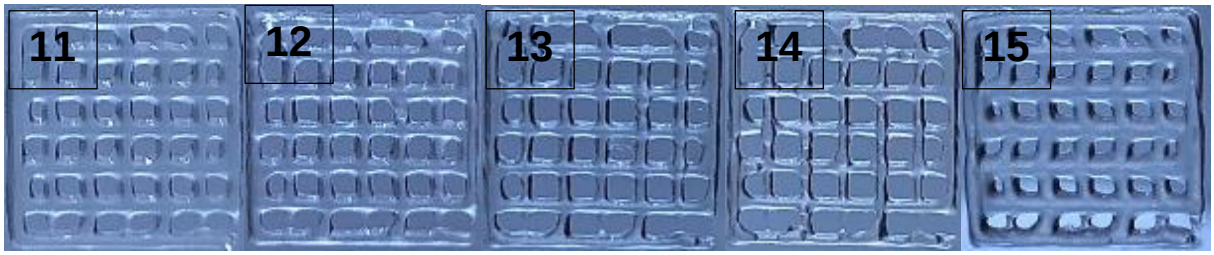

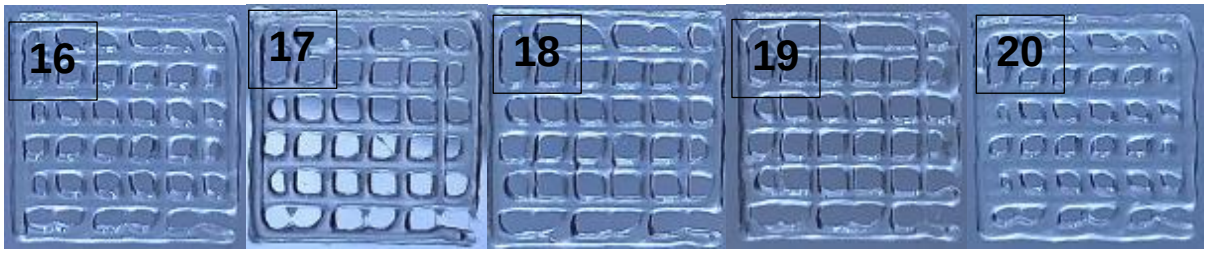

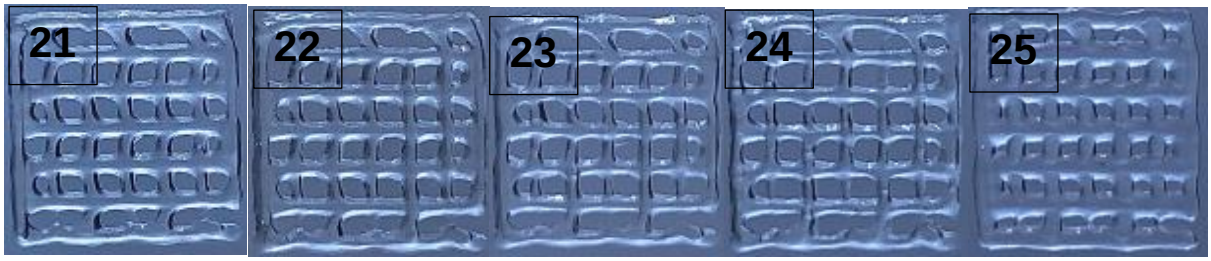

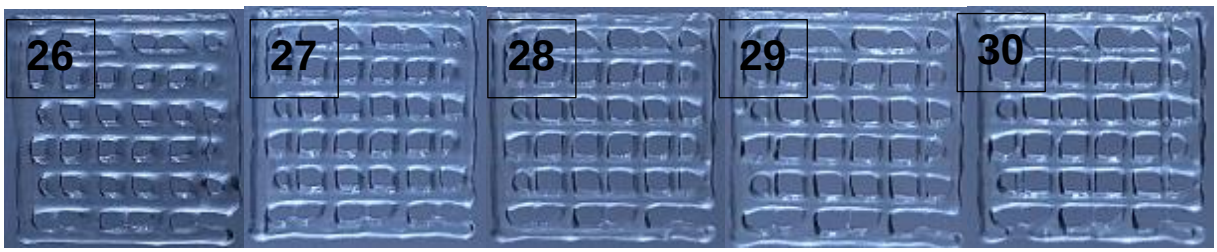

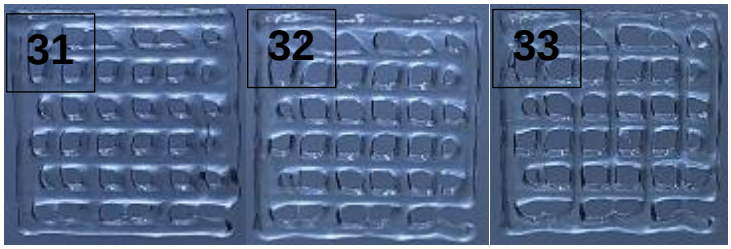

C.9.4 37ºC 22G

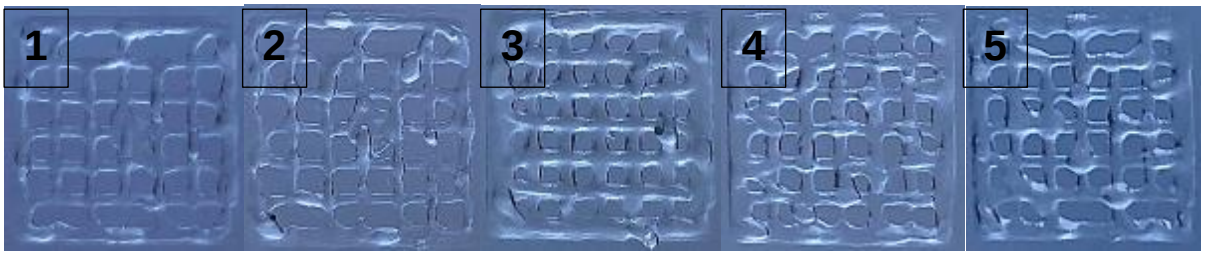

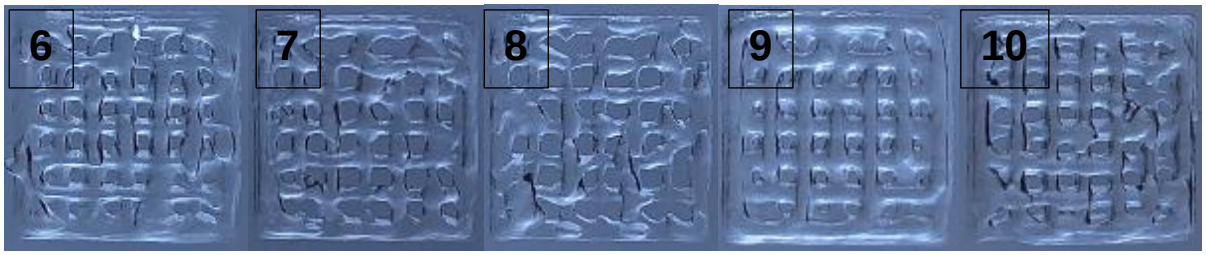

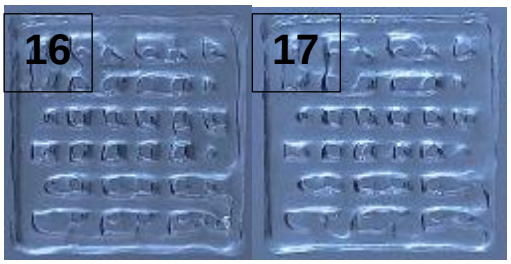

C.9.5 37ºC 25G

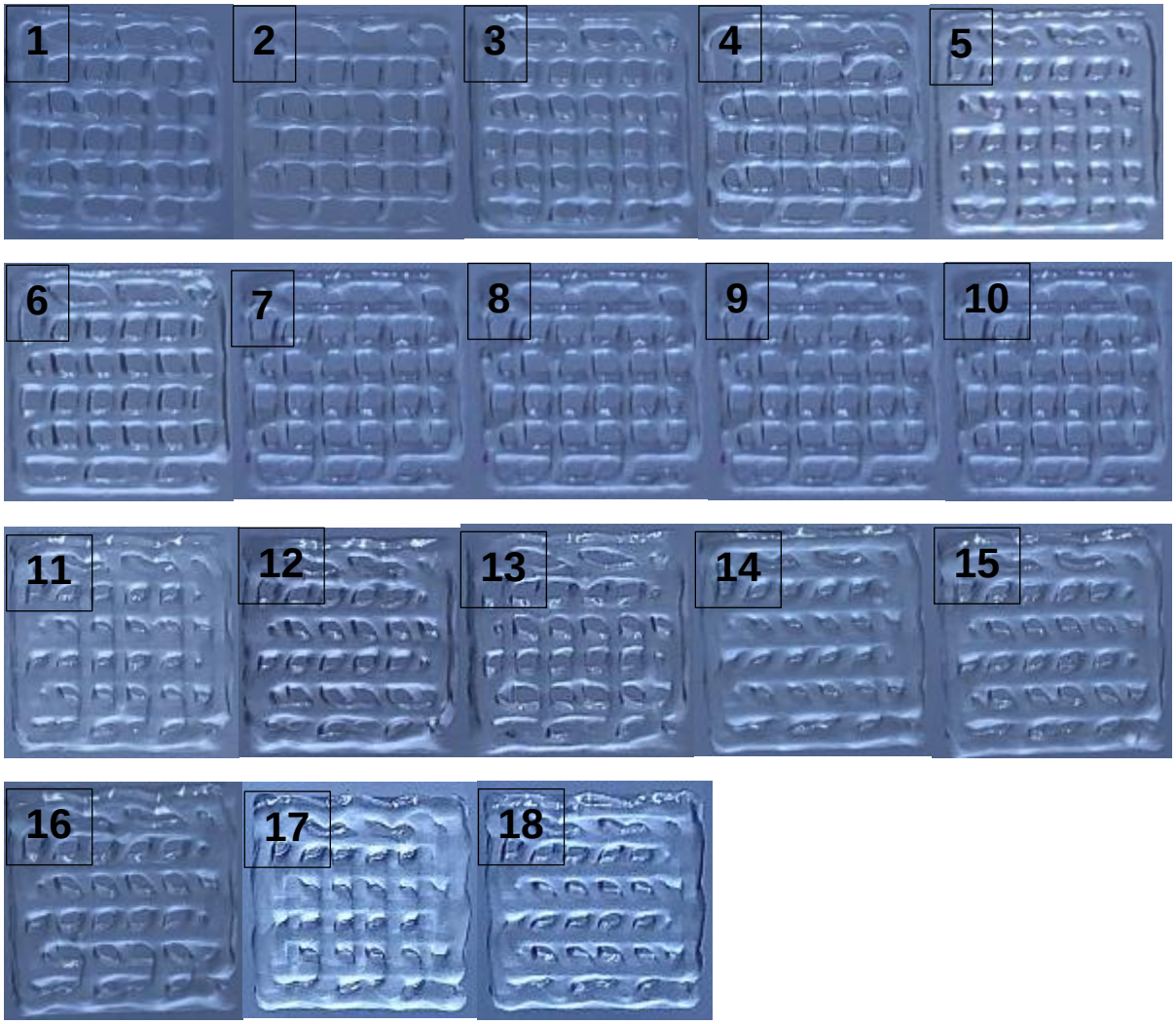

C.9.6 37ºC 27G

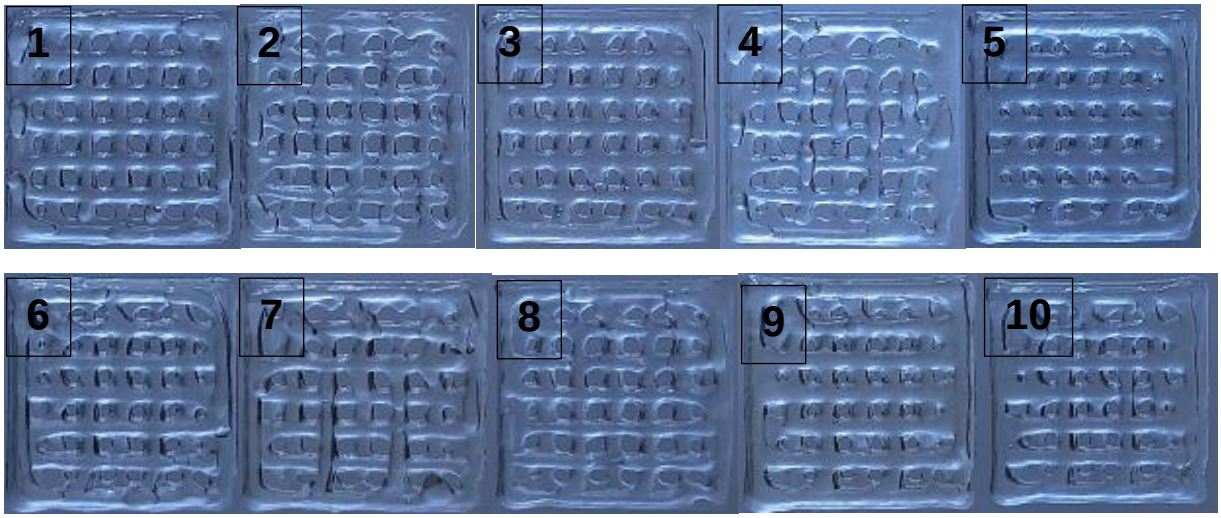

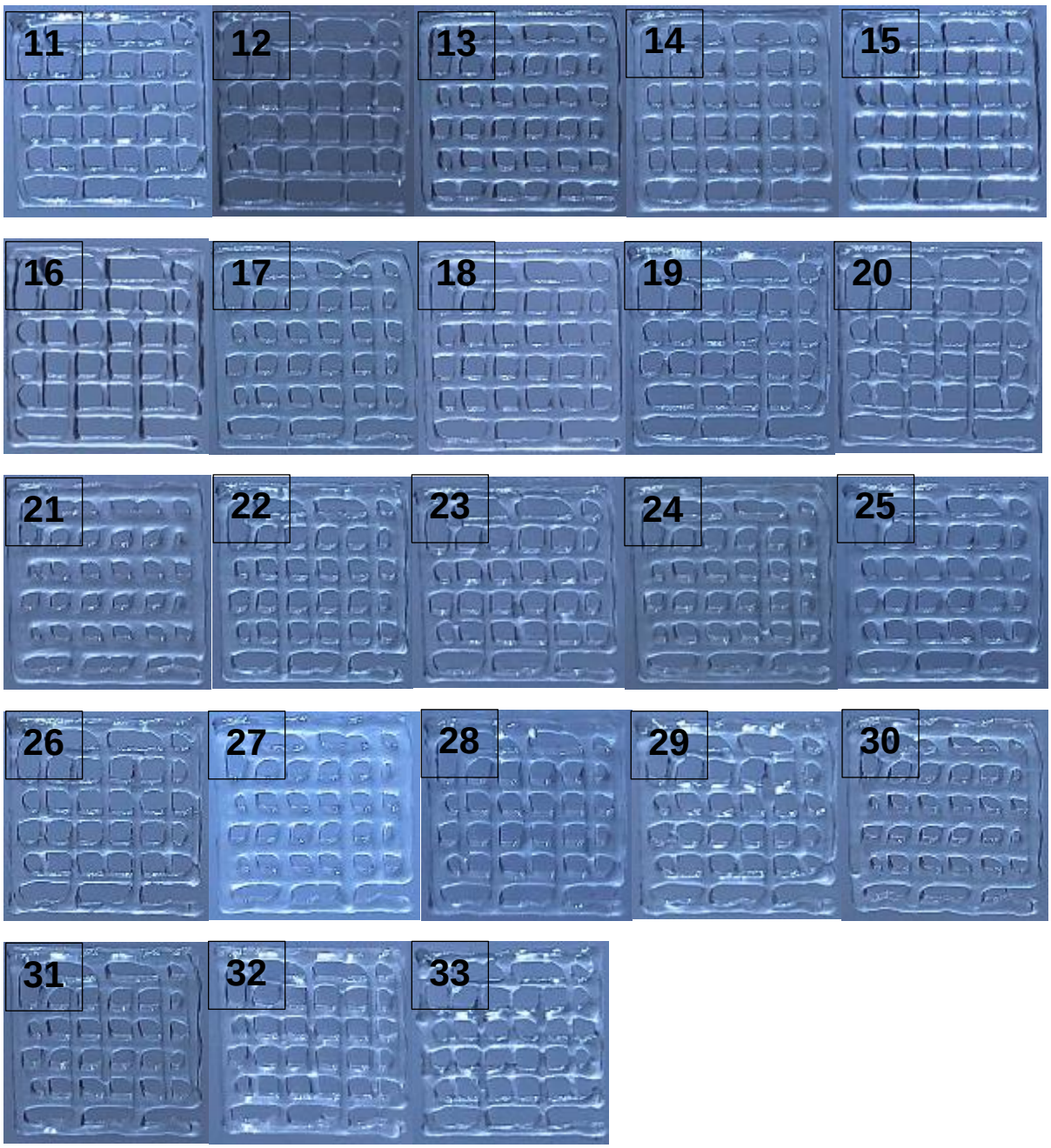

C.9.7 65kPa 25mm/s triplicates

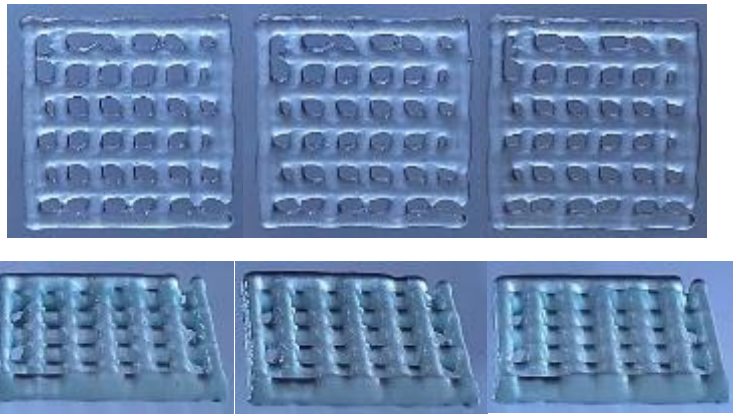

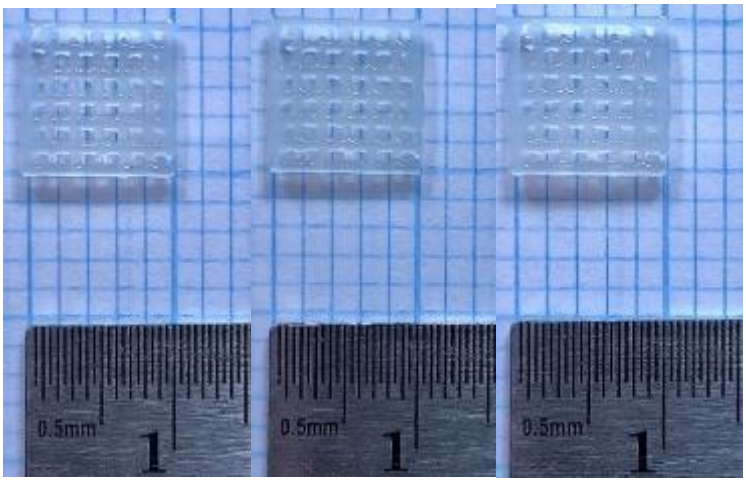

C.9.8 66kPa 26mm/s triplicates

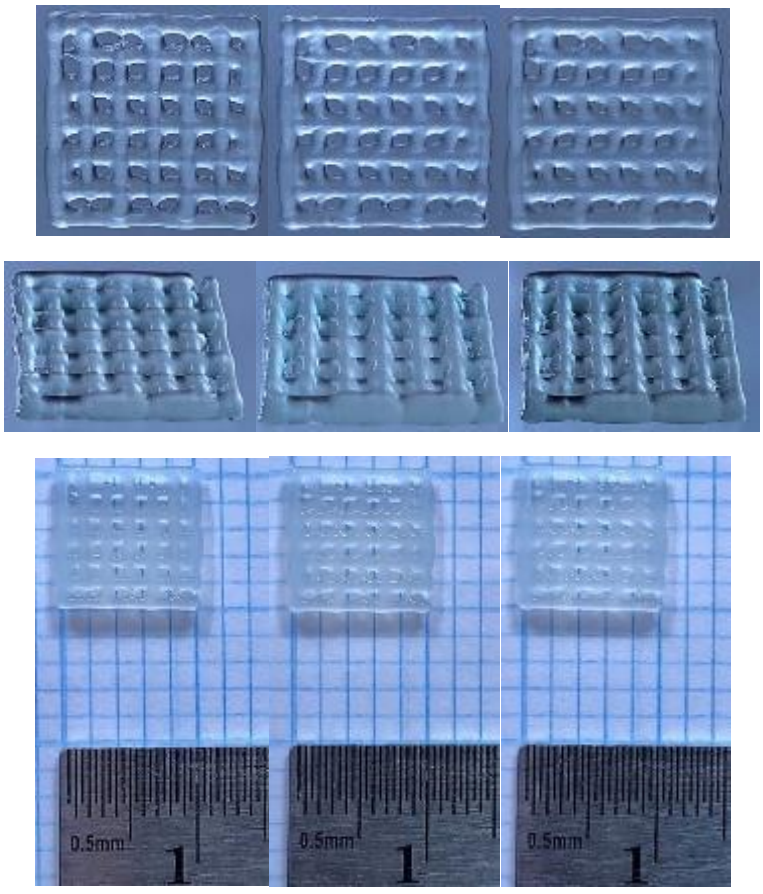

C.9.9 67kPa 27mm/s triplicates

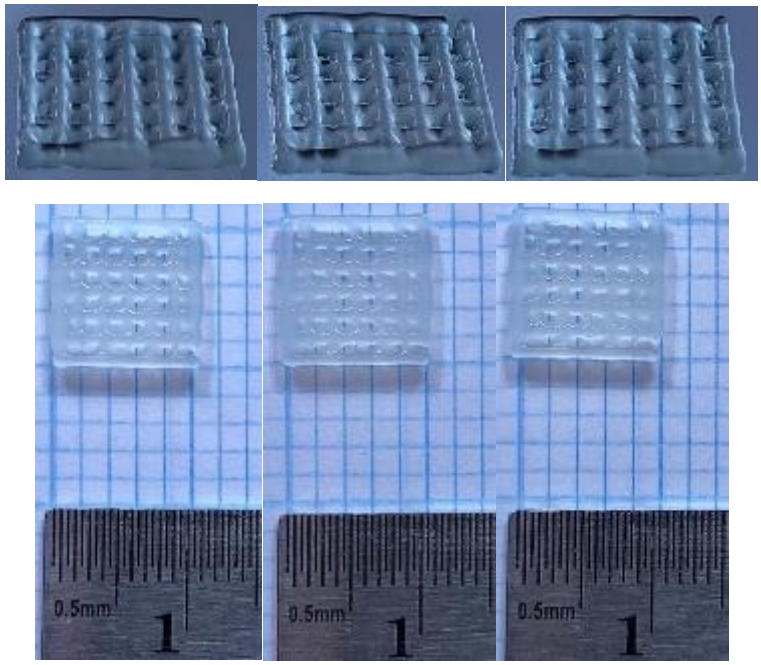

C.9.10 68kPa 28mm/s triplicates

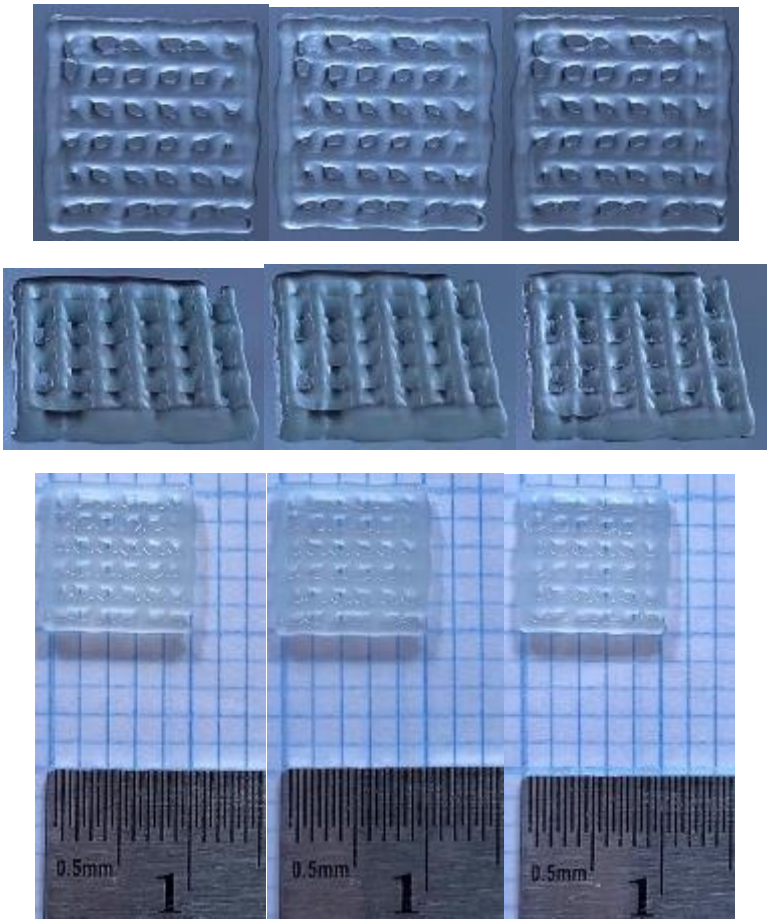

C.9.11 69kPa 29mm/s triplicates

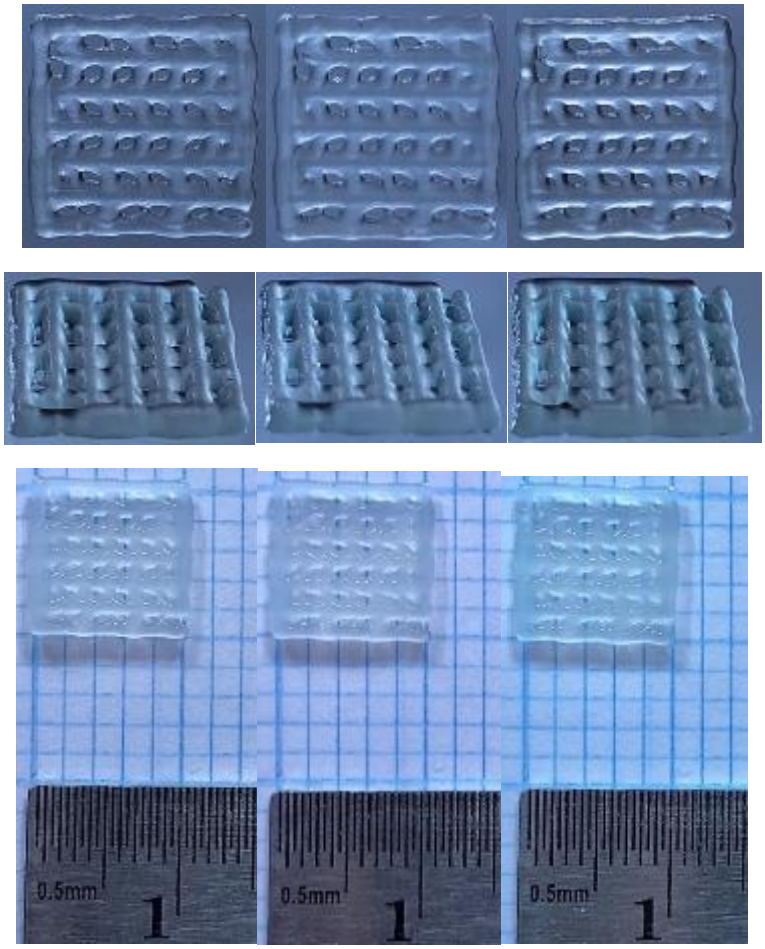

C.9.12 70kPa 30mm/s triplicates

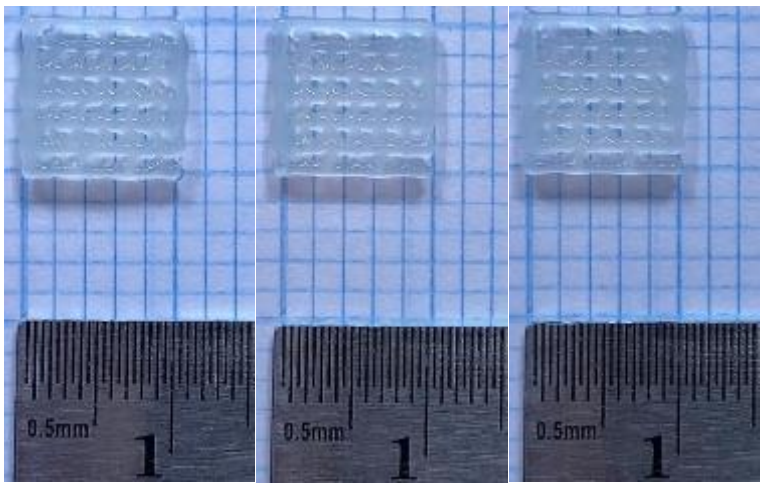

C.9.13 71kPa 31mm/s triplicates

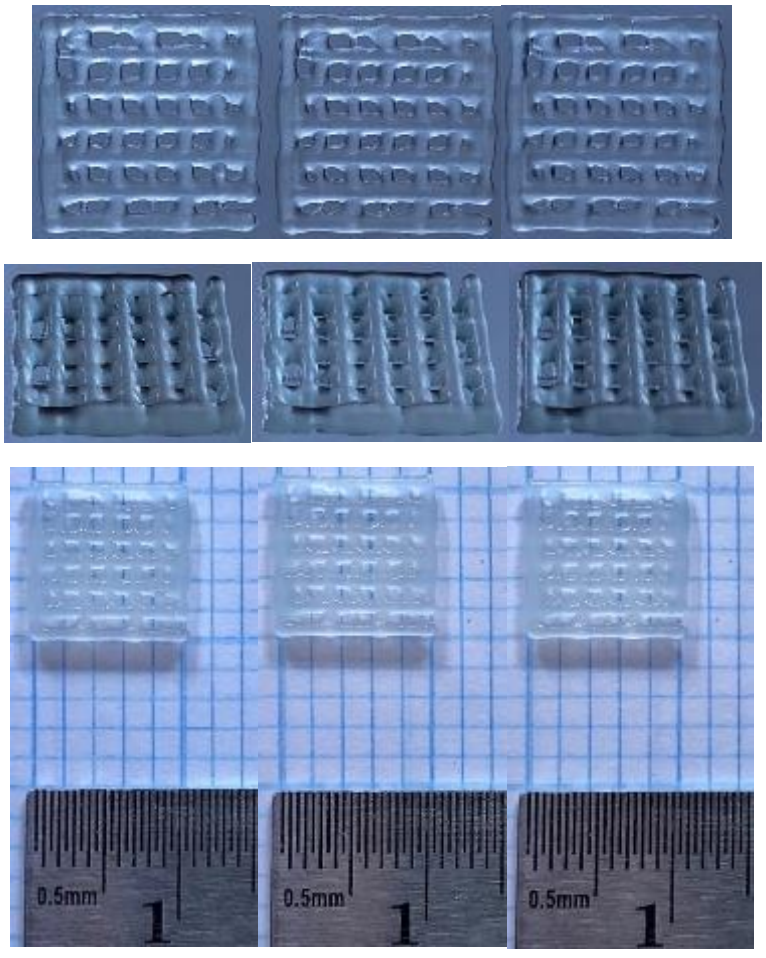

C.9.14 72kPa 32mm/s triplicates

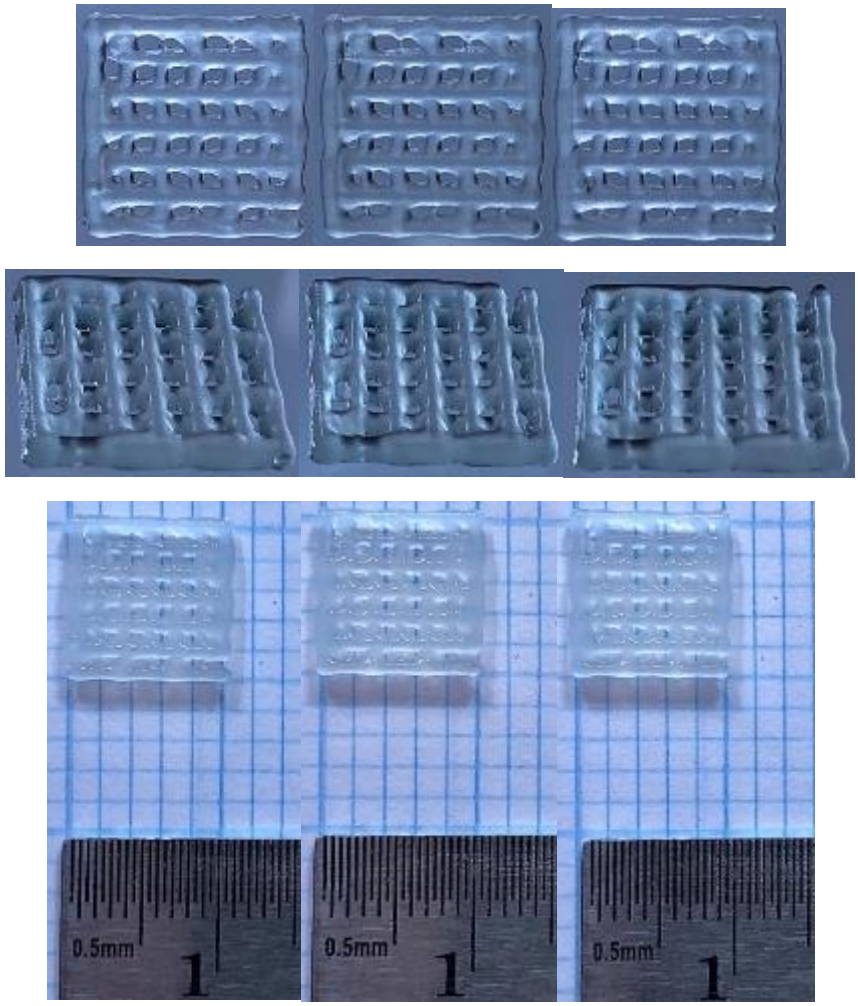

C.9.15 73kPa 33mm/s triplicates

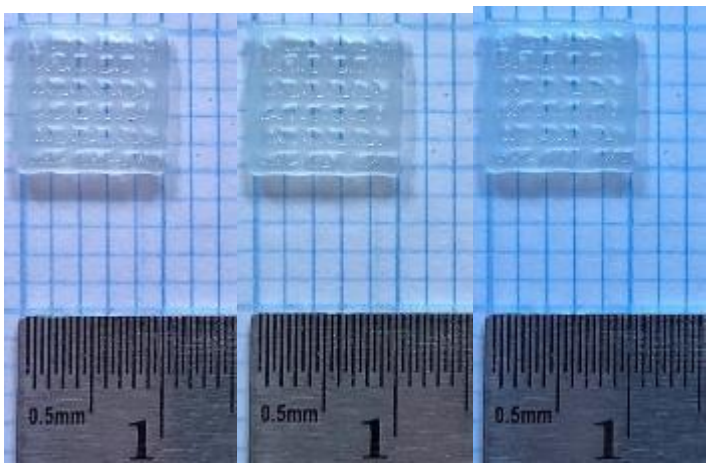

C.9.16 74kPa 34mm/s triplicates

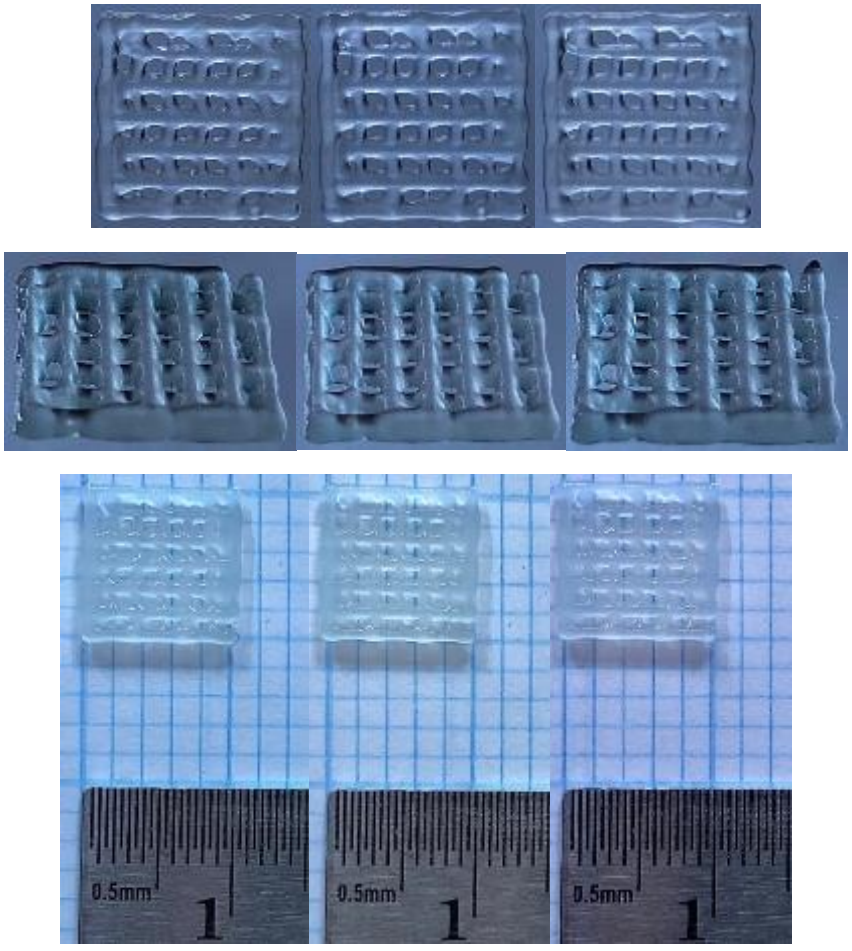

C.9.17 75kPa 35mm/s triplicates

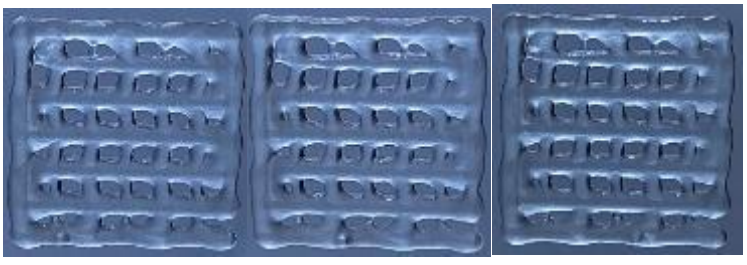

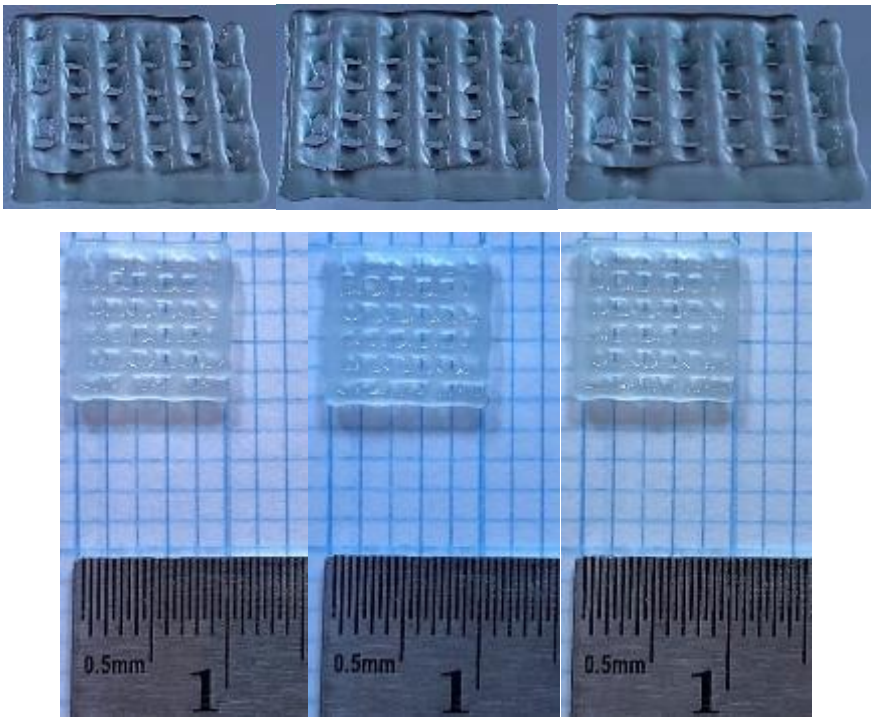
0.5mm
1
0.5mm
1
0.5mm
1

ANNEXURE D: ETHICS COMMITTEE LETTER

Private Bag X1290, Potchefstroom
South Africa 2520

Tel: 086 016 9698
Web: http://www.nwu.ac.za

North-West University Health Research Ethics Committee (NWU-HREC)

Tel: 018 299-1206
Email: Ethics-HRECApply@nwu.ac.za (for human studies)

10 September 2019

RESEARCH ETHICS COMMITTEE LETTER OF DECISION: NO RISK

Based on the review by the North-West University Health Research Ethics Committee (NWU-HREC) on 10/09/2019, the NWU-HREC hereby clears your study as a no risk study. This implies that the NWU-HREC grants its permission that, provided the general conditions specified below are met, the study may be initiated, using the ethics number below.

Study title: Print parameter optimisation for three-dimensional bioprinting of hydrogel scaffolds
Principal Investigator/Study Supervisor/Researcher: Prof LH du Plessis
Student: M van der Linde - 25073559

Ethics number:

N	W	U	-	0	0	5	1	0	-	1	9	-	A	1
Institution				Study Number						Year			Status	

Status: S = Submission; R = Re-Submission; P = Provisional Authorisation; A = Authorisation

Application Type: Single study
Commencement date: 10/09/2019

Risk: **No Risk**

General conditions:

The following general terms and conditions will apply:

- *The commencement date indicates the first date that the study may be started.*
- *In the interest of ethical responsibility, the NWU-HREC reserves the right to:*
  - *request access to any information or data at any time during the course or after completion of the study;*
  - *to ask further questions, seek additional information, require further modification or monitor the conduct of your research;*
  - *withdraw or postpone clearance if:*
    - *any unethical principles or practices of the study are revealed or suspected;*
    - *it becomes apparent that any relevant information was withheld from the NWU-HREC or that information has been false or misrepresented;*
    - *submission of the required amendments, or reporting of adverse events or incidents was not done in a timely manner and accurately; and/or*
    - *new institutional rules, national legislation or international conventions deem it necessary.*
- *NWU-HREC can be contacted for further information via Ethics-HRECApply@nwu.ac.za or 018 299 1206*

The NWU-HREC would like to remain at your service and wishes you well with your study. Please do not hesitate to contact the NWU-HREC for any further enquiries or requests for assistance.

Yours sincerely,

Digitally signed by Wayne Towers
Date: 2019.09.10 20:54:26 +02'00'

Prof Wayne Towers
Chairperson NWU-HREC

Digitally signed by Prof Minrie Greeff
DN: cn=Prof Minrie Greeff, o, ou, email=minrie.greeff@nwu.ac.za, c=ZA
Date: 2019.09.11 07:35:19 +02'00'

Prof Minrie Greeff
Head of the Faculty of Health Sciences Ethics Office

Current details: (13210572) G:\My Drive\My Documents 20190227\NWU-HREC\NWU-HREC_Applications\NWU-HREC_Applications-2019\Applications 09-20191015\NWU-00510-19-S1(LH du Plessis-M van der Linde)-NR\NWU-00510-19-S1(LH du Plessis-M van der Linde)-LoD\9.1.5.4.3_LOD_NWU-00510-19-A1.docm
10 September 2019

File reference: 9.1.5.4.3

ANNEXURE E: PROOF OF ETHICS TRAINING AND ASSESMENT

NWU®
NORTH-WEST UNIVERSITY
NOORDWES-UNIVERSITEIT
YUNIBESITI YA BOKONE-BOPHIRIMA

Private Bag X6001, Potchefstroom
South Africa 2520

Tel: +2718 299-1111/2222
Web: http://www.nwu.ac.za

Faculty of Health Sciences Ethics Office for Research, Training and Support

Tel: 018 299 2092
Email:minrie.greeff@nwu.ac.za

Ms Monja van der Linde

8 March 2019

Dear Ms van der Linde

PROOF OF ATTENDANCE AND ASSESSMENT

This letter certifies that you have attended the 2-day ethics training entitled:

The Basics of Health Research Ethics

(Accreditation number: PSB002/110/01/2019 from University of Free-State CPD accreditation department accredited by the HPCSA)

Presenter: Prof M Greeff (Head of the Health Sciences Ethics Office for Research, Training and Support) on the **22nd – 23rd January 2019.**

This letter of attendance, serves as proof of ethics training and assessment and is valid for three (3) years and expires on 31 January 2022. (Where applicable, Ethics CEUs awarded: 14 CEUs)

Yours sincerely

Digitally signed by Prof Minrie Greeff
Date: 2019.03.20 15:07:38 +02'00'

Prof Minrie Greeff
Head of Health Sciences Ethics
Office for Research, Training and Support

Prof Jeanetta du Plessis
Deputy Dean: Research and Innovation
Faculty of Health Sciences

Current details: (20536890) G:\My Drive\9. Research and Postgraduate Education\9.1.5.7 Training\ 9.1.5.7.6_Letter of Attendance_Template_BCHRE.docm
8 March 2019

File reference: 9.1.5.7.6

ANNEXURE F: LANGUAGE EDITING CERTIFICATE

To whom it may concern

Cecile van Zyl
Language editing and translation
Cell: 072 389 3450
Email: Cecile.vanZyl@nwu.ac.za

12 March 2021

Dear Mr / Ms

Re: Language editing of dissertation: Print parameter optimisation for three dimensional bioprinting of hydrogel scaffolds

I hereby declare that I language edited the above-mentioned dissertation, Chapter 1 to 4 and Annexure A to C, by Ms Monja Hibbert (student number: 25073559).

Please feel free to contact me should you have any enquiries.

Kind regards

Cecile van Zyl

Language practitioner

BA (PU for CHE); BA honours (NWU); MA (NWU)
SATI number: 1002391